GEORGIA DOT RESEARCH PROJECT 20 – 15

Final Report

RECOMMENDATIONS FOR NONDESTRUCTIVE TESTING (NDT) OF CONCRETE COMPONENTS FOR PERFORMANCE-BASED SPECIFICATIONS

Office of Performance-based Management and Research
600 West Peachtree Street NW | Atlanta, GA 30308

August 2022

<table>
<tr><td>1. Report No.:
FHWA-GA-22-2015</td><td colspan="2">2. Government Accession No.:</td><td>3. Recipient's Catalog No.:</td></tr>
<tr><td colspan="2" rowspan="2">4. Title and Subtitle:
Recommendations for Nondestructive Testing (NDT) of Concrete Components for Performance-Based Specifications</td><td colspan="2">5. Report Date:
August 2022</td></tr>
<tr><td colspan="2">6. Performing Organization Code:
N/A</td></tr>
<tr><td colspan="2">7. Author(s):
Laurence J. Jacobs (PI), PhD
Kimberly E. Kurtis (coPI), PhD
Ryan J. Sherman, (coPI), PhD, PE
David C. Burney</td><td colspan="2">8. Performing Organ. Report No.:
20-17</td></tr>
<tr><td colspan="2" rowspan="2">9. Performing Organization
School of Civil & Environmental Engineering
Georgia Institute of Technology
Atlanta, GA 30332-0355</td><td colspan="2">10. Work Unit No.:
N/A</td></tr>
<tr><td colspan="2">11. Contract or Grant No.:
PI#0017413</td></tr>
<tr><td colspan="2" rowspan="2">12. Sponsoring Agency
Georgia Department of Transportation (SPR)
Office of Performance-based Management and Research
600 West Peachtree St. NW
Atlanta, GA 30308</td><td colspan="2">13. Type of Report and Period Covered:
August 2020–August 2022</td></tr>
<tr><td colspan="2">14. Sponsoring Agency Code:
N/A</td></tr>
<tr><td colspan="4">15. Supplementary Notes:
Prepared in cooperation with the U.S. Department of Transportation, Federal Highway Administration.</td></tr>
<tr><td colspan="4">16. Abstract:
This research investigates non-destructive testing (NDT) techniques for the quality assurance of portland cement concrete pavements and structures. Responses were collected from a survey distributed amongst AASHTO Committee of Materials and Pavements (CoMP) members regarding their use of NDT technologies. Relevant literature was reviewed to determine the fundamental capabilities and limitations of NDT techniques and comparisons were drawn between commercially available devices. Finally, a series of validation tests were performed to confirm that specific NDT devices can perform as expected. From the information gathered, recommendations are made regarding the implementation of NDT technologies for the enforcement of concrete performance-based specifications.</td></tr>
<tr><td colspan="3">17. Key Words:
Nondestructive Testing, Performance-based Specifications, Pavements, Structures</td><td>18. Distribution Statement:
No restriction</td></tr>
<tr><td>19.Security Classification (of this report):
Unclassified</td><td>20. Security Classification (of this page):
Unclassified</td><td>21. No. of Pages:
118</td><td>22. Price:
Free</td></tr>
</table>

GDOT Research Project 20-15

Final Report

RECOMMENDATIONS FOR NONDESTRUCTIVE TESTING (NDT) OF CONCRETE COMPONENTS FOR PERFORMANCE-BASED SPECIFICATIONS

By
Laurence J. Jacobs
Ph.D.
Kimberly E. Kurtis
Ph.D.
Ryan J. Sherman
Ph.D., P.E.
David C. Burney

Georgia Institute of Technology Research Corporation

Contract with
Georgia Department of Transportation

In cooperation with
U.S. Department of Transportation
Federal Highway Administration

August 2022

SI* (MODERN METRIC) CONVERSION FACTORS

APPROXIMATE CONVERSIONS TO SI UNITS

Symbol	When You Know	Multiply By	To Find	Symbol
		LENGTH		
in	inches	25.4	millimeters	mm
ft	feet	0.305	meters	m
yd	yards	0.914	meters	m
mi	miles	1.61	kilometers	km
		AREA		
in^2	square inches	645.2	square millimeters	mm^2
ft^2	square feet	0.093	square meters	m^2
yd^2	square yard	0.836	square meters	m^2
ac	acres	0.405	hectares	ha
mi^2	square miles	2.59	square kilometers	km^2
		VOLUME		
fl oz	fluid ounces	29.57	milliliters	mL
gal	gallons	3.785	liters	L
ft^3	cubic feet	0.028	cubic meters	m^3
yd^3	cubic yards	0.765	cubic meters	m^3
		NOTE: volumes greater than 1000 L shall be shown in m^3		
		MASS		
oz	ounces	28.35	grams	g
lb	pounds	0.454	kilograms	kg
T	short tons (2000 lb)	0.907	megagrams (or "metric ton")	Mg (or "t")
		TEMPERATURE (exact degrees)		
°F	Fahrenheit	5 (F-32)/9 or (F-32)/1.8	Celsius	°C
		ILLUMINATION		
fc	foot-candles	10.76	lux	lx
fl	foot-Lamberts	3.426	$candela/m^2$	cd/m^2
		FORCE and PRESSURE or STRESS		
lbf	poundforce	4.45	newtons	N
lbf/in^2	poundforce per square inch	6.89	kilopascals	kPa

APPROXIMATE CONVERSIONS FROM SI UNITS

Symbol	When You Know	Multiply By	To Find	Symbol
		LENGTH		
mm	millimeters	0.039	inches	in
m	meters	3.28	feet	ft
m	meters	1.09	yards	yd
km	kilometers	0.621	miles	mi
		AREA		
mm^2	square millimeters	0.0016	square inches	in^2
m^2	square meters	10.764	square feet	ft^2
m^2	square meters	1.195	square yards	yd^2
ha	hectares	2.47	acres	ac
km^2	square kilometers	0.386	square miles	mi^2
		VOLUME		
mL	milliliters	0.034	fluid ounces	fl oz
L	liters	0.264	gallons	gal
m^3	cubic meters	35.314	cubic feet	ft^3
m^3	cubic meters	1.307	cubic yards	yd^3
		MASS		
g	grams	0.035	ounces	oz
kg	kilograms	2.202	pounds	lb
Mg (or "t")	megagrams (or "metric ton")	1.103	short tons (2000 lb)	T
		TEMPERATURE (exact degrees)		
°C	Celsius	1.8C+32	Fahrenheit	°F
		ILLUMINATION		
lx	lux	0.0929	foot-candles	fc
cd/m^2	$candela/m^2$	0.2919	foot-Lamberts	fl
		FORCE and PRESSURE or STRESS		
N	newtons	0.225	poundforce	lbf
kPa	kilopascals	0.145	poundforce per square inch	lbf/in^2

* SI is the symbol for the International System of Units. Appropriate rounding should be made to comply with Section 4 of ASTM E380.
(Revised March 2003)

Table of Contents

LIST OF FIGURES

LIST OF TABLES

CHAPTER 1. INTRODUCTION

MOTIVATION

Current practice uses destructive drilling and coring to determine if concrete meets stated specifications, such as 28-day compressive strength. While this approach has been widely practiced, the procedures can be time-consuming and have the potential to negatively impact the long-term performance of the concrete pavement, bridge deck, piles, or structural element. As an alternative, a number of candidate nondestructive testing (NDT) techniques exist which have the potential to replace coring. These NDT techniques provide critical measurements for the quality assurance of concrete components, including quantitative measures of the in-place concrete properties, which enable the development of criteria for a performance-based specification. A shift toward performance-based specifications for concrete would allow contractors flexibility to enhance the performance of their mixes, while maintaining low costs. Ultimately, performance-based specifications would positively impact Georgia through higher reliability, longer service life and economic savings associated with concrete infrastructure.

There have been significant advances in the development of quantitative NDT techniques to characterize concrete properties, such as strength and porosity. Many companies now provide NDT devices based on waves (acoustic and electromagnetic), vibrations and mechanical phenomenon. These devices have a wide variety of accuracy, robustness, sensitivity and selectiveness to critical concrete properties.

With growing interest in the development and adoption of performance-based specifications, there is a need to identify NDT methods that can be readily implemented in the field to assess concrete quality and ensure specifications are met. Development of performance-based specifications could provide an alternative means to design concrete that meets specific performance-related goals, such as limits on permeability (to resist ingress of corrosion-causing aggressive chlorides), as well as minimum strength and cover depth criteria. Instead of specifying materials, means, and proportions, as current prescriptive specifications do, a performance-based specification indicates the functional requirements for concrete in the plastic and hardened states—as measured by standard test methods—and allows the concrete producer to design a mixture that meets those requirements.

Research and development have shown that NDT techniques hold tremendous promise for this application, and recent instrumentation advances suggest there are field-ready, inexpensive, commercially available devices capable of accurately measuring critical concrete material properties. A non-inclusive list of NDT techniques investigated includes: ultrasonic pulse velocity (UPV), impact-echo (IE), ground penetrating radar (GPR), cover meter, and surface resistivity meters. Each technique offers unique advantages as well as disadvantages that will limit their applicability. For example, electromagnetic wave-based techniques, such as GPR, are sensitive to the dielectric properties of a material, making them excellent means to detect the presence and condition of steel reinforcing bars, but relatively insensitive to concrete material properties (Popovic 2017, Arndt 2009, Lesnicki 2013). The positive and negative aspects of each technology must be evaluated with respect to its ability to be integrated into a performance-based specification. The relative sensitivity of each measurement technique to material characteristics relevant for performance is also important in evaluating potential NDT methods.

OBJECTIVES

The objectives of this research project are to:

1. Document available concrete NDT tools and their use by transportation agencies.
2. Understand the underlying physics, reliability, and sensitivity of candidate NDT tools.
3. Establish critical properties of concrete components and suitable acceptance criteria for performance-based concrete material specifications.
4. Validate the most promising NDT tools to demonstrate overall effectiveness.

REPORT ORGANIZATION

The project final report is organized into five chapters. Chapter 2 presents beneficial outcomes from a survey that was created and distributed to members of the AASHTO Committee of Materials and Pavements (CoMP). Respondents were asked to give feedback on what NDT devices were used, what they were used for, and the positive/negative aspects of their performance in service. Chapter 3 consists of a literature review of NDT techniques commonly used for measurement of concrete components, with an emphasis placed on quality assurance applications. The chapter is organized by NDT technique; at the end of each subsection, comparisons are drawn between commercially available devices. Chapter 4 summarizes testing performed at the Georgia Tech structures and materials laboratory to validate the ability of given NDT devices to perform as expected. The findings of this research project are summarized in Chapter 5 in the form of recommendations for the implementation of NDT techniques for the acceptance or rejection of concrete components.

CHAPTER 2. AASHTO SURVEY

INTRODUCTION

To gather information on the usage of NDT technologies for quality assurance across the United States, a survey was created and distributed to members of the AASHTO Committee of Materials and Pavements (CoMP). The survey was conducted in collaboration with a second GDOT research project that was investigating performance-based concrete material specifications. The first half of the survey collected data regarding the usage of performance-based specifications (PBS), while the second half collected data regarding the usage of NDT technologies. A diagram detailing the survey questions is included in Appendix A. In total, 31 responses were collected and reviewed. Two different responses were collected from the Maryland, Alabama, Florida, and North Dakota Departments of Transportation. The responses provided beneficial feedback on which NDT technologies and devices are being used in-service, what applications owners are using a given technology for, and how the devices perform (i.e., both positive/negative aspects).

COMMON NDT USAGES

The first question in the NDT section of the survey asked respondents for what applications their agencies use NDT technologies. Responses were provided by 19 of the total 31 survey respondents. The results are shown in Figure 1. The responses from this question, along with some responses from the PBS section, provide valuable insight on the current state of NDT and the general perception of various NDT technologies.

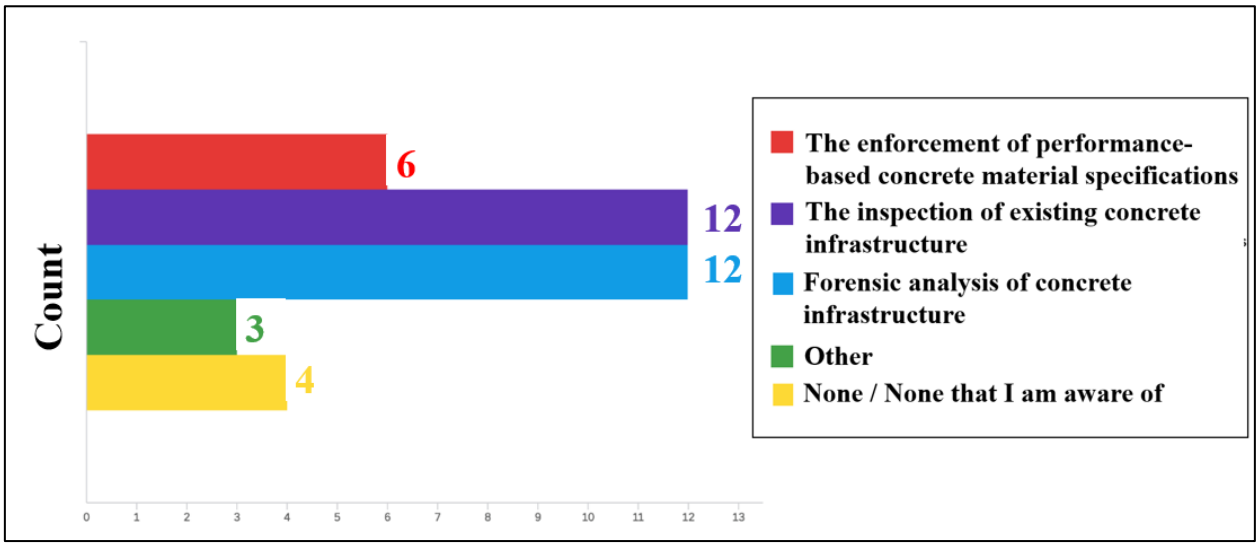

Figure 1. Graph. NDT Applications Indicated by 19 Respondents

Most respondents (63% of the 19) indicated that their agencies used NDT technologies for the inspection of existing concrete infrastructure. Similarly, 63% of respondents indicated usage for forensic analysis. However, only 32% of respondents indicated usage of NDT technologies for the enforcement of PBS. Of the 13 respondents whose agencies do not utilize NDT technologies for PBS, 4 enforce PBS through other means (e.g., coring). One respondent specified destructive determination of pavement depth, despite the wide variety of commercially available devices available for the application. The results suggest that while NDT technologies are commonly used for inspection and forensic applications, often they are not viewed as having a level of reliability capable of specification enforcement. Further, in a subsequent survey question, respondents were asked about PBS barriers to implementation. The most common response (54% of 13 respondents) was “difficulties with enforcement,” while another respondent replied that a “lack of confidence” was the main barrier to implementation.

The final question of the survey concerned the barriers to implementation of more NDT technologies. The responses are displayed in Figure 2. Interestingly, the most common responses were “cost of equipment” and “personnel limitations” rather than “lack of equipment reliability.”

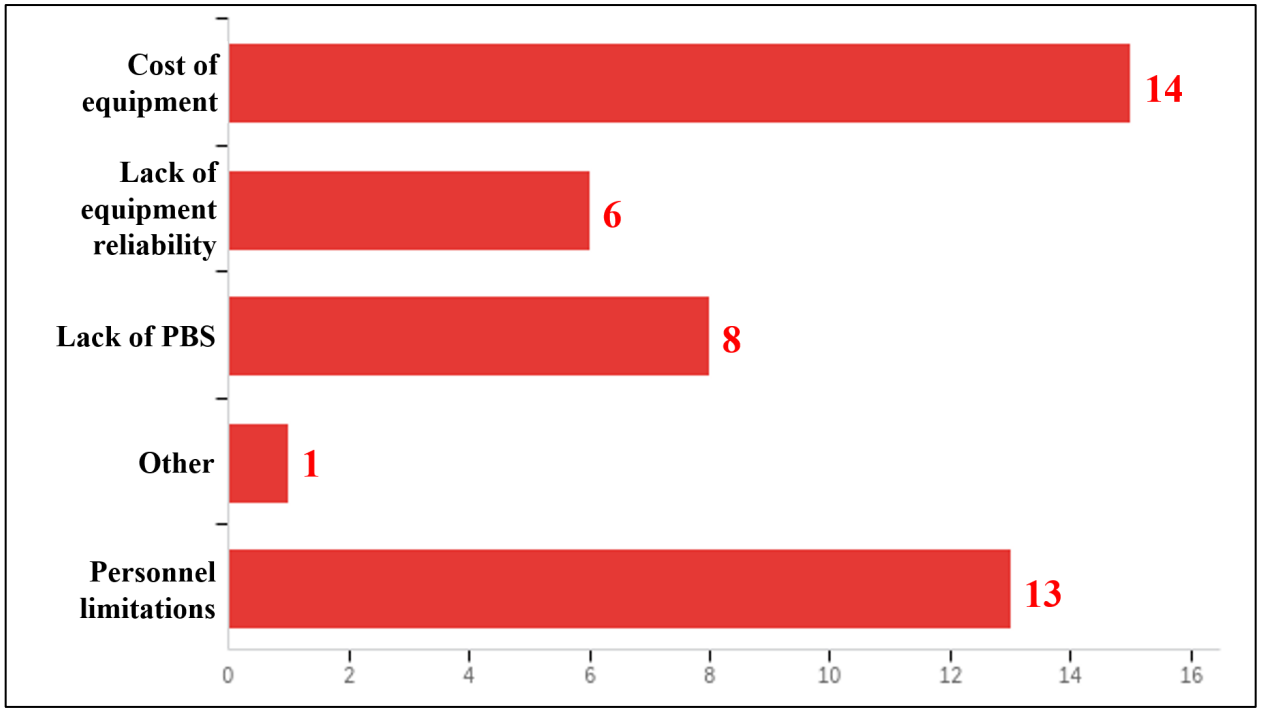

Figure 2. Graph. Barriers to Implementation of NDT Technologies

One of the most beneficial outcomes of the survey was gaining information on which NDT techniques are most used by agencies across the country. This knowledge can help GDOT determine which techniques are ready for implementation and what contexts are appropriate for a given technique. Responses were provided by 14 of the total 31 survey respondents. The survey responses for which NDT technologies used by various agencies are shown in Figure 3.

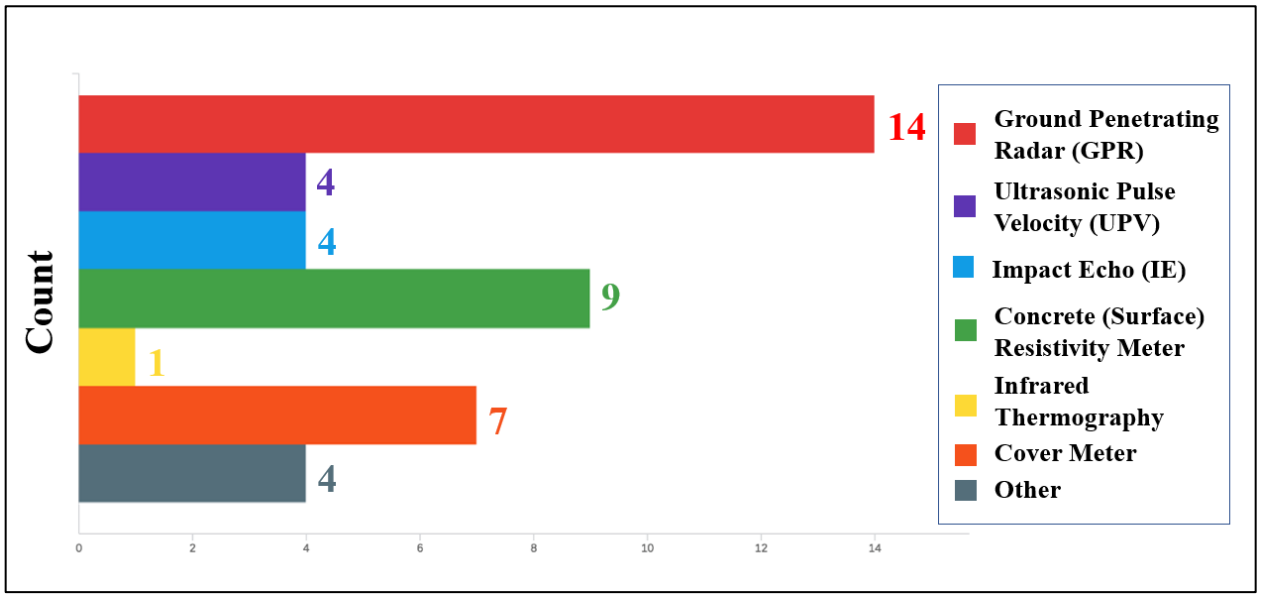

Figure 3. Graph. Use of Various NDT Technologies Indicated by 14 Respondents

GPR was the most-used technology (used by all 14 question respondents), with 28.5% of users (4 out of the 12 who specified application) indicating that the technology was used for the enforcement of specifications. Three of the four respondents who used GPR to enforce specifications indicated that the primary application was evaluation of dowel bar depth and alignment. A respondent from the Tennessee DOT specified use of the GSSI Structure scan for locating rebar as part of the verification of precast components. Respondents used GPR technologies for a variety of other applications as well: delamination of cover, pavement depth, cover depth, and void detection. Due to the wide range of applications for GPR, the popularity of the technology is not necessarily an indication of it being preferred to other NDT technologies. One other important note from the survey results is that GSSI was the most used GPR manufacturer.

The second-most used technology was the concrete surface resistivity meter (64.3% of respondents). Use on cylinders and cores for research projects and mix design acceptance was

specified. The responses suggest that the majority of testing is performed in a laboratory setting rather than in the field, most likely because of the high sensitivity to saturation and pore solution composition inherent to the methodology (Liu 2010), both of which vary depending on field conditions. It was reported that the Illinois DOT is conducting a research project to understand how local materials may influence measurements. The most used resistivity meter (two out of three specified devices) was the Proceq Resipod.

The third-most used technology was the cover meter (50% of respondents). The most common uses were for determining concrete cover and for locating rebar during coring operations. One respondent specified cover meter use for forensics and inspection rather than quality assurance. Of the two respondents who specified which cover meter devices were used, both indicated that they used "various" cover meters, which is an indicator of the large number of commercially available cover meter devices.

Use of UPV was reported by 28.5% of respondents. Inspection and forensics were specified as common use cases. The Indiana DOT has reported reliable use of the technology to monitor crack depth over time. Three out of three respondents who specified what UPV device was used, specified usage of the Germann Instrument's MIRA device, an ultrasonic shear wave imaging device.

Use of impact echo was reported by 28.5% of respondents. Impact echo was used for detecting delamination of overlays and the determination of pavement thickness. The Olson Engineering Impact Echo device was the only device specified.

Other technologies were reported to a lesser extent. Only one respondent indicated use of infrared thermography, which was used to verify rebar placement. The Illinois DOT uses Schmidtt hammers to identify locations of potentially low strength concrete for coring; the Tennessee DOT uses them for the verification of precast concrete components.

Additional specific devices and technologies that were identified include:

- The MIT-Scan-T2, an eddy current-based device which involves the embedding of a steel plate between the pavement and subgrade, allowing for the measurement of pavement depth.
- The Germann Instruments CAPO-test (pullout test method for the estimation of concrete strength, standardized by ASTM C900)
- The falling weight deflectometer (FWD)
- Cross-hole sonic logging for the acceptance of drilled shafts (standard practice for the Arkansas DOT, included in a special provision for drilled shaft construction).
- The MIT-Scan2-BT, another dowel bar measurement device which functions similarly to a cover meter (i.e., utilizes the principle of electromagnetic induction to detect eddy currents generated on steel reinforcement).

Three users indicated non-destructive measurement of pavement smoothness as an enforced PBS, but no devices were specified.

DEVICE RATINGS

The survey also collected ratings from the respondents regarding the in-service performance in terms of cost efficiency, time efficiency, and ease of use. For each category, devices were rated on a 3-point scale, with 1 being "would not use again," 2 being "would use again under certain conditions," and 3 being "would use again." As a point of reference, the mean rating of all devices was 2.76/3 for cost efficiency, 2.83/3 for time efficiency, and 2.56/3 for ease of use. The overall mean rating was 2.72/3, which suggests a general sense of satisfaction with the devices being used. Device rating results are shown visually in Figures 4–8, at the end of this section.

Cover meter devices received the highest performance rating, with an average of 2.89/3. Cover meter ratings are shown in Figure 4.

The GPR results are shown in Figure 5. GPR devices received a relatively high average performance rating of 2.88/3. Of the three respondents who specified use of GSSI GPR devices, all three gave the device 3/3 ratings for each of the three categories. No other GPR manufacturers were specified. The MIT Scan2-B2 received low ratings as compared to the GPR, with a 2/3 for both cost efficiency and ease of use, and a 3/3 for time efficiency. The MIT Scan T2 received perfect 3/3 ratings for all three categories.

Surface resistivity meter ratings are shown in Figure 6. The average rating was 2.67/3. Both Proceq Resipod users rated the device 3/3 for all three categories.

UPV ratings are shown in Figure 7. The technology received a relatively low mean rating of 2.25/3. Both MIRA users rated their device 2/3 for all three categories. One respondent explained that a researcher found the analysis software to be not as powerful as expected and the data analysis options to be limited considering the capabilities of the device.

Impact Echo ratings are shown in Figure 8. The technology received an overall rating of 2.75/3. The Olson Engineering Impact Echo user rated their device 3/3 for all three categories.

The only infrared thermography user rated their device 2/3 for all three categories. The cross-hole sonic logging user rated their device 3/3 for all three categories. One user of the Schmidt hammer rated their various devices 2/3 for cost efficiency and 3/3 for time efficiency and ease of use.

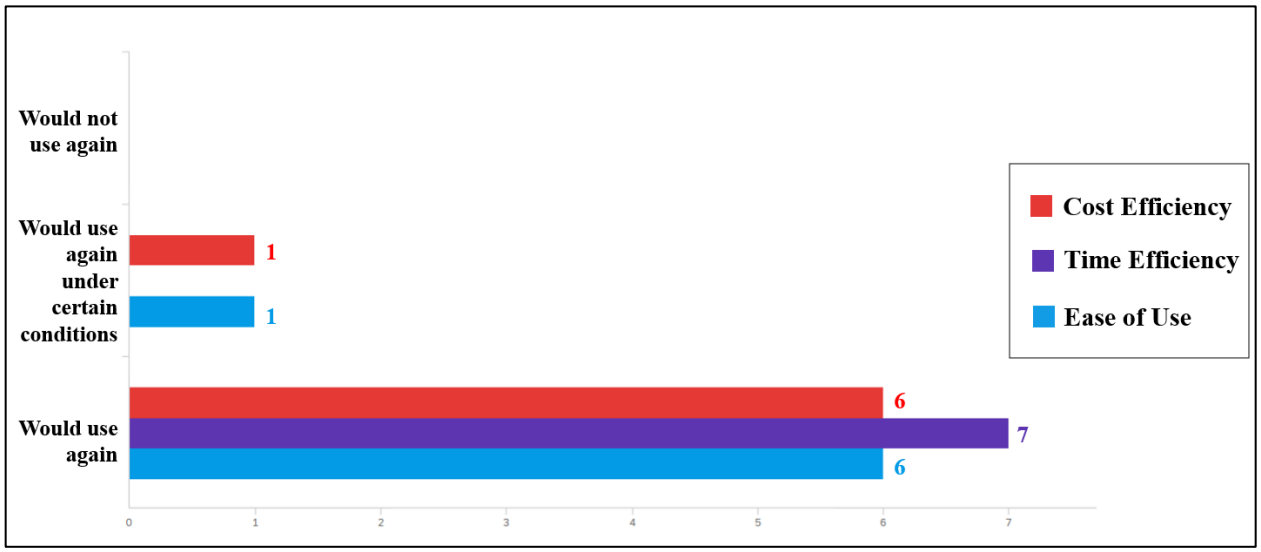

Figure 4. Graph. Cover Meter Performance Ratings

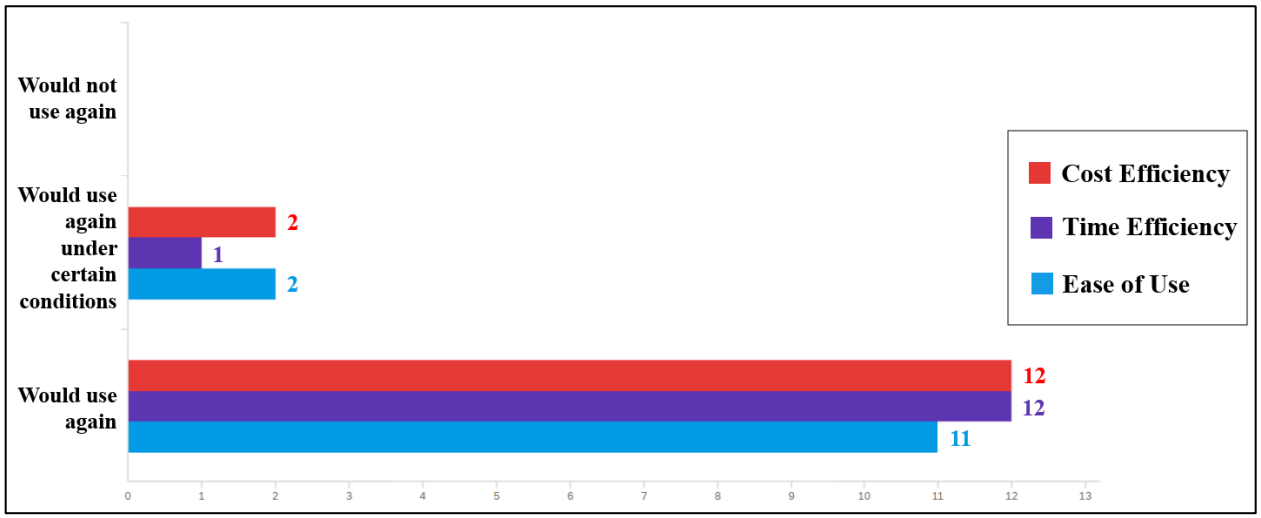

Figure 5. Graph. GPR Performance Ratings

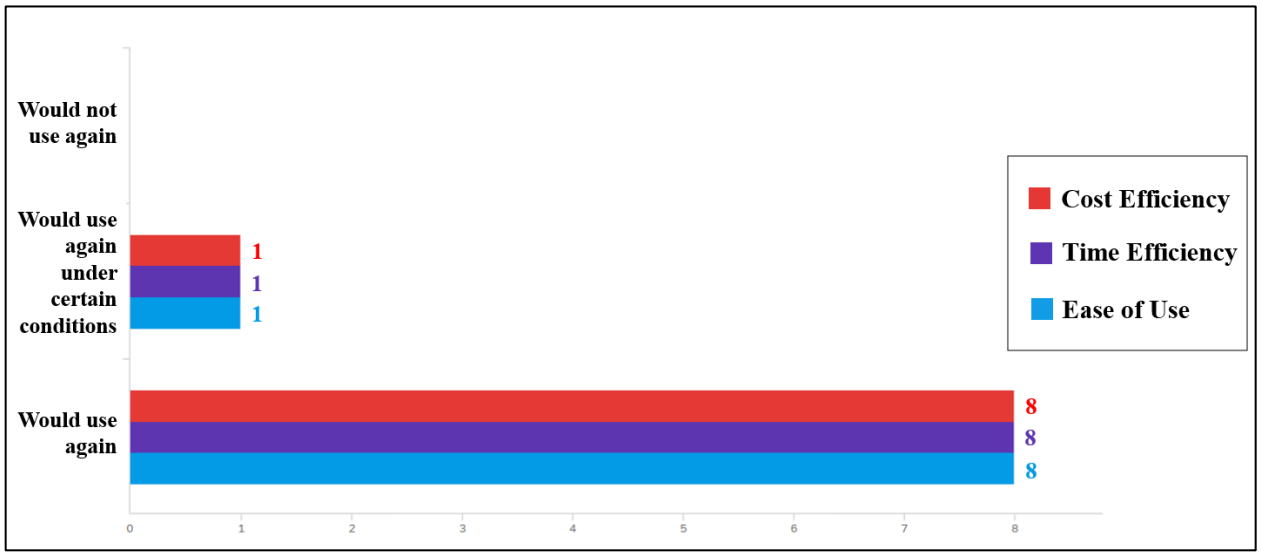

Figure 6. Graph. Concrete (Surface) Resistivity Meter Performance Ratings

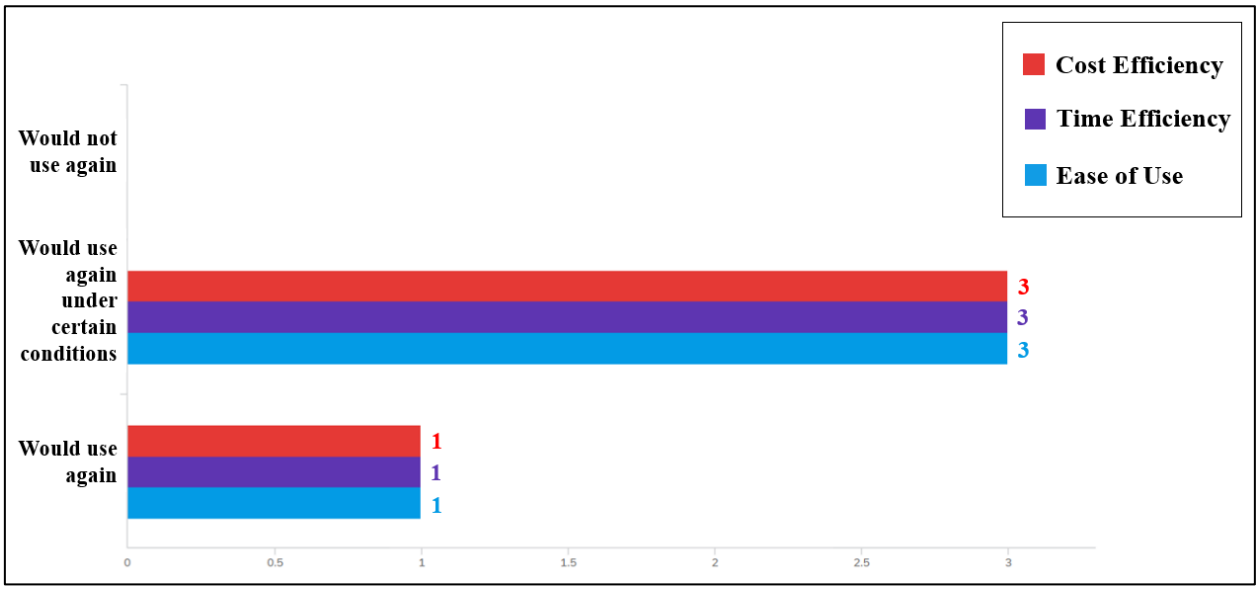

Figure 7. Graph. UPV Performance Ratings

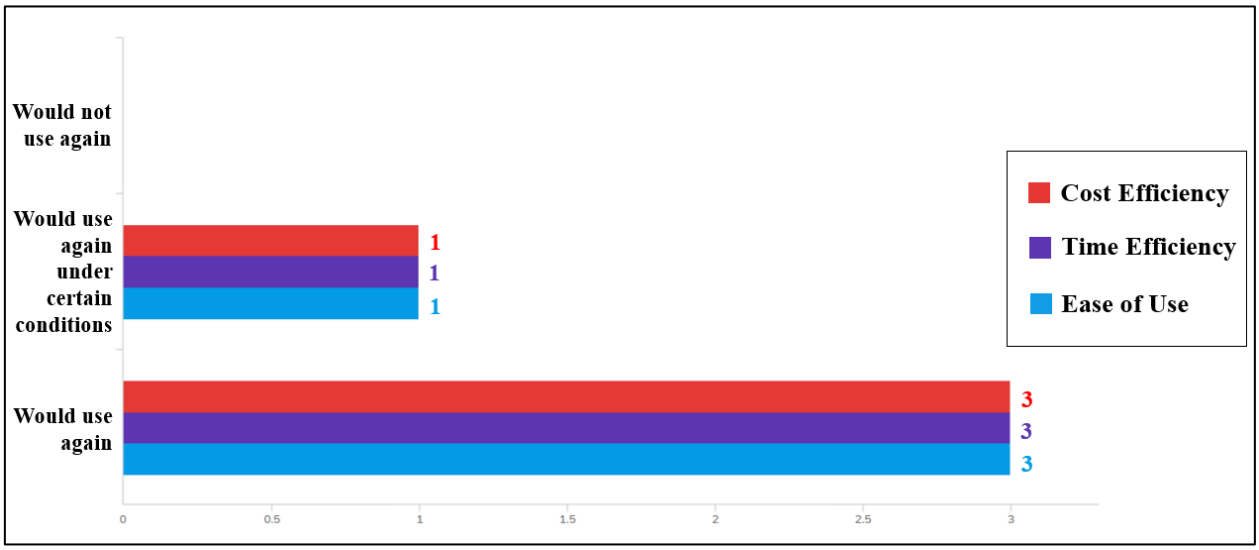

Figure 8. Graph. Impact Echo Performance Ratings

FUTURE IMPLEMENTATION OF NDT TECHNOLOGIES

The survey also collected data regarding any additional NDT technologies which agencies were considering. The responses made the Georgia Tech team aware of emerging NDT technologies and

gave a general sense of their perception. Overall, the results show a growing popularity for surface resistivity and the maturity method.

- Three respondents reported considering surface resistivity meters.
- Two respondents reported considering the maturity method, which involves real-time estimation of concrete strength by monitoring embedded temperature sensors.
- The Tennessee DOT is currently joining Transportation Pooled Fund Project 1499 for real-time strength monitoring and is considering both MIT scan devices.
- The Colorado DOT is considering implementation of the super air meter, a device which is able to provide information on air void size in fresh concrete as well as total air content, allowing a better prediction of concrete freeze thaw durability (Ley 2014).
- The Missouri DOT is considering thermal imaging for asphalt pavements.
- The Illinois DOT is considering the measurement of shrinkage for bridge deck concrete, but has yet to decide on a test method.

DISCUSSIONS

The survey results for NDT usage suggest that while the technologies are commonly used for inspection and forensic applications, a lack of confidence exists for their usage to enforce PBS. Despite the reported apprehension, lack of equipment reliability was the second least common barrier to implementation of NDT technologies. Furthermore, the device ratings suggested a general sense of satisfaction for the technologies in use. Most NDT users expressed confidence in device performance under certain conditions. Given these results, there is an opportunity for further implementation of NDT technologies for quality assurance applications. The results for future

considerations indicate a movement towards further implementation of PBS and NDT technologies for their enforcement.

CHAPTER 3. LITERATURE REVIEW

GROUND PENETRATING RADAR

Overview

Short pulse radar, more commonly known as ground penetrating radar (GPR), is an electromagnetic (EM) wave-based NDT technology. The technique works similarly to radar technologies used in other industries, most notably the geotechnical industry, and began to be implemented for the inspection of concrete infrastructure in the early 1900s (Stain 1919). By transmitting electromagnetic waves with frequencies typically between and receiving their reflections, the devices can detect and locate subsurface objects. Devices typically display results with the horizontal scan distance on the x axis, and depth (calculated from the measured two-way transit time and determined wave velocity) on the y axis. Signal strength expressed with changes in hue or value, depending on the device and selected viewing settings. The procedure is standardized by ASTM D4748-10, ASTM D6087-08, and AASHTO R 37-04.

EM waves are transmitted into the concrete's surface, and travel through the material at a velocity given by equation 1:

$$V = \frac{C}{\sqrt{\epsilon}} \quad (1)$$

where C = the speed of light in a vacuum, and ϵ = the concrete's dielectric constant. A material's dielectric constant, also known as relative permittivity, is defined as the ratio between its permittivity

and the permittivity of a vacuum. A material's permittivity reflects its ability to become polarized in the presence of an electromagnetic field.

Each time an EM wave passes through a material interface that is greater than about half of the wavelength (ACI 228 2R-13), part of the wave is reflected, and the rest of the wave is transmitted through the material. Wave frequencies are typically between 500 MHz and 2.5 GHz (Maierhofer 2003). The magnitude of the reflected wave, R, is dependent on the dielectric constants (the ratio between the electric permittivity of a material and the electric permittivity of a vacuum) of the two materials and is given in Equation 2

$$R = I \times \frac{\sqrt{\varepsilon_c} - \sqrt{\varepsilon_2}}{\sqrt{\varepsilon_c} + \sqrt{\varepsilon_2}} \quad (2)$$

where I = initial wave amplitude, ε_c = concrete dielectric constant of first material, and ε_2 = dielectric constant of second material. A list of dielectric constants for common civil engineering materials is given in Table 1. When the second material has a higher dielectric constant, the reflection coefficient is negative, indicating a change in polarity.

Table 1. Material Dielectric Constants From (ASTM D 4748-10)

Material	Concrete	Air	Water	Asphalt	Granite	Gravel
ε	4-10	1	81	2-4	5-8	4-8

Steel has an infinite dielectric constant, therefore 100% of the wave is reflected at concrete-steel interfaces. This makes GPR an excellent means for measuring reinforcing steel. Reflections are also produced at concrete-air interfaces allowing for the detection of voids and delaminations with the measurement of rebar. Voids and delaminations greater than about half of the wavelength can be

detected. Weak reflections are to be expected from concrete-gravel interfaces, which limits the technology's ability to measure pavement thickness.

The work done in (Soutsos 2001) shows that while changes in concrete composition can affect the dielectric constant (referred to as relative permittivity in the paper), the moisture content has a much greater influence. In the study, the dielectric constants of a wide range of concrete specimens (ordinary portland cement, concrete with pulverized fly ash, concrete with ground granulated blast furnace slag, and high strength concrete) were measured at different levels of saturation with an electromagnetic wave frequency of 500 MHz. The results are shown in Figure 9.

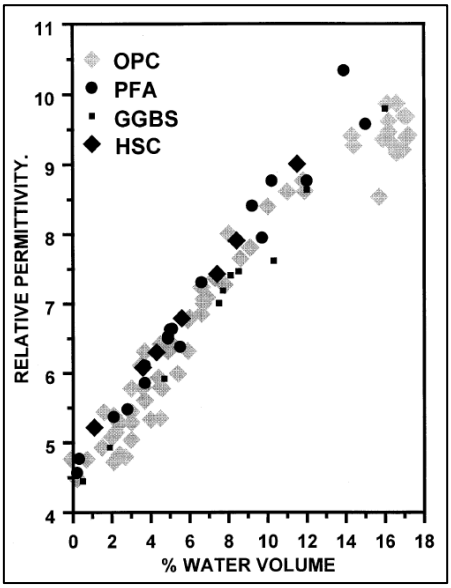

Figure 9. Graph. From (Soutsos 2001), the Relationship Between Concrete's Dielectric Constant and Moisture Content

The strong correlation between the concrete dielectric constant and moisture content can be utilized to estimate the moisture content in the concrete cover (Koyan 2018). This may be of interest for ensuring sufficient moisture during curing or assessing the potential for rebar corrosion.

Most commercially available GPR devices use a hyperbolic fitting to allow the user to estimate the EM wave speed (and thereby the concrete dielectric constant). As the device approaches a rebar, part of the transmitted EM wave diffuses and reflection from the rebar is measured. The two-way EM wave transit time increases as the device approaches the object. The square distance between the device and object is given by the Pythagorean Theorem, which results in the depth/transit time forming a hyperbolic curve with respect to distance along the line scan.

The precision associated with the hyperbolic fitting is most affected by the operator's ability to distinguish the hyperbolic curve. As the ratio between the amplitude of the reflected wave and the amount of noise (reflected waves that are not of interest) increases, the hyperbolic curve becomes more distinguished. In general, the best results will be achieved with dry concrete, short cover depths, and uncongested areas. When necessary, cores can be taken to confirm the EM wave velocity.

Without velocity calibration needed, GPR can reliably measure the horizontal spacing between rebar and the relative depth of rebar. The measurement of relative rebar depth can be useful for the identification of potential coring locations. Once cores are taken, the EM wave velocity can be calculated and applied to the rest of the rebar. A cover survey of 103 bridges in Georgia (Emmenegger 2020) found that variations in cover depth within a bridge deck is much more common than a constant bias from the design cover.

EM Wave Attenuation

The amplitude of an EM wave over distance and time can be determined by the general solution to the wave equation, given in Equation 3 (Neto 2006)

$$A(x,t) = A_o \times e^{-\alpha x} \times e^{i\omega(t-x/v)} \quad (3)$$

where, A_o is the wave's initial amplitude, α is the attenuation coefficient, x is distance, t is time, i is the imaginary unit, ω is the angular frequency, and v is the phase velocity. The attenuation coefficient is known to increase with moisture content due to increased conductivity (Garcia 2008). For this reason, GPR can be less effective when measurements are taken on early age concretes with high moisture content. The attenuation coefficient is also known to increase in the presence of chloride ions and can be used to determine the potential for rebar corrosion (Senin 2016) although most commercially available concrete GPR devices do not automatically quantify attenuation. Depending on the device, GPR measurements can be taken for depths up to 20 inches (Maierhofer 2003). With sufficient horizontal rebar spacing, GPR devices can measure multiple layers of reinforcement.

Commercially Available Devices

According to the AASHTO CoMP survey results, GSSI was the most used GPR manufacturer. All GSSI users rated their devices 3/3 for ease of use, time efficiency and cost efficiency. The GSSI StructureScan Pro can be used with a four-wheel cart for large surfaces, or a smaller device with one wheel for small or curved surfaces (i.e., bridge piers). The device can be used with a 1.6 GHz antenna (0.85 inch resolution for a dielectric constant of 7) or a 2.6 GHz antenna (1.39 inch resolution for a dielectric constant of 7). The device can take measurements up to 18 inches.

The Proceq GPR devices are distinguished by their use of stepped frequency continuous waves (SFCW). The wave frequency is varied as measurements are being taken, removing the need for the operator to select the appropriate antenna for the desired penetration depth and resolution. The downside of SFCW is that frequencies are produced which are not necessarily needed. The Proceq GP 8000 produces frequencies from 0.2 GHz to 4.0 GHz and has four wheels. The device can take measurements up to 31.5 inches deep. The GP 8800 is a smaller device with two wheels and produces frequencies from 0.4 GHz to 6 GHz. The device can take measurements up to 25 inches deep.

Rather than using a hyperbolic fitting, the Hilti PS 1000 X-Scan renders an image of the detected rebar and the user selects the dielectric constant that produces the most circular rebar cross section. By observing manufacturer demonstrations at the World of Concrete Conference, the Georgia Tech Team has determined that this procedure is less precise than the hyperbolic fitting.

The Sensoft NOGGIN GPR device is available in a number of configurations that may be more practical for the scanning of large areas including but not limited to a handheld cart (SmartCart) and a trailer attachment (SmartChariot).

The Georgia Tech team recommends the Proceq GP 8000 or the GP 8800 when the device will be used for a wide variety of applications, or if simultaneous rebar and bridge deck depth measurements are desired. If similar measurements will be taken repeatedly, the Georgia Tech team recommends the GSSI StructureScan Pro.

COVER METER

Overview

Concrete cover meters are eddy current based devices used for the measurement of rebar depth, spacing and diameter. An alternating current flows through a coil in the device, inducing an alternating magnetic field along the longitudinal axis. The changing magnetic field induces eddy currents on nearby electrically conductive objects which are detected as changes in the measured current in a second coil in the device. A diagram of the cover meter measurement principle is shown in Figure 10.

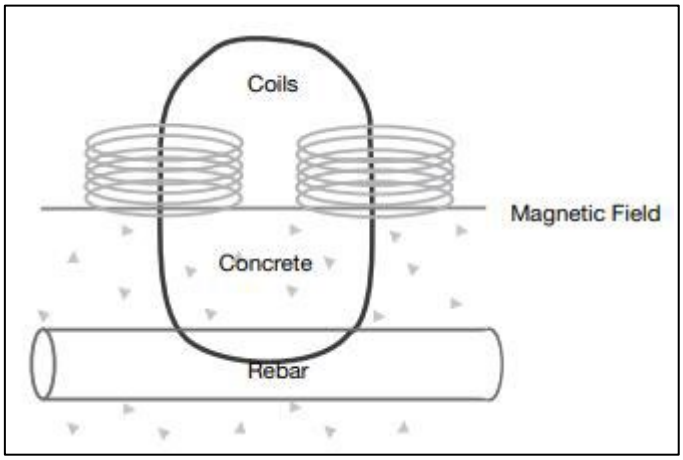

Figure 10. Diagram. Cover Meter Measurement Principle From (Proceq 2017)

Both concrete and air are unable to become magnetized and have low electrical conductivities. Therefore, unlike GPR measurements, cover meter measurements are uninfluenced by concrete-air interfaces and can take measurements when closer to the member's edge.

Rebar diameters can be measured by producing variations in the distance between the coil and the concrete surface. This is typically done by adding spacing blocks of known thicknesses beneath the

device. Cover meters are less sensitive to changes in diameter than cover depth. The signal strength can be related to cover depth by an inverse fourth power law and is known to increase approximately linearly with bar diameter (Alldred 1993).

Limitations

Eddy currents can be produced on any steel within the cover meter sphere of influence (about 8 inches (Proceq 2017) and hurt the measurement accuracy. Some devices provide corrections for rebar parallel to the rebar of interest (Proceq 2017). Most commercial cover meters have coils positioned such that the primary magnetic field is strongest along a plane parallel to the rebar's axis to minimize the effect of eddy currents produced on nearby perpendicular reinforcement. In a study of various factors affecting the accuracy of cover meters (Barnes 2008), it was found that for a 2.36 inch cover, the effect of taking a scan on top of a perpendicular rebar was a 0.0637 inch decrease in the measured cover when the top layer of rebar was being measured. Devices are unable to correct for steel beneath the rebar (e.g., rebar chairs, additional layers of steel), and cannot make measurements on multiple layers of parallel rebar unless there is a large offset.

Fluctuations in temperature causes changes in the electrical resistivity of the device components and can lead to a bias in cover measurements. Some devices account for temperature fluctuations through recalibration (Proceq 2017), while others contain embedded temperature sensors (James Instruments 2018).

Commercially Available Devices

- The Proceq Profometer 650 has three measurement modes: a normal mode, a spot mode for areas with a high concentration of steel, and a large mode for covers up to 7 inches. The device can automatically make corrections for closely spaced parallel rebar. Rebar diameter measurements can be taken for cover depths up to 2.5 inches.
- The James Instruments Rebarscope has two measurement modes: a short mode and a deep mode for covers up to 8 inches.
- The Elcometer Model 331 has interchangeable search heads including a standard search head, a narrow pitch search head, a deep cover search head, and a search head specifically calibrated for high tensile and stainless steel rebar with higher conductivities. The need for multiple search heads may be inconvenient, but it may allow for more room for coil arrangements, thereby improving the device accuracies.

The AASHTO CoMP survey results indicate that it is common practice to use multiple cover meter devices due to the differences in performance depending on application.

ELECTRICAL RESISTIVITY AND FORMATION FACTOR

Overview

The electrical resistivity of concrete is commonly measured as an indication of the moisture transport properties (i.e., diffusivity, permeability, and sorptivity), and is used to assess the resistance to a variety of moisture-dependent durability factors, including the initiation of rebar corrosion, alkali-silica reactions (ASR), freeze-thaw degradation, and sulfate attack. After the initiation of corrosion, the resistivity can also be related to the rate of corrosion, as it influences the

ability of ions to travel from anodic to cathodic sites on the rebar. The electrical resistivity of a material, ρ, is defined in equation 4,

$$\rho = \frac{RA}{l} \quad (4)$$

where R = the resistance of a material to an electrical current passed through it, A = cross-sectional area of the material, and l = path length of the current through the material. AASHTO T 358-17 includes a table relating concrete resistivity to chloride ion penetration, shown in Table 2.

Table 2. Relationship Between Concrete Resistivity and Chloride Ion Penetration (from AASHTO T 358-17)

Chloride Ion Penetration	Surface Resistivity Test	
	100-by-200-mm (4-by-8-in.) Cylinder (kΩ-cm) a = 1.5	150-by-300-mm (6-by-12-in.) Cylinder (kΩ-cm) a = 1.5
High	<12	<9.5
Moderate	12–21	9.5–16.5
Low	21–37	16.5–29
Very low	37–254	29–199
Negligible	>254	>199

a = Wenner probe tip spacing

The first widespread method of measuring concrete resistivity, known as the rapid chloride permeability test, was developed in the early 1980s (Whiting, 1981) and is now standardized in ASTM C 1202 and AASHTO T 277. The test involves placing electrodes on either side of a concrete specimen and measuring the total charge (the integral of current with respect to time) passed through the specimen when subjected to a given voltage. The results are often expressed as

charge passed, but the resistivity can also be calculated by substituting the voltage divided by the current for electrical resistance in Equation 4.

More recently, the measurement of surface resistivity has gained popularity due to the ease and speed of the measurement procedure relative to bulk resistivity measurements. The surface resistivity measurement procedure is standardized by AASHTO T 358-17. Devices include four electrodes spaced evenly along a line: two outer electrodes generate alternating currents and two inner electrodes measure voltage. The results have been found to be uninfluenced by changes in current frequency (ACI 228-2R-13, Morris, 1996). Currents produced by the Proceq Resipod surface resistivity meter are known to penetrate approximately 3.5 inches into the concrete, an appropriate depth for assessing corrosion resistance as well as other durability concerns. Surface resistivity results have been found to correlate well with bulk resistivity results for a variety of concrete mixtures (Ghosh, 2015), which is unsurprising considering the theoretical similarities between the two methods. Combined with a change point detection analysis, surface resistivity has the potential to be used for the acceptance of supplementary cementitious materials (SCMs) when the materials used and mixture proportions are held constant (Rios, 2021).

Formation Factor

While electrical resistivity has been shown to correlate well with the measurement of chloride penetration (AASHTO T 259) within individual studies, the relationships differ between studies and for specimen with large differences in mix design (McDonald, 1994). This is in part due to the dependence of the concrete resistivity on the pore solution conductivity, which is influenced by the material cement composition, use of admixtures and SCMs, mixture proportions, and concrete age

(Weiss, 2018). However, the pore solution conductivity, is not a good predictor of concrete transport properties. To account for differences in pore solution chemistry, the formation factor, *F*, described in (Weiss, 2018), is calculated with Equation 5

$$F = \frac{\rho}{\rho_o} \tag{5}$$

where ρ_o = pore solution resistivity. Because of its independence from the pore solution conductivity, the formation factor is inversely proportional to the product of the concrete porosity and pore connectivity. The formation factor has been shown to correlate well with experimental water absorption results (Moradllo, 2018). Concretes with high formation factors have also been shown to be less susceptible to ASR degradation (Chopperla, 2022).

In addition, the formation factor can be related to the diffusion coefficient of the concrete and then used to predict the initiation of corrosion by applying the Nernst-Einstein relationship given in Equation 6

$$\frac{C_x - C_o}{C_s - C_o} = 1 - \text{erf}\left[\frac{x}{2\sqrt{\frac{D_o}{F} \times t}}\right] \tag{6}$$

where *t* = time, C_x= chloride concentration at depth x, C_o= original chloride concentration, C_s = chloride concentration at the concrete surface, and D_o = chloride ion self-diffusion coefficient (2.19 x 10^{-8} square feet per second) (Weiss, 2018). Corrosion initiates when C_x exceeds the chloride concentration threshold.

Limitations

As discussed previously, while the pore solution conductivity of concrete is known to affect the measurement results, it can be accounted for with calculation of the formation factor. Concrete moisture content, degree of cement hydration, and ambient temperature during testing have all been found to have a significant influence on concrete resistivity (Weiss, 2016), which for the most part limits the measurement to laboratory applications. Concrete age was also found to be an important factor in an internal GDOT study (Collins, 2019). In situ measurements can still be used as a relative measure of concretes moisture properties.

Manufacturer Comparisons

The Georgia Tech team recommends surface resistivity measurements over bulk resistivity measurements because of the speed and ease of the test method. A comparison between two commercially available surface resistivity meters is given in Table 3. For a given category, green cells are used to indicate the superiority of a device with a brighter shade indicating a more significant difference in properties. Yellow is used to indicate neutrality.

Table 3. Surface Resistivity Device Comparisons

Device	Operating Temperature	Accuracy	Price	Resistivity Range
Proceq Resipod	32 - 122 F	12 - 16 kΩcm (± 0.2 or 1%) 90 - 120 kΩcm (± 0.3 or 2%) >100 kΩcm (± 2 or 5%)	$4,470	0 to 1000 kΩcm
Giatech SURF	59 – 113 F	< 100 kΩcm (± 0.1 or 1%) > 100 kΩcm (± 1 or 1%)	$5,500	0.1 to 1000 kΩcm

The Giatech SURF device has slightly superior specified accuracies than the Proceq Resipod; however, the operating temperature ranges is most significant difference between the devices. The temperature range, as well as the physical geometry of the Giatech SURF device, limits the use of the device to the testing of concrete cylinders in a laboratory environment. As mentioned in the limitations section, measurements in the field cannot be reliably used to compare concrete mixtures, but the flexibility of the Proceq Resipod device gives it the potential to be used in the field as a relative measure for a given concrete mixture if all measurements are taken within a single day.

It should also be noted that Sensytec manufactures an embedded Bluetooth sensor called SensyRoc that measures electrical resistivity and temperature for the implementation of the maturity method. While the sensor could provide a useful metric for the monitoring the development of transport properties as the concrete cures, prior correlations would have to be conducted because of the previously mentioned limitations. Without correlations, large differences in electrical resistivity measurements could be an indication of significant changes in concrete quality.

ULTRASONIC PULSE VELOCITY

Overview

Ultrasonic pulse velocity is a common NDT technique that involves the transmitting and receiving of stress waves. The majority of devices perform what is colloquially known as pitch-catch measurements where a vibration produced by one piezoelectric transducer propagates through the concrete as a longitudinal wave (P-wave) and is received by a second transducer placed elsewhere on the concrete. Pulse-echo devices involve the transmission and detection of stress waves from a single transducer. The P-wave travels through the concrete at a speed determined by Equation 7

$$V_p = \sqrt{\frac{E(1-v)}{\rho(1+v)(1-2v)}} \quad (7)$$

where Vp = P-wave velocity through concrete, E = concrete dynamic modulus of elasticity, ρ = concrete density, and v = concrete Poisson's ratio. Measurements can be taken in direct transmission, indirect transmission, or semi-direct transmission, with the three measurement orientations defined in Figure 9.

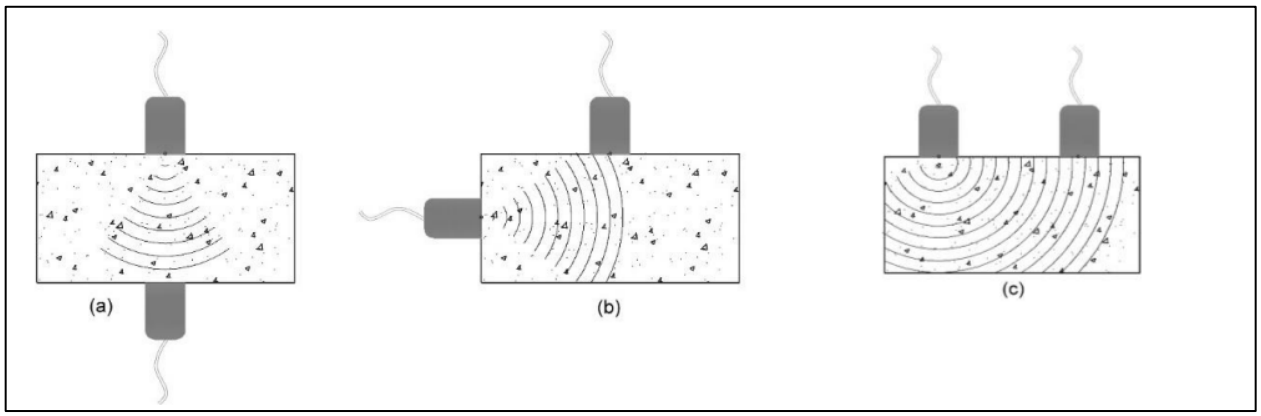

Figure 11. Diagram. DUPV Diagram From (Ndagi 2019) (a) Direct Transmission Measurement (b) Semi-Direct Transmission Measurement (c) Indirect Transmission Measurement

Detection of Voids and Defects

At material interfaces larger than a half of a wavelength with significant differences in acoustic impedances, a portion of the stress wave is reflected, while the rest transmits through. The reflection coefficient, R, is given in Equation 8

$$R = \frac{Z_2 - Z_1}{Z_2 + Z_1} \quad (8)$$

where Z_2 = acoustic impedance of material 2, and Z_1 = acoustic impedance of material 1 (concrete). A list of acoustic impedances for common civil engineering materials is given in Table 2. By comparing this table with the table of dielectric constants in the UPV section (Table 1), it can be

seen that stronger reflections are produced at concrete-air interfaces for stress waves than for EM waves. For concrete-steel interfaces, however, much weaker reflections are produced for stress waves than for EM waves. It is for this reason that stress-wave-based NDT techniques are in general more effective than GPR for the detection of voids and defects, but less effective for the measurement of reinforcing steel.

Table 3. Acoustic impedances and Reflection Coefficients From (Carino 2015)

Material	Specific acoustic impedance, kg/(m^2 s)	Reflection coefficient at interface
Air	412	-1.00
Water	1.48 x 10^6	-0.65 to -0.75
Soil	0.3 to 4 x 10^6	-0.3 to -0.9
Concrete	7 to 10 x 10^6	
Steel	47 x 10^6	0.65 to 0.75

For pulse-echo and indirect transmission measurements, the reflections produced at material interfaces can be measured directly. For pitch-catch UPV measurements taken in direct transmission, a diffused portion of the wave can travel around small voids and be detected, in which case the voids can be detected as decreases in apparent wave velocity. Significant defects smaller than a half wavelength, such as small voids, cracking, and honeycombing can also be detected as decreases in apparent wave velocity. Stress wave attenuation is known to be more sensitive to microcracking than P-wave velocity (Khanal 2020), but its quantification is difficult due to the dependence of wave amplitude on the pressure applied to transducers.

The depth of a surface crack can be calculated using the technique outlined in (Bungey 2006). Two measurements are taken with the transducers on either side of the crack, with the distance from the

crack varied. After being transmitted, the stress wave diffracts when it reaches crack's tip, and the diffracted wave is received by the second transducer. A form of the equation from (Bungey 2006) is generalized for arbitrary transducer distances in Equation 9

$$h = \frac{1}{2} \times \sqrt{\frac{x_2{}^2 t_1{}^2 - x_1{}^2 t_2{}^2}{t_2{}^2 - t_1{}^2}} \quad (9)$$

where h = crack depth, x_1 = first distance from transducer to crack, x_2 = second distance from transducer to crack, t_1 = first transit time, and t_2 = second transit time. A visual depiction of the crack depth measurement procedure is shown in Figure 12.

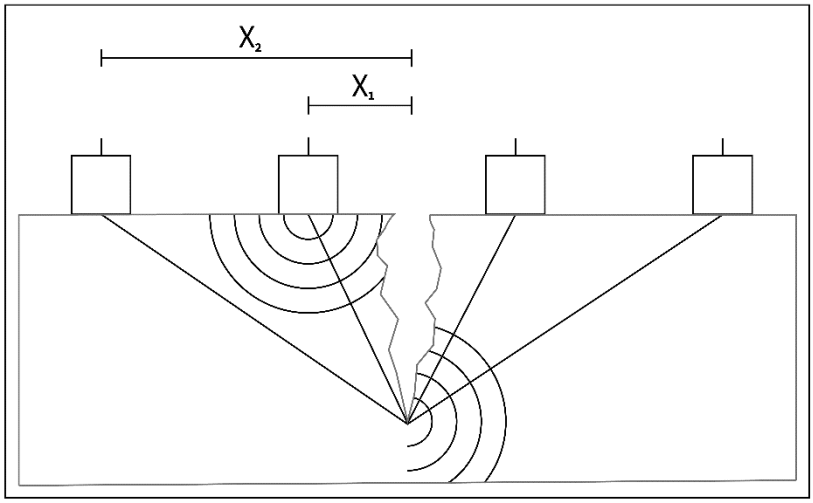

Figure 12. Illustration. UPV Crack Depth Measurement Procedure

The Effect of Rebar

Due to the increased velocity of stress waves in steel, an increase in UPV measurements is found when rebar lies along the stress wave path length. The effect is greatest when the rebar is running parallel to the stress wave path. In general, the speed of the stress wave in the presence of rebar is difficult to predict and depends on the stress wave velocity through the concrete as well as the quality of the concrete–steel bond. The work done in (Saleem 2017) utilizes this fact to access the

quality of the concrete-steel bond. Taking UPV measurements nearby rebar should be avoided, but this is not always possible. A methodology for accounting for the presence of rebar was outlined in a past version of the British Standard (BS 1881-203), and updated correction factors are provided in (Fodil 2019).

Compressive Strength Correlations

Although there is no empirical relationship, UPV measurements are commonly used to estimate concrete compressive strengths due to the correlation between the two values. Despite this, there are a number of factors which affect the two values differently including but not limited to concrete paste fraction, aggregate type, moisture content, air content, and concrete age. For these reasons, UPV measurements can only be reliably used for compressive strength estimations as for mixtures for which a correlation has already been developed (as described in ACI 228-1R-19), or as a relative measure for a given in-situ concrete mixture.

Ultrasonic SAFT Devices

More contemporary UPV devices contain arrays of dry point contact transducers which transmit and receive ultrasonic shear waves. Signals are processed using the synthetic aperture focusing technique (SAFT) to generate 2D contour plots. Because the offset between transducers is known, the S-wave velocity can be determined without calibration. The result are devices which are able to quickly take measurements without coupling and can accurately detect defects and measure member depth. A detailed report on the Germann Instruments MIRA device was published by the Illinois DOT (Popovic 2017).

Commercially Available Devices

Several manufacturers produce typical pitch-catch UPV devices with similar performances. These devices include the Olson UPV device, the Proceq Pundit 200, and the James Instruments VuCon. Controls Group produces another pitch-catch UPV device, the 58-E4800 UPV tester, which automatically calculates the wave attenuation. The Germann Instruments MIRA device and the Proceq PD8000 are two commercially available ultrasonic shear wave tomography devices. The Proceq PD8000 can take measurements at greater depths (up to 6.6 ft) than the MIRA device (up to 2.58 ft). The Georgia Tech Team recommends the Proceq PD8000 device.

IMPACT ECHO

Overview

Impact echo is another stress-wave based NDT technique which is commonly used for the measurement of concrete thickness and the detection of defects such as voids, delaminations, and honeycombing. The technique is standardized by ACI 228.2R-13 and ASTM C-1383-15. Unlike the UPV technique, the longitudinal stress wave velocity (P-wave) can be estimated through the measurement of the surface wave (S-wave) velocity. The surface of the concrete is impacted nearby two transducers with a known spacing, and the difference between recorded transit times is used to calculate the S-wave speed. The P-wave velocity can then be estimated by assuming a Poisson's ratio of 0.2, for which the ratio between the S-wave and P-wave velocities is 0.61 (Malhotra 2003).

During testing, an impact on the concrete's surface produces a high-energy, low-frequency (5–40 kHz) (Khanal 2020), transient stress wave and the reflections are recorded with transducers. The size of impactor is inversely proportional to the maximum waveform frequency. Lower frequency

waves will result in lower resolutions and greater penetration depths. Due to the lower frequencies, the technique has a lower resolution but greater penetration depth than the UPV technique. The large penetration depth allows the technique to be commonly used for the quality assurance of piles. At each material interface with significant differences in acoustic impedances, reflections are produced. The same reflection coefficients discussed in the UPV section apply to the Impact Echo technique.

For a thin, plate like structure—defined in ASTM C1383-15 as having a width at least 5 times its depth—a fast Fourier Transform (FFT) can be performed allowing the operator to see the responses in frequency space, and the peak frequency is typically the rebounding of the wave from a void or the bottom and top half of the slab. The velocity, along with the peak frequency from the concrete's opposite surface, can then be used to calculate the depth to the reflection, D, can be calculated with Equation 10:

$$D = \frac{V_p}{2f} \tag{10}$$

where V_p = stress wave velocity through the concrete plate, and f = frequency. A visual depiction of the technique is shown in Figure 10.

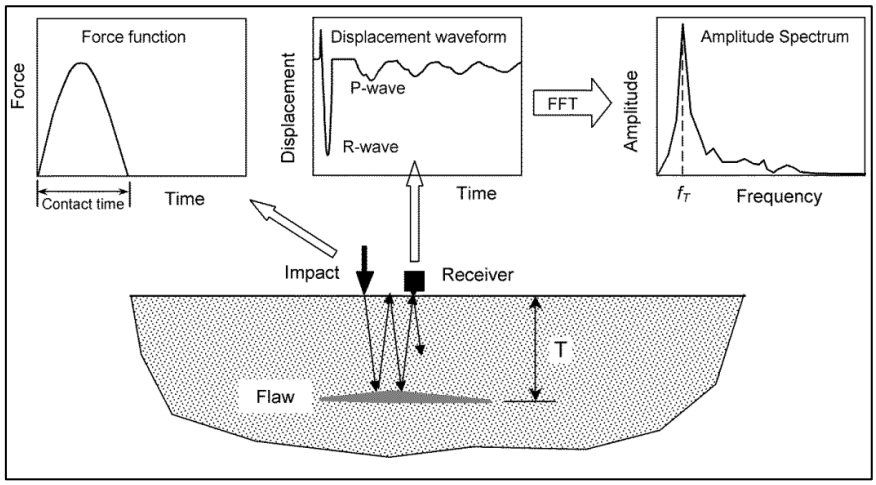

Figure 13. Diagram. Impact Echo Diagram From (Carino 2015)

The range of detectable flaw sizes is depicted in Figure 11. As with the UPV technique, flaws must be at least half the wavelength to produce reflections. Smaller but significant defects, such as small voids and honeycombing, may be detected as decreases in the measured thickness due to decreases in the apparent wave velocity. The depth of surface cracks can also be measured using a procedure similar to the one described in the UPV section.

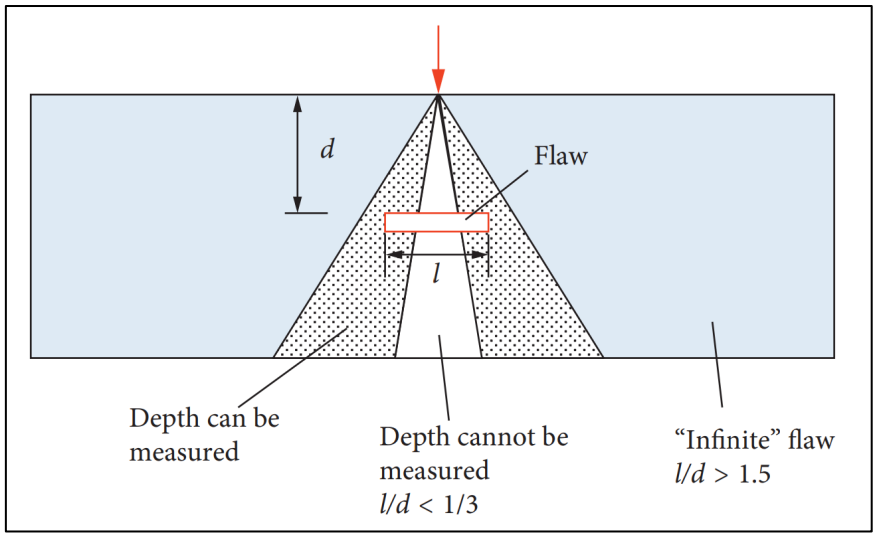

Figure 14. Diagram. Range of Detectable Flaw Sizes For Impact Echo From (Liu 2019)

Limitations

The wave speed calibration can result in error when the Poisson's ratio of the concrete varies from the assumed value, or when there are differences in concrete stiffness or density at the concrete's surface. The cumulative error between the determination of wave speed and the peak frequency increases with depth (ASTM C1383-15).

Commercially Available Devices

The James Instruments VuCon and Germann Instruments DOCter are both typical impact echo devices. Germann Instruments also offers the MIRADOR software for use with the DOCter which allows for the automatic generation of 2D contour plots. The FprimeC Impact device also automatically generates 2D contour plots, although it does not appear to allow for P-wave speed determination using the S-wave measurements. Similarly, the Olson CTG-2 impact device and the Proceq PI8000 require knowledge of the concrete P-wave speed or calibration with an 8 inch × 12 inch cylinder, which either requires coring, or is likely to lead to errors due to differences in curing conditions. The Georgia Tech team recommends the Germann Instruments impact echo device. The James Instruments VuCon device should be just as effective but has less sophisticated data processing software which would significantly increase the amount of time required for data processing.

OTHER TECHNOLOGIES

Maturity Method

The maturity method is a technique that uses the measurement of concrete temperature over time to estimate concrete compressive strength. Relationships between the temperature and concrete

strength are determined for a specific concrete mixture with cylinders which can either be prepared in a laboratory or cast in the field with an embedded sensor. Once the relationship has been developed, temperature sensors embedded in the field concrete can be remotely monitored for the estimation of compressive strength. The maturity method is standardized by ASTM C 1074 – 17 and ACI 228.1R-19

Several temperature sensors specifically designed for the maturity method are commercially available.

- The Giatec SmartRock sensors have the capability for dual-temperature monitoring, which as well as estimating the strength development at two depths, can be used to monitor temperature differentials for shrinkage cracking.
- As discussed in the electrical resistivity section, the Sensytec SensyRoc measures electrical resistivity as well as temperature.
- Nex ConCure manufacturers temperature sensors which are inserted through a thin embedded plastic tube and can be reused. While this provides an economical option, the embedment of the tube could negatively affect the concrete durability.

Infrared Thermography

Infrared Thermography (IT) is an NDT technique which involves the measurement of thermal radiation from the concrete surface. Sound concrete has a higher thermal conductivity than delaminations or voids, and therefore large delaminations and voids that are close to the concrete surface can be detected as areas of high or low radiation when the concrete is heating or cooling. IT

cameras are commonly mounted on vehicles for the rapid assessment of pavements and bridge decks and tunnels.

CHAPTER 4. VALIDATION TESTING

METHODOLOGY

Samples Overview

Five sets of samples were used in the validation testing program. A set of nineteen 4 inch × 8 inch cylinders, cast in a previous Georgia Tech research project to represent typical concrete pavement mixtures, were used to study the factors which affect the relationship between UPV measurements and compressive strength. Samples with a variety of water-to-cement ratios were selected to produce a range of compressive strengths. Samples with a variety of paste fractions and coarse aggregate sizes were selected because of the known effects of the parameters on the UPV measurements through changes in concrete density and stiffness, and their known effects on the concrete compressive strength through changes in cement content and the size of the aggregate-cement paste interfacial transition zone (ITZ). Samples with a variety of air contents were selected. This is a concrete property for which is difficult to achieve consistency, which causes changes in UPV readings through changes in density and is known to decrease the concrete's compressive strength. The cylinders are designated C01–C19. Sample mix designs are given in Table 18 in Appendix C.

A set of two reinforced concrete slabs and two reinforced concrete beams, also cast for a previous Georgia Tech course (Kurtis 2013), were used for the measurement of rebar and the detection of

various embedded artificial voids and defects. The samples are referred to as Test Slab 1, Test Slab 2, Test Beam 1, and Test Beam 2. Details on the slab dimensions and embedded objects, along with images of the slabs before casting, are shown in Figures 35–38 in Appendix B. The mix designs and materials used for these samples are unknown.

Five additional samples were designed and cast to test specific capabilities of NDT devices. This set of samples will be referred to as the structures samples. The Alternative Rebar Sample contained carbon steel rebar, epoxy coated rebar, galvanized rebar, and stainless-steel rebar to determine the effect of rebar type on measurement accuracy. The Rebar Size Sample contained various sizes of carbon steel reinforcement to determine the effect of rebar size on cover meter accuracy, although under most conditions the sample had too high of a concentration of steel for accurate measurements to be taken. For both the Alternative Rebar Sample and the Rebar Size Sample, the rebars were cast in a fanned orientation to allow for the determination of cover meter resolution (the minimum distance between reinforcing bars that allows for them to be distinguished). The Dowel Bar Sample was 12 inches deep and included two #11 (11/8 inch diameter) carbon steel dowel bars and two #8 epoxy coated dowel bars embedded 6 inch deep. One of each dowel bar type was intentionally misaligned in both the horizontal and vertical direction. The Bridge Deck Sample contained two layers of #4 and #5 rebar and an embedded galvanized steel stay-in-place (SIP) deck form. The sample was designed to test the ability of the cover meter and GPR to measure multiple layers of rebar and to determine the GPR's ability to measure bridge deck thickness. Sample details and images taken prior to casting are shown in Figures 39–44 in Appendix B. Sample mix designs are given in Appendix C.

Two sets of 4 inch × 8 inch cylinders were cast by the Georgia tech RP 20-19 team to validate the use of surface resistivity measurements for material and mix design acceptance in a laboratory setting. The first set of cylinders used GDOT Class AAA specifications as the basis for the mix designs. Four distinct mix designs were used:

- A control mixture (labelled as PC-AAA)
- A mixture with a 20% weight replacement of portland cement with quartz (labelled as Qz-AAA)
- A mixture with a 8% weight replacement of portland cement with metakaolin (labelled as MK-AAA)
- A mixture with a 20% weight replacement of portland cement with Class F fly ash (labelled as F-AAA).

Three cylinders were cast for each mixture. A second set of cylinders used GDOT Class A specifications as the basis for the mix designs. Four distinct mix designs were used:

- A control mixture (labelled as PC-A)
- A mixture with a 10% weight replacement of portland cement with an impure, uncalcined clay (labelled as Clay-A)
- A mixture with a 20% weight replacement of portland cement with Class F fly ash (labelled as F-A)
- A mixture with a 5% reduction in portland cement content accompanied by an increase in fine aggregate and decrease in coarse aggregate (labelled as RPC-A). Three cylinders were cast for each mixture. Sample mix designs are given in Tables 18 and 19 in Appendix C.

Materials

For all mixtures, the ASTM C150 Type I/II cement (supplied by Argos from a plant in Roberta, Georgia) was used. The cement properties (oxide compositions, fineness, and specific gravity) are given in Table 4.

Table 4. Argos Type I/II Cement Properties

Property	Value for UPV–Fc Cylinders	Value for Surface Resistivity and Structures Samples	Unit
XRF			
SiO2	20.68	19.2	%
Al2O3	4.57	4.5	%
Fe2O3	3.24	3	%
CaO	63.51	62.8	%
MgO	3.09	3.6	%
SO3	2.88	3.1	%
Na2O	0.0875	0.5	%
K2O	0.42	0	%
TiO2	0.22	0.3	%
P2O5	0.066	-	%
ZnO	0.036	-	%
Mn203	0.028	-	%
SrO	0.054	-	%
Cr2O3	0.007	-	%
LOI	1.92	2.6	%
Sum of Conc.	100.78	99.6	%
QXRD Composition			
C3S	52	-	%
C2S	17	-	%
C3A	6	-	%
C4AF	10	-	%
Total Alkali (Na2Oeq)	0.36	-	%
Blaine Fineness	2050	-	ft2/lb
45 microns	95.92	-	%
Limestone	2.315	-	%
Specific Gravity	3.16	3.17	-

A standard natural sand from a quarry in Stockbridge, Georgia (supplied by Vulcan Materials) was used for all mixtures other than the test slabs and beams. The fine aggregate properties and gradation are given in Table 5.

Table 5. Standard Manufactured Sand Properties

Sieve	% Passing
⅜″	100
#4	99.8
#8	80.9
#16	58.3
#30	40.0
#50	21.3
#100	6.7
#200	2.24
Pan	0.00
Specific Gravity (SSD)	2.46
Fineness Modulus	2.53

A crushed granitic gneiss was used as the coarse aggregate for the UPV–compressive strength and surface resistivity samples and was supplied by Vulcan Materials from a quarry in Stockbridge, Georgia. A #67 stone was used for the surface resistivity samples, and #57, #67, and #4 stone was used for the UPV–compressive strength samples. Coarse aggregate properties and gradations are given in Tables 6–8.

Table 6. #57 Crushed Granitic Gneiss Used for UPV–Compressive Strength Samples

Sieve Opening Size	% Passing
1 ½″	100
1″	97.7
¾″	80.3
½″	35.5
⅜″	15.2
#4	1.0
#8	0.5
Pan	0.00
Specific Gravity (Bulk SSD)	2.65

Table 7. #67 Crushed Granitic Gneiss Used for UPV–Compressive Strength and Surface Resistivity Samples

Sieve	% Passing
1″	100
¾″	98.3
½″	56.8
⅜″	30.1
#4	1.5
#8	0.5
Pan	0.00
Specific Gravity (Bulk SSD)	2.65

Table 8. #4 Crushed Granitic Gneiss Used for UPV–Compressive Strength Samples

Sieve	% Passing
2″	100
1 ½″	94.9
1″	35.2
¾″	10.5
½″	3.1
⅜″	1.4
Pan	0.00
Specific Gravity (Bulk SSD)	2.65

A crushed granitic gneiss was used as the coarse aggregate for the structures samples and was supplied by Vulcan Materials from a quarry in Lithia Springs. A #57 stone, #67 stone, and #467 stone were used. Coarse aggregate gradations and specific gravities are given in Table 9.

Table 9. Structural Sample Crushed Granitic Gneiss

Sieve	#67 % Passing	#57 % Passing	#467 % Passing
1 ½″	100	100	100
1″	100	98.3	88.8
¾″	99.5	91.9	57.0
½″	59.7	43.2	31.6
⅜″	32.1	2.4	14.4
#4	3.4	2.4	1.4
#8	0.6	0.5	0.0
Pan	0.0	0.0	0.0
Specific Gravity (Bulk SSD)	2.61	2.61	2.61

For the UPV–compressive strength samples, varying doses of a vinsol-resin based air entraining admixture (Daravair 1000, GCP), were used to achieve and stabilize a range of air contents. A different air entraining admixture (MasterAir AE 200) was used for the structures samples. Varying doses of a polycarboxylate based ASTM C494 Type A/F, ASTM C1017 Type 1 high range water reducing admixture or "superplasticizer" (ADVA 198, GCP) were used for the UPV–compressive strength samples as well as the structure samples. For the surface resistivity sample containing uncalcined clay (Clay-A), a polycarboxylate based superplasticizer (MasterGlenium 7920) was used at 0.5% weight of cementitious solids to improve workability. Admixture densities are given in Table 10.

Table 10. Admixture Information

Admixture	Density	Manufacturer Recommended Dosage Range
Daravair 1000 Air Entraining Admixture	8.5 lbs/gal	0.450–3.05 fl oz / 100 lbs of cement
MasterAir AE 200 Air Entraining Admixture	8.4 lbs/gal	0.125–1.5 fl oz / 100 lbs of cement
ADVA 198 Superplasticizer	9.0 lbs/gal	3.00–5.75 fl oz / 100 lbs of cementitious materials
MasterGlenium 7920	9.0 lbs/gal	—

The properties for the SCMs used for the UPV–compressive strength and surface resistivity samples are given in Table 11. Both fly ashes were sourced from Boral Materials in Catersville, Georgia; the metakaolin was provided by Metamax, BAST in Gordon, Georgia; the quartz filler was sourced from MIN-U-SIL Fin Ground Silica, US Silica in Berkeley Springs, West Virginia; and the impure, uncalcined clay was sourced from Purebase Corporation in Ione, California.

Table 11. SCM Properties

Property	ASTM C618 Class F Fly Ash (UPV-Fc Samples)	ASTM C618 Class F Fly Ash (SR Samples)	Metakaolin (ASTM C618 Class N Pozzolan)	Impure Uncalcined Clay	Quartz	Unit
SiO2	57.19	51.3	52.7	59.7	>99	%
Al2O3	13.19	23.3	44.6	24.0	0.0	%
Fe2O3	4.50	13.3	0.4	2.9	0.0	%
SO3	1.50	0.5	0.0	0.2	0.0	%
CaO	15.01	2.8	0.1	0.2	0.0	%
Na2O	2.12	0.8	0.0	0.8	0.0	%
MgO	3.66	1.0	0.0	0.4	0.0	%
K2O	0.93	2.4	0.1	0.3	0.0	%
P2O5	0.24	-	-	-	-	%
TiO2	0.85	1.3	1.6	1.7	0.0	%
SrO	0.13	-	-	-	-	%
BaO	0.08	-	-	-	-	%
Sum	99.41	96.7	99.5	90.2	>99	%
Moisture	0.038	-	-	-	-	%
Carbon	0.30	-	-	-	-	%
LOI	0.38	2.9	3.5	13.1	3.3	%
D_{10}	-	3.05	1.2	-	1.7	µ
D_{50}	-	15.3	3.63	7.58	8.81	µ
D_{90}	-	58.3	9.88	-	24.3	µ
Volume Weighted Mean Particle Size	16.58	-	-	-	-	µ
Specific Gravity	2.53	-	-	-	-	-

Mixing

Mixtures were designed for aggregates in the saturated surface dry (SSD) condition. For each mixture, the actual amount of water added was adjusted based on the moisture content. Concrete was prepared at Georgia Institute of Technology's Structures and Materials Laboratory in a Crown C9 tilting drum mixer, following the procedure specified in ASTM C192. First coarse aggregate was added, followed by fine aggregate and air entraining admixture, if applicable. These materials were mixed briefly to ensure uniformity before the addition of cement along with two-thirds of the mixing water. After additional mixing, water reducing admixture was added with the remainder of the water. The structural samples were mixed in two batches, with the second immediately following the first, and were consolidated using a handheld vibrator.

Figure 15. Photo. Concrete Mixing From (Shalan 2016)

Pressure air content measurements were taken in accordance with ASTM C231 for the UPV–compressive strength and structures samples, and gravimetric air content measurements were taken in accordance with ASTM C138 for UPV–compressive strength samples. After measurements were taken, mixtures were molded into three 4 inch × 8 inch cylinders. Concrete was placed in two

volumetric layers, which were rodded using 25 strokes, and tapped 15 times as specified by ASTM C192. The cylinders were then sealed for 24 hours.

(a) Gravimetric Air Content From (Shalan 2016) (b) Pressure Air Content From (Shalan, 2016)

Figure 16. Photo. Measurement of Fresh Properties

Curing

The structures samples were cured outdoors, sealed in 2-millimeter-thick plastic until testing. The UPV–compressive strength samples were cured for three years in the Structures Lab fog room at 100% relative humidity and room temperature (71 ± 2° F), continuously moistened by sprinklers. The surface resistivity samples were cured in saturated limewater at room temperature (71 ± 2° F).

COVER METER AND GPR COMPARISONS

Two commercially available cover meter devices (Proceq Profometer 650 AI and James Instruments Rebarscope) and one commercially available GPR device (Proceq GP 8000) were evaluated for the measurement of rebar location.

Measurement Procedures

The Profometer cover meter device was calibrated before each scan. The normal mode was used for Test Slab 1 measurements, the large mode was used for Test Slab 2 and Dowel Bar specimen measurements, and the spot mode was used for the alternative reinforcement specimen. Line scans on the test slab specimens were taken with the cover meter between the rebar perpendicular to the bars being measured, such that the perpendicular rebar were 5 inches from the measurement line on either end. While the procedure was within the sphere of influence for the device, most commercial cover meters have coils positioned such that the primary magnetic field is strongest along a plane parallel to the axis of the rebar to minimize the effect of eddy currents produced on nearby perpendicular reinforcement. In a study of various factors influencing the accuracy of cover meters (Barnes, 2008), it was found that for a 2.36-inch cover, the result of taking a scan on top of a perpendicular bar was a 0.0637-inch decrease in the measured cover.

GPR area scans were taken for void detection, and line scans were used for all other measurements. During the GPR post-measurement analysis, the gain settings were selected to enhance the signal of interest. Through a series of experiments, it was determined that in most cases, adjustments to gain settings can influence the measurement precision by changing the ability of the operator to detect the reinforcement; however, the adjustments will cause negligible bias to the measurements. For

example, considering a #4 rebar at a cover depth of 2-9/16 inches, the maximum error due to incorrect gain settings was determined to be 0.2 inches. The dielectric constants were determined using the built-in hyperbolic curve fitting of the Proceq GP 8000.

For both test slabs, the reinforcement spacing is 10 inches on center, which is beyond the 8-inch radius sphere of influence given in the Profometer Operating Instructions (Proceq, 2017). Therefore, it can be assumed that the parallel neighboring rebars have a negligible effect on the cover measurements. The initial assumption was supported by the fact that when the neighboring rebar corrections were included in the Profometer, no influence on the measured cover values were observed.

The true cover thicknesses of Test Slabs 1 and 2 were determined by drilling holes. For the Dowel Bar and Alternative Reinforcement Samples, the rebars were accessible from the outside of the specimen; as such, ground truth values were measured directly. An image depicting the measurement of dowel bar alignment is shown in Figure 17.

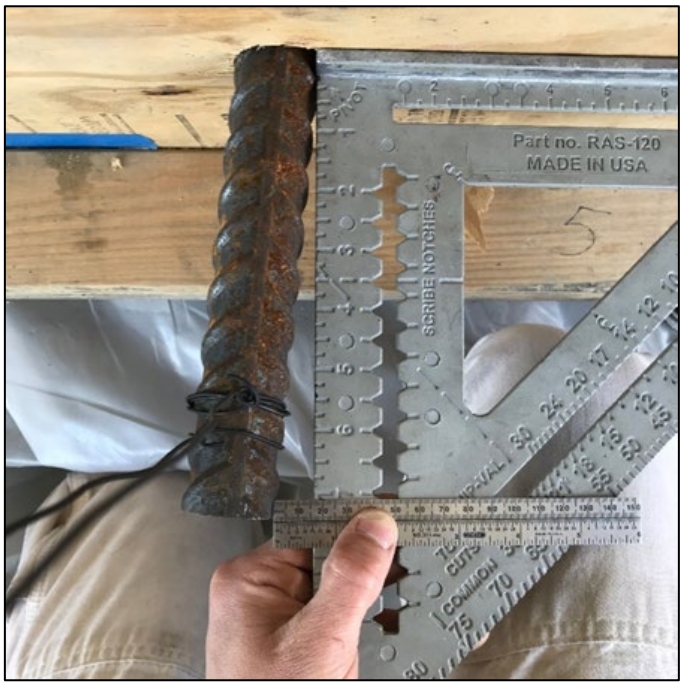

Figure 17. Photo. Dowel Bar Horizontal Alignment Measurement

Cover Depth Accuracy

For Test Slab 2, cover measurements were taken on both reinforcement layers. The results are shown in Figure 18. The top layer had an average cover of 2.61inches and the bottom layer had an average cover of 3.08 inches. The GP 8000 was unable to take accurate measurements on Test Slab 2 rebars 1, 5, 6, 10, 6-b, and 10-b due to physical limitations related to the size of the device and interference from the edge of the specimen. Further, the GP 8000 was also unable to make measurements on rebars 7-b and 9-b due to interference from the embedded Styrofoam cylinder and cylindrical void respectively. For the GPR, electromagnetic (EM) waves can be reflected as they pass through the concrete-air interface due to differences in the dielectric constants between the materials. Conversely, the cover meter measurements are unaffected by boundaries and voids. The magnetic permeabilities of both concrete and air are near unity and have a negligible effect on the

magnetic field strength. In addition, both materials have minor conductivities such that significant eddy currents are not produced.

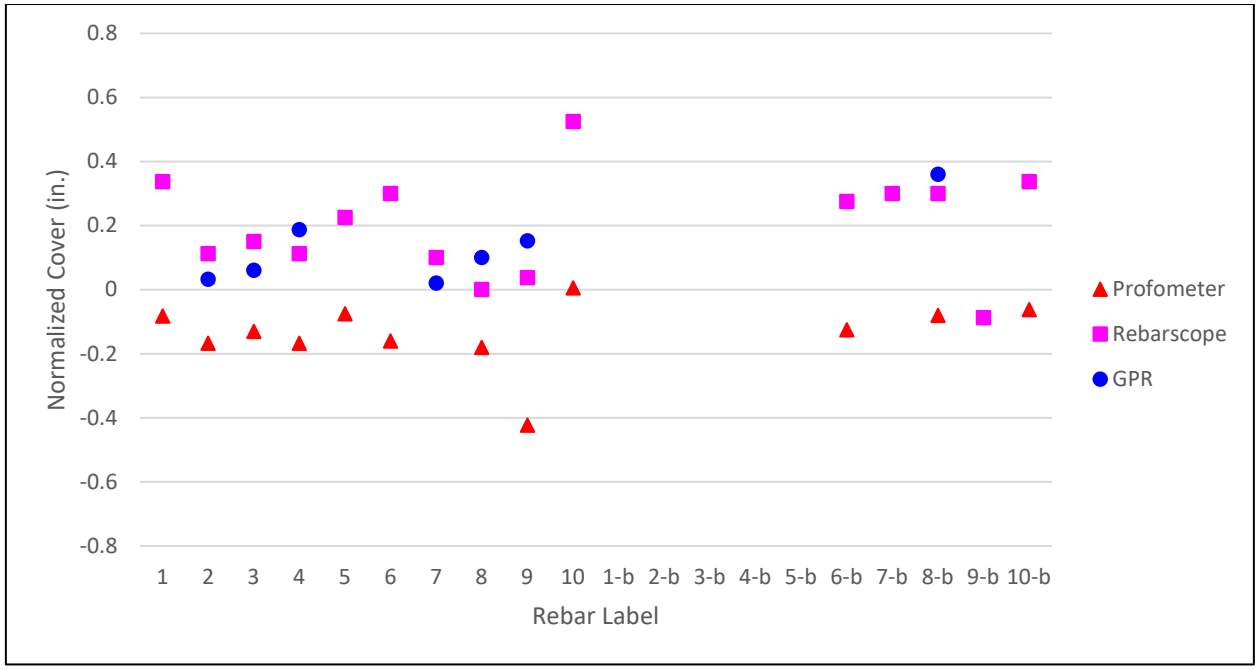

Figure 18. Graph. Test Slab 2 Cover Measurements

The GP 8000, Profometer, and Rebarscope had mean accuracies of 0.13 inches, 0.13 inches, and 0.19 inches, respectively. These errors are slightly lower than what was found in a previous study (Barnes, 2008); a 0.2-inch error for a cover of 3.15 inches and a 0.16-inch error for a cover of 2.42 inches. Similar accuracies were achieved despite a larger bar diameter of 1.1 inches (N24) being used. Cover meter signal strength is known to increase approximately linearly with bar diameter (Alldred, 1993).

For Test Slab 1, measurements were taken on the bottom reinforcement layer which had a mean actual cover of 4.39 inches (Figure 19). For all three devices, inaccurate measurements were

obtained for rebar 7, most likely due to a large amount of rebar ties / steel wire used to position the embedded sack of gravel in that location. In addition, rebars 6 and 10 were too close to the edge of the specimen for accurate measurements to be recorded with the GP 8000.

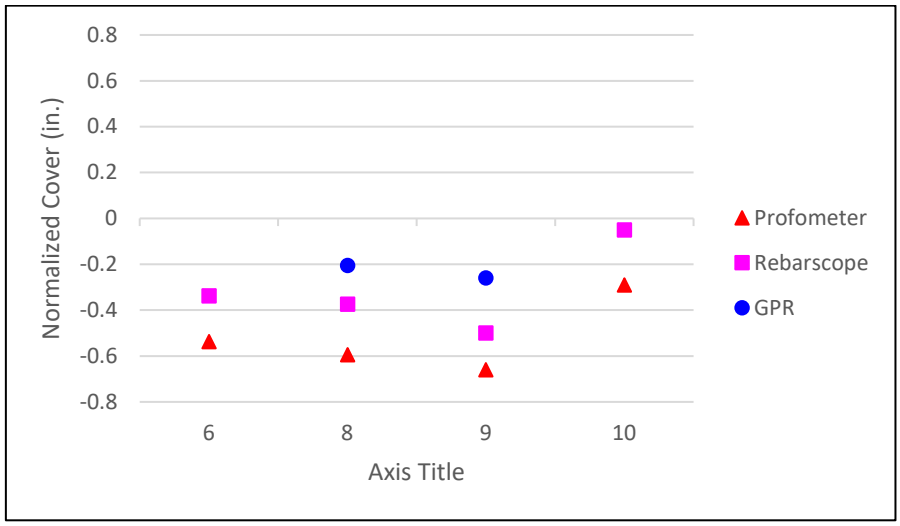

Figure 19. Graph. Test Slab 1 Cover Measurements

For rebars 8 and 9, the GP 8000 had the greatest accuracy (0.21 inches and 0.26 inches, respectively). In comparison, the Profometer achieved accuracies of 0.60 inches and 0.66 inches and the Rebarscope achieved accuracies of 0.375 inches and 0.5 inches. In general, GPR devices can be expected to have better accuracies at greater depths, which is consistent with the measured results. Overall, the Rebarscope performed better than the Profometer with mean accuracies of 0.32 inches and 0.52 inches, respectively. The cover meter errors are significantly higher than the errors found for the Test Slab 2 measurements, and the errors found in (Barnes, 2008), due to the increase in cover depth. Cover meter signal strength is approximately related to cover depth by an inverse fourth power law (Alldred, 1993). As the signal strength decreases with increasing cover depth, greater inaccuracies are found.

For all three devices, a bias can be seen in the cover measurements for Test Slabs 1 and 2. For the GP 8000, this bias is most likely associated with the determination of dielectric constant. The negative biases associated with cover meter measurements is most likely due to interference from embedded conductive objects. The positive biases found in the Rebarscope Test Slab 2 measurements could be due to changes in the resistivity of electrical components resulting from changes in ambient temperature. The Profometer accounts for differences in temperature through recalibration; whereas the Rebarscope contains temperature sensors and adjusts calculations to account for changes in temperature (James Instruments, 2018).

Measurements taken on carbon steel reinforcement at a cover of 2 inches in the Alternative Reinforcement Sample had a mean accuracy of 0.045 inches. The calculated error is much lower than what was found for all three devices during the Test Slab 2 measurements. This result is further evidence of the influence of cover depth on measurement accuracy.

Dowel Bar Measurements

With the Profometer and GP 8000, line scans were taken along each face of the Dowel Bar Sample. Diagrams were generated to scale of the measured and actual dowel bar positions, as shown in Figure 20. The dowel bars labelled A and D are #11 carbon steel bars and the dowel bars labelled B and C are #8 epoxy coated bars.

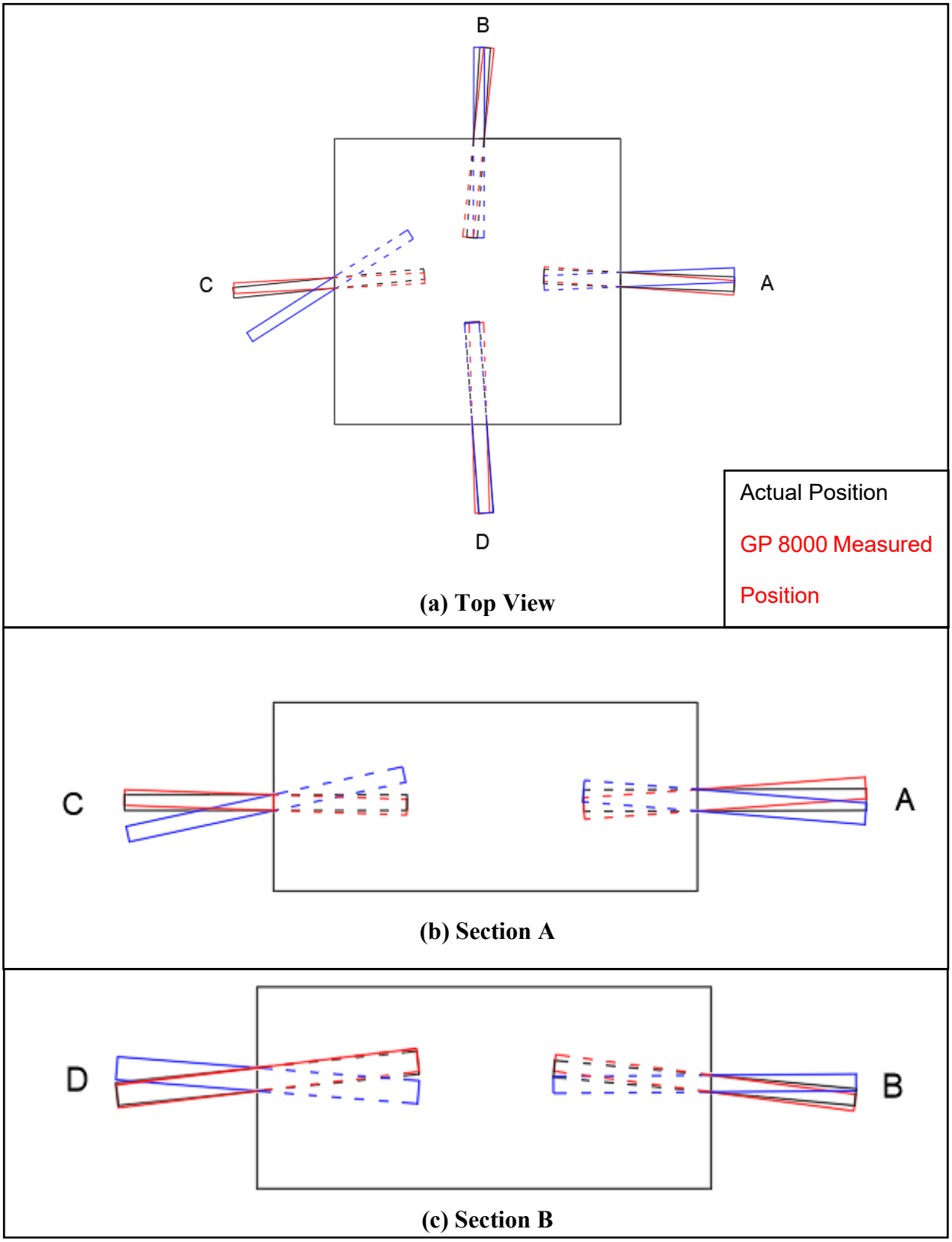

Figure 20. Diagram. Comparisons Between Measured and Actual Dowel Bar Positions (to-scale)

With the depth and distances obtained, the position and alignment of each reinforcing bar was calculated with trigonometry. The resulting values were then compared to the true values to determine if the accuracy was sufficient to enforce the specified dowel placement tolerance. Section 430 of the GDOT Specifications (Portland Cement Concrete Pavement) requires dowel bars to be placed within 1.0 inch of the plan position horizontally and vertically. Further, the Specification limits horizontal and vertical misalignment to 0.375 inches per foot dowel bar length. The calculated alignments, given in both inches and inches per foot of dowel bar length, are shown in Table 12. Red font is used to indicate errors larger than the alignment tolerance.

Table 12. Dowel Bar Alignment Measurements

Dowel Bar Label	GP 8000 Vertical Alignment Error inches (inches/ft)	Profometer Vertical Alignment Error inches (inches/ft)	GP 8000 Horizontal Alignment Error inches (inches/ft)	Profometer Horizontal Alignment Error inches (inches/ft)
A	0.063 (0.042)	0.32 (0.21)	0.12 (0.077)	0.31 (0.21)
B	0.14 (0.090)	0.38 (0.25)	0.09 (0.063)	0.35 (0.23)
C	0.125 (0.083)	0.80 (0.53)	0.03 (0.021)	1.2 (0.78)
D	0.031 (0.020)	0.68 (0.45)	0.15 (0.10)	0.72 (0.48)

The GP 8000 had an average error of 0.093 inches (0.063 in/ft), which was far less than the average Profometer error of 0.59 inches (0.39 inches/ft). For all measurements, the GP 8000 had errors much less than the 1 inches placement tolerance as well as the 0.375 inches/ft alignment tolerance. The Profometer had errors less than the placement tolerance for all except one measurement; however, the device had insufficient accuracy for the alignment tolerance. The signal strength for cover meters decreases rapidly with increasing cover, while the amplitude of an electromagnetic wave decreases exponentially over a distance. Based on the measured data, it is clear that the depths

in the current study are small enough compared to the depth limits of the devices to enable accurate results to be obtained.

In addition, it was found that the bar diameter had a greater effect on the accuracy of the Profometer than the GPR. This can be seen in the difference between the average measurement errors for the #11 bar and #8 epoxy bars, which was 0.17 inches for the Profometer and 0.0054 inches for the GPR. The result is due to the signal of the cover meter increasing approximately linearly with increasing bar diameter (Alldred, 1993), whereas amplitude of the electromagnetic wave received by the GPR is primarily dependent on the amount of attenuation in the concrete.

Conclusions

From the experimental studies conducted using the cover meter and GPR devices, the following conclusions can be drawn:

1. Of the three devices studied, the Profometer had the greatest accuracy for measuring the cover depth of carbon steel rebar for cover depths between 2.38 inches and 3.19 inches. A mean error of 0.14 inches was calculated for the Profometer in this cover depth range. At a cover depth of 2 inches, the mean accuracy of the Profometer improved to 0.045 inches.
2. The GP 8000 had the greatest accuracy for measuring the cover depth of carbon steel rebar at depths greater than 4.25 inches. For a mean cover depth of 4.44 inches, the device had a mean accuracy of 0.23 inches. The Rebarscope performed better than the Profometer for this cover depth, with mean accuracies of 0.32 inches and 0.52 inches. It is expected that either the Rebarscope or GP 8000 would have the best accuracy for covers between 3.19 inches

and 4.25 inches depending on the conditions (i.e., amount of interference, rebar diameter, ambient temperature, etc.).

3. The GP 8000 had sufficient accuracy to enforce the GDOT dowel bar tolerances (i.e., 1 inch placement and 3/8 inch/ft alignment) with a mean accuracy of 0.093 inches (0.063 inches/ft). All but one Profometer measurement had sufficient accuracy for the placement tolerance; however, insufficient accuracy was found for the alignment tolerance, with a mean accuracy of 0.590 inches (0.393 inches/ft).

COVER METER TESTING

Alternative Rebar

Measurements were taken on the Alternative Reinforcement specimen to determine the effect of using alternative reinforcement types on cover measurement accuracy. Five rebar alternatives were used for the study: #5 grade 60 carbon steel, #5 stainless steel, #5 Galvabar, #6 epoxy coated grade 60 carbon steel, and #6 grade 60 carbon steel. All measurements were taken using the Profometer 650 Spot Mode, and the results are displayed in Figure 6. For some rebars, measurements were unable to be taken due to rebar congestion and the presence of steel lifting inserts. For other rebars, measurements were able to be taken, but the accuracy was negatively influenced by identifiable interferences (depicted as blue squares in Figure 21).

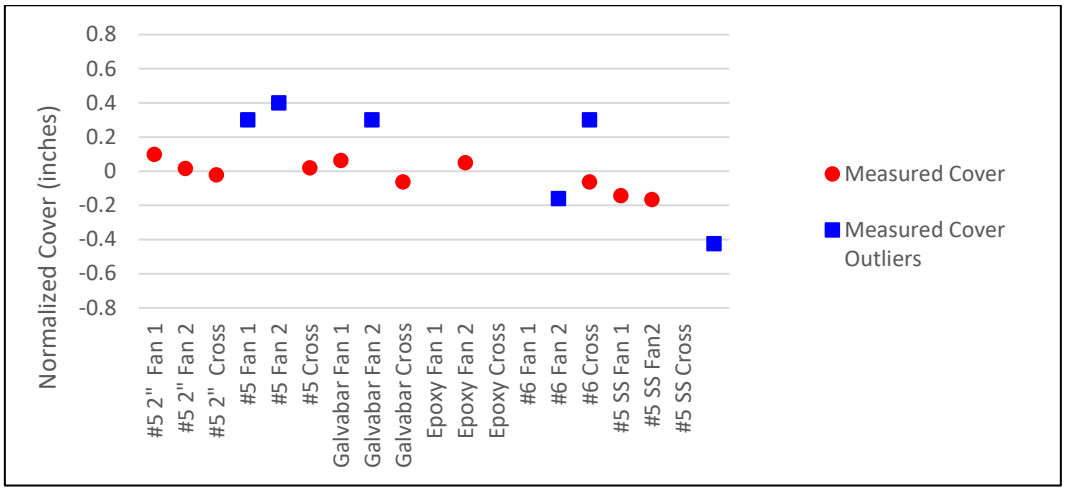

Figure 21. Graph. Alternative Reinforcement Specimen Cover Measurements

The Galvabar cover depth was measured with a mean accuracy of 0.0625 inches and the epoxy coated rebar cover depth was measured with an accuracy of 0.05 inches. Both errors are smaller than the results for the carbon steel rebar at a cover of 3.08 inches (0.15-inch accuracy). The stainless-steel rebar was measured with the same accuracy as carbon steel, with an average error of 0.15 inches, despite stainless steel having a higher electrical conductivity compared to carbon steel, resulting from differences in composition. The epoxy coating has a very low electrical conductivity, and while the zinc coating of the Galvabar has a higher electrical conductivity than steel, the coating is thin enough that any eddy currents produced have a negligible influence on the measured magnetic field. Stainless steel is known to have a higher electrical conductivity than carbon steel, but differences were not significant enough to influence the results. Overall, the impact of using stainless steel, epoxy coated, and galvanized reinforcement had a negligible effect on the measurement accuracy.

Perpendicular Neighboring Rebar

To determine the influence of nearby rebar positioned perpendicular to the rebar of interest, line scans were recorded on Test Slab 1 and Test Slab 2 at varied distances to the perpendicular reinforcement. The results are shown in Figure 22.

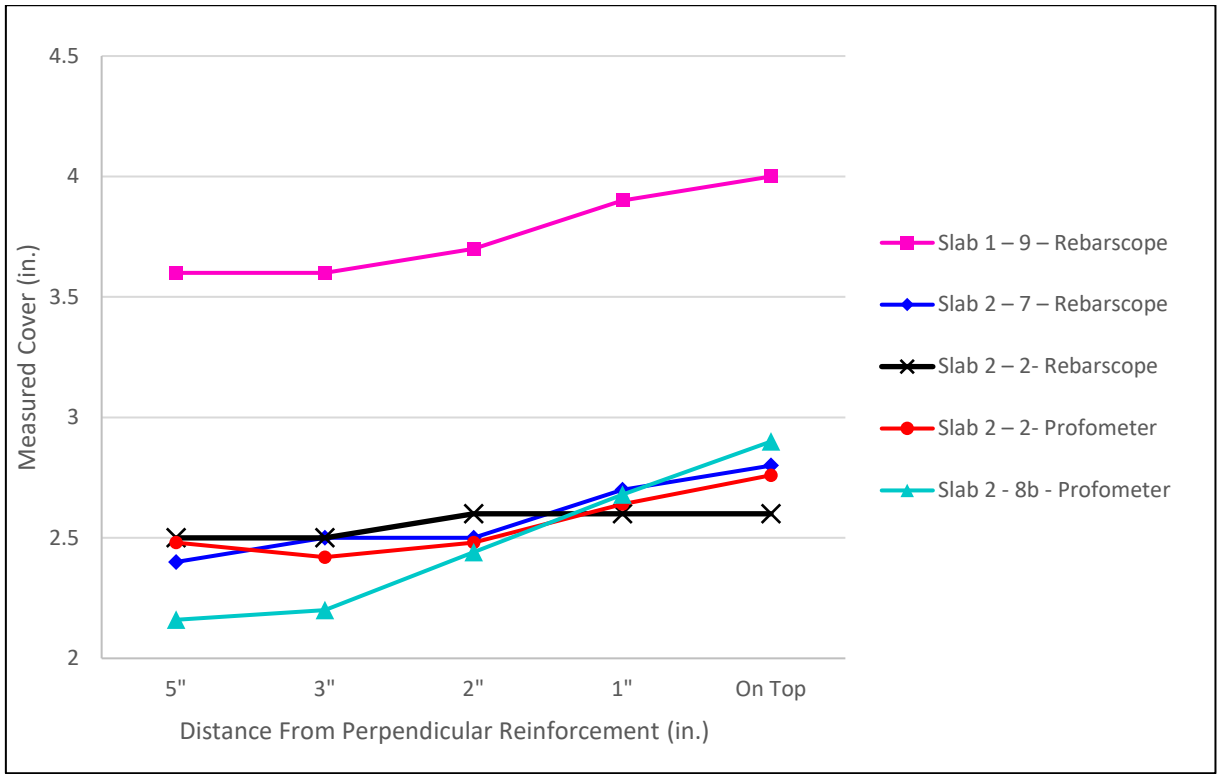

Figure 22. Graph. The Influence of Perpendicular Rebar on Cover Depth Accuracy

For Test Slab 2-2, where the perpendicular rebar are below the rebar of interest, a small difference in measured cover depth was found (0.10 inches for the Rebarscope, and 0.28 inches for the Profometer), similar to the 0.11 inches difference found in the literature (Barnes, 2008). A much greater difference was found for the other rebar (0.40 inches for the Rebarscope, and 0.74 inches for the Profometer), which were below the perpendicular reinforcement. For most situations, accurate

cover measurements are less critical on the second layer of reinforcement because the deeper cover results in longer periods to depassivate and corrode than the first layer of reinforcement.

Cover Meter Resolution

The fanned rebar layout of the Alternative Reinforcement specimen was utilized to determine the resolution of the cover meters (minimum spacing for rebars to be distinguished) for a #5 rebar at a cover depth of 2 inches. The Profometer had a superior resolution of 1.63 inches compared to the 1.50 inches resolution found with the Rebarscope. Both cover meters experienced an increase in measured cover depth after the rebars were distinguished. The measured cover of the Profometer went from 2.18 inches to 1.94 inches, as compared to the measured cover of the Rebarscope that went from 2.3 inches to 2.1 inches. As can be seen in Figure 4, where the red cross indicates the resolution determined by the testing during the current study, the performance of Profometer was similar, but superior to what was specified in the operating instructions.

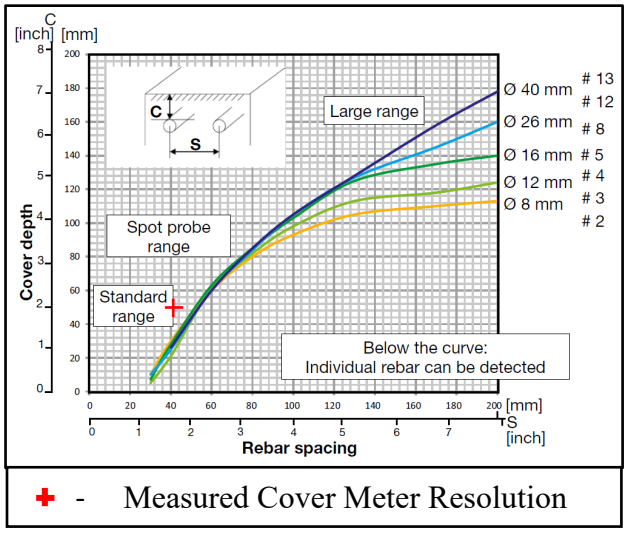

Figure 23. Graph. A Comparison Between the Resolution Specified in the Operating Instructions, with the Experimentally Determined Resolution

Diameter Measurements

Comparisons were made between the ability of Profometer and Rebarscope to measure rebar diameter. At a cover of 2.75 inches, the diameter of a #5 bar was measured by the Rebarscope to be 1.15 inches, having an error of 0.687 inches. The large error was highly unexpected, given that the instruction manual claims that diameter measurements can be taken for covers up to 4.2 inches. The Profometer was unable to measure the rebar diameter at the 2.75 inch cover depth, which is consistent with the operating instructions, which state that diameter measurements cannot be made at depths greater than 2.5 inches (Proceq, 2017). At a cover of 2 inches, the diameter of a #5 bar was correctly measured to be 0.625 inches by the Profometer and measured to be 0.56 inches by the Rebarscope, having an error of 0.07 inches.

Conclusions

From the cover meter results, the following conclusions can be drawn:

1. The use of ASTM A775 Grade 60 Epoxy coated steel rebar and ASTM A 1094 Grade 60 Galvabar at a mean depth of 3.08 inches had a negligible effect on cover depth measurement. The cover of ASTM A 995 Grade 60 stainless steel rebar at an average depth of 3.09 inches was measured with an accuracy of 0.15 inches, a 0.0059 inches increase from the measurement of ASTM A615 grade 60 carbon steel rebar.
2. The effect of perpendicular rebars on cover depth measurements was quantified for #4 carbon steel rebar at cover depths ranging from 2.69 inches to 4.50 inches. Multiple line scans were conducted, moving progressively closer to the perpendicular rebar, with the final line scan being directly on top of the perpendicular bar. The decrease in measured cover was

found to be greatest for the Profometer. The maximum measured difference in cover was 0.28 inches and 0.74 inches for the top and bottom rebar layers, respectively.

3. For a #5 carbon steel rebar at a depth of 2.08 inches, the resolution (minimum distance between rebar in order for them to be distinguished) of the Profometer was determined to be 1.625 inches, while the resolution of the Rebarscope was determined to be 1.50 inches.
4. Neither cover meter device was able to accurately measure the diameter of a #5 rebar at a depth of 2.75 inches. For a #5 rebar at a depth of 2 inches, the Profometer was able to accurately identify the diameter (bar diameter measurements are discretized), while the Rebarscope measured the diameter to be 0.56.

GPR TESTING

Void Detection

An area scan was taken on Test Slab 2 using the GP 8000. A cylindrical embedded void with a radius of 3 inches and height of 1 inches was detected. The void can be seen in the bottom left corner of the rendering shown in Figure 24. The object seen in the top right corner of the rendering is an embedded lifting insert.

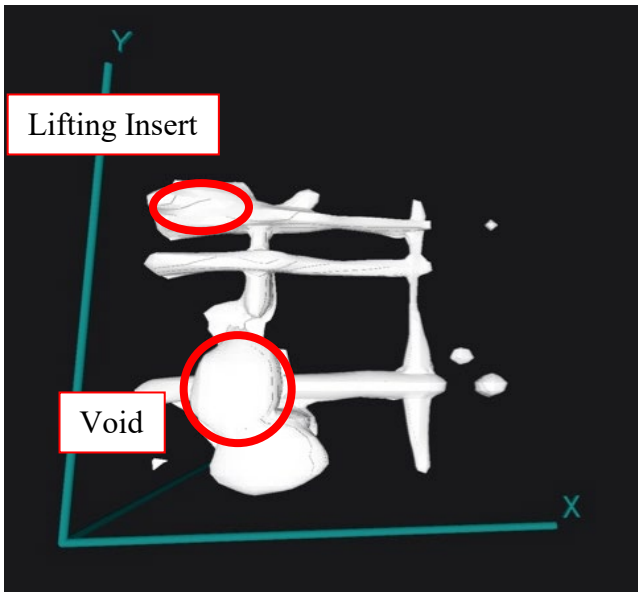

Figure 24. Rendering. Test Slab 2 GPR Area Scan Rendering Depicting Reinforcement and Embedded Void

The ability the GPR to detect any the interface between two materials having a significant difference in dielectric constants can be an advantage of the GPR over the cover meter, which can only measure electrically conductive materials. The quality of the concrete-rebar bond and member thickness can be checked simultaneously with the measurement of rebar. Delaminations, large voids, and honeycombing can also be detected using a GPR device.

Thickness Measurement

The thickness of the Dowel Bar, Bridge Deck, Test Slab 1, and Test Slab 2 specimens were measured with the GP 8000. The EM wave velocity was determined through hyperbolic fitting of the signal from a rebar embedded in the same specimen. Unlike the other measurements, time-gain compensation was used to account for wave attenuation and produce the clearest signal. Actual thicknesses were measured using a tape measure at the nearest edge of the specimen. The results are shown in Table 13.

Table 13. GP 8000 Thickness Measurements

Specimen	Actual Thickness (inches)	Measurement Error (inches)	Notes
Dowel Bar B	12	0.300	Stored indoors
Test Slab 1	5.625	0.275	Stored outdoors
Test Slab 2	4.25	0.25	Stored outdoors
Bridge Deck	8.5	0.300	Stored indoors High concentration of steel Embedded bridge deck pan

For all four specimens, similar accuracies were achieved, with all errors less than 0.3 inches. The measurement for the bridge deck specimen was negatively influenced by interference from a high concentration of steel; however, a stronger reflection was detected due to the embedded galvanized steel pan (steel is a strong reflector of EM waves). For the measurement of pavement thickness, lower accuracy can be expected because there will likely be a greater difference in dielectric constants between concrete and air than concrete and subgrade.

Inter-Operator Precision of Post-Measurement Analysis

To determine the GPR inter-operator precision, nine operators performed the GPR post-measurement analysis for four different measurement files. A trained and experienced GDOT engineer (Christopher Collins) acted as one of the operators as well as the lead graduate research assistant (David Burney) who gained GPR experience from performing all testing during the duration of the current project. Additionally, seven operators were trained for approximately 15 minutes before being asked to analyze the four measurement files on their own. The analysis included manual selection of gain settings, hyperbolic fitting for the determination of dielectric constant, and indication of the rebar depth (determination of EM wave transit time).

The files used were from measurements taken on the Dowel Bar Specimen, the Bridge Deck Specimen, Test Slab 1, and Test Slab 2 to examine a variety of conditions which may affect GPR precision. Relevant specimen properties are given in Table 14.

Table 14. Relevant Measurement Properties

Specimen	Average Measured Rebar Depth (inches)	Average Concrete Dielectric Constant	Notes
Dowel Bar Specimen	5.88 inches	5.56	Stored indoors
Bridge Deck Specimen	3.26 inches	7.20	Stored indoors High concentration of steel
Test Slab 1	4.72 inches	5.96	Stored outdoors
Test Slab 2	2.50 inches	7.84	Stored outdoors

For each specimen, a standard deviation between measurements was determined for the dielectric constant setting. It was observed that the standard deviation between dielectric constant settings increases approximately linearly with the dielectric constant, as can be seen in Figure 25.

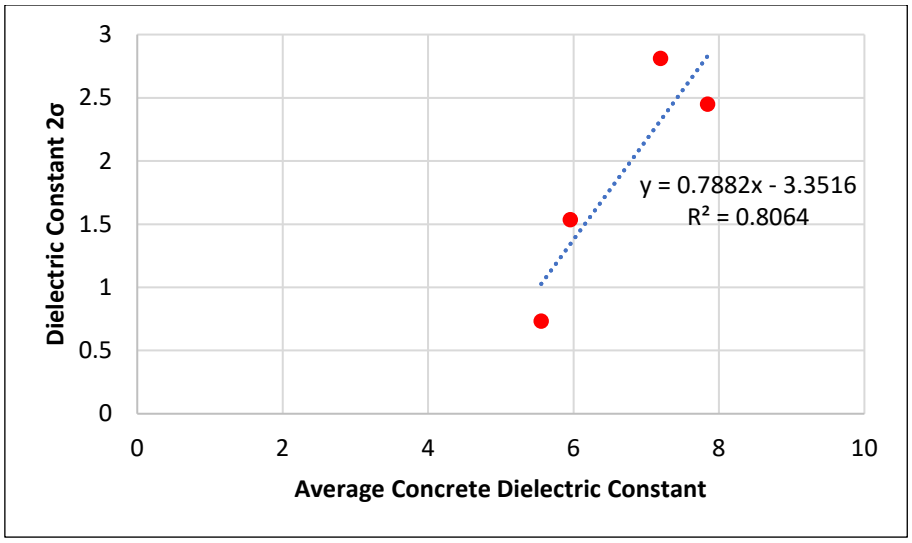

Figure 25. Graph. Relationship Between Dielectric Constant and Dielectric Constant Precision

To separate the determination of the EM wave transit time from the selection of dielectric constant (which is used to calculate the EM wave speed), depths were converted to transit times using equation 11.

$$t = d \times \frac{\sqrt{\varepsilon}}{c} \tag{11}$$

Where t = one-way transit time, d = depth, ε = concrete dielectric constant, and c = speed of light in a vacuum. The standard deviation between calculated transit times was then calculated for each measurement file. The standard deviations were 0.013 ns for the Dowel Bar Specimen, 0.016 ns for the Bridge Deck Specimen, 0.013 ns for Test Slab 1, and 0.012 ns for Test Slab 2. The average standard deviation was 0.014 ns. There were no observed correlations for the precision of transit time selection, although the increased standard deviation for the Bridge Deck Specimen was most likely due to wave interference.

Quantile-quantile plots, shown in Appendix D., were used to test the normalcy of the value distribution. The plots show that the data is approximately normally distributed. For normally distributed data, it can be assumed that 95% of the values fall within two standard deviations of the mean. Using this assumption, and the linear fit from Figure 25, the 95-percentile upper and lower bounds (equations 12 and 13) can be generated for depth measurements.

$$d_{LowerBound} = \frac{c}{\sqrt{1.7882\varepsilon - 3.3516}} \times (t - 0.027\ ns) \tag{12}$$

$$d_{UpperBound} = \frac{c}{\sqrt{0.2118\varepsilon + 3.3516}} \times (t + 0.027\ ns) \tag{13}$$

The bounds are more applicable when expressed in terms of depth. The transit times are converted to depths in equations 14 and 15.

$$d_{LowerBound} = \frac{c}{\sqrt{1.7882\varepsilon - 3.3516}} \times \left(\frac{d \times \sqrt{\varepsilon}}{c} - 0.027\ ns\right) \quad (14)$$

$$d_{UpperBound} = \frac{c}{\sqrt{0.2118\varepsilon + 3.3516}} \times \left(\frac{d \times \sqrt{\varepsilon}}{c} + 0.027\ ns\right) \quad (15)$$

The precision, given in equation 16, can then be calculated as the difference between the bounds.

$$P_{Depth} = d_{UpperBound} - d_{LowerBound} \quad (16)$$

The standard deviation of depth measurements (which reflects the cumulative precision of dielectric constant and transit time selection) was also determined for each measurement file. The average standard deviation was 0.25 inches, which was significantly higher than the average difference between the measured depths of the two experienced operators (0.08 inches). The results suggests that operator experience has a great influence on the precision of GPR cover depth measurements. The methodology outlined for the development of the model given in Equations 14-15 could be repeated with trained GDOT engineers using the same measurement files.

CONCLUSIONS

From the GPR results, the following conclusions can be drawn:

1. An embedded cylindrical void with a radius of 3 inches and a depth of 1 inch was successfully detected with the Proceq GP 8000.
2. Specimen depths were measured for depths between 4.25 inches and 12 inches, with EM wave reflections from a concrete-air and concrete-steel interfaces. The maximum measurement error was 0.3 inches
3. The inter-operator precision was studied for the post measurement determination of dielectric constant and EM wave transit time. A model was developed to predict the precision given a dielectric constant and rebar cover depth. It was found that the precision of

cover depth measurements was significantly improved when experienced GPR operators performed the post-measurement analysis.

SURFACE RESISTIVITY TESTING

In testing performed by the Georgia Tech–GDOT RP 20-19 team, surface resistivity measurements were taken on 4 inch × 8 inch cylinders to validate the applicability of the test method for acceptance of materials and concrete mix designs. For the class AAA cylinders, surface resistivity measurements were taken daily for 56 days after casting. For the Class A cylinders, the first measurements were taken at 28 days after casting and then measurements were taken at 7 day intervals until 56 days. Measurements were taken with the Proceq Resipod following the procedure specified in AASHTO T 358. Measurements were taken such that the device was parallel with the cylinder's axis. For each cylinder, eight total measurements were taken—two at each circumferential mark spaced at 90 degree intervals around the cylinder's circumference. As specified in AASHTO T 358, results were multiplied by a factor of 1.1 to compensate for the curing in limewater.

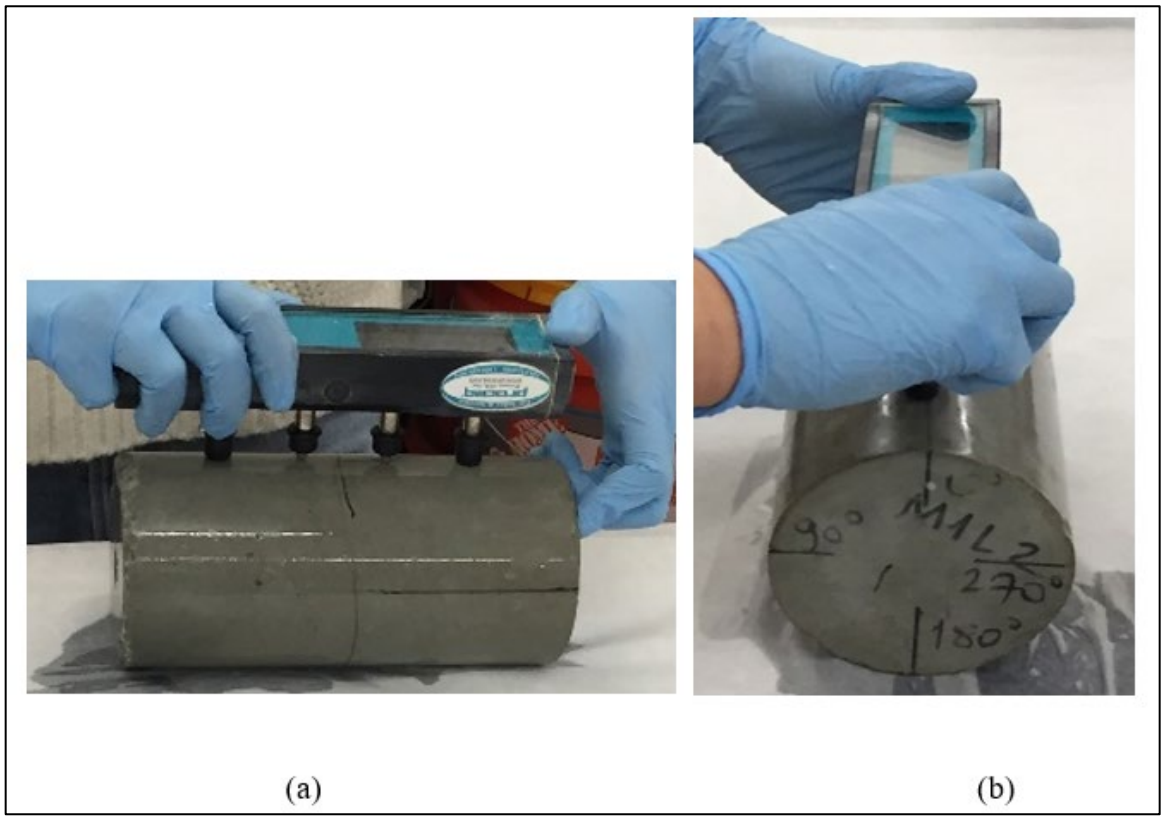

Figure 26. Photo. Surface Resistivity Testing (a) Front view (b) Side view

Surface resistivity results are shown in Figures 26–29 where the positive and negative error bars represent one standard deviation. The results presented in Figures 26 and 27 show that the surface resistivity measurements were capable of detecting the improvements in moisture transport properties due to the decreases concrete porosity and capillary pore connectivity that is to be expected based on the theoretical understanding of the materials used. The delayed increase in resistivity seen in the fly ash mixture is due to the general understanding that fly ash reactions occur much later in the cement hydration, whereas metakaolin is known to react much earlier. The results presented in Figure 28 show that lower surface resistivity values were measured on the quartz sample, representing the negative effect on transport properties that is to be expected with the replacement of cement with inert quartz filler.

Similarly, Figure 29 shows the expected increase in surface resistivity for mixtures with Class F fly ash, and a slight decrease in resistivity with the replacement of cement with an impure, uncalcined clay. An increase in resistivity is found for the cylinders with a 5% reduction in cement content and an increase in fine aggregate content, however based on the theoretical understandings of cement hydration, it is unlikely that this mixture would actually have lower porosity or pore connectivity. The increase in surface resistivity is most likely a symptom of the fact that sand has a higher electrically resistivity than the cement paste.

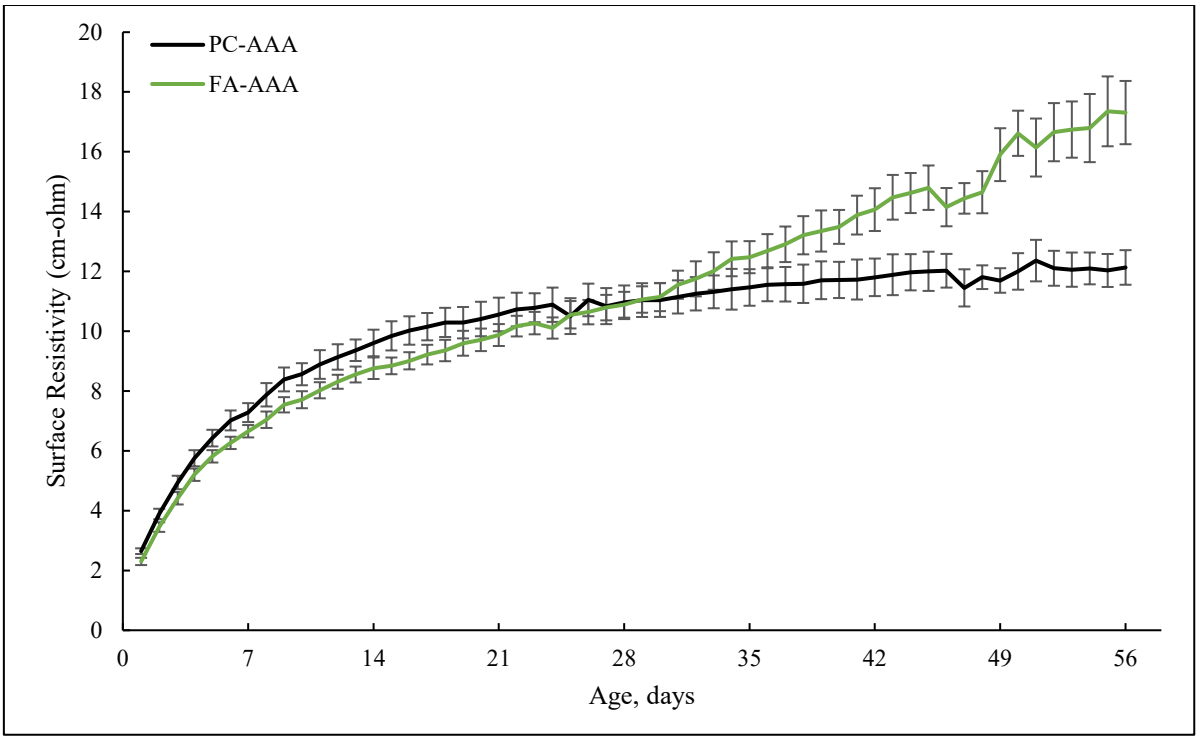

Figure 27. Graph. Surface Resistivity Successful Identification of the Improved Moisture Transport Properties Due to the Addition of Class F Fly Ash

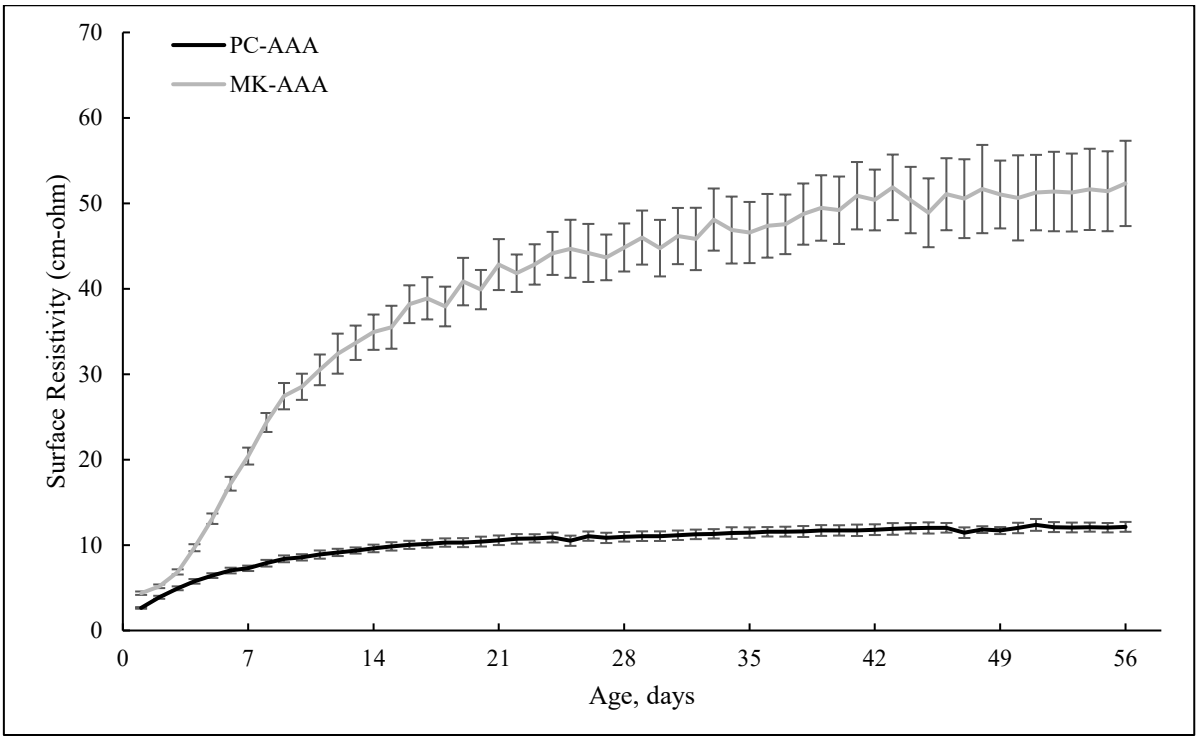

Figure 28. Graph. Surface Resistivity Successful Identification of the Improved Moisture Transport Properties Due to the Addition of Metakaolin

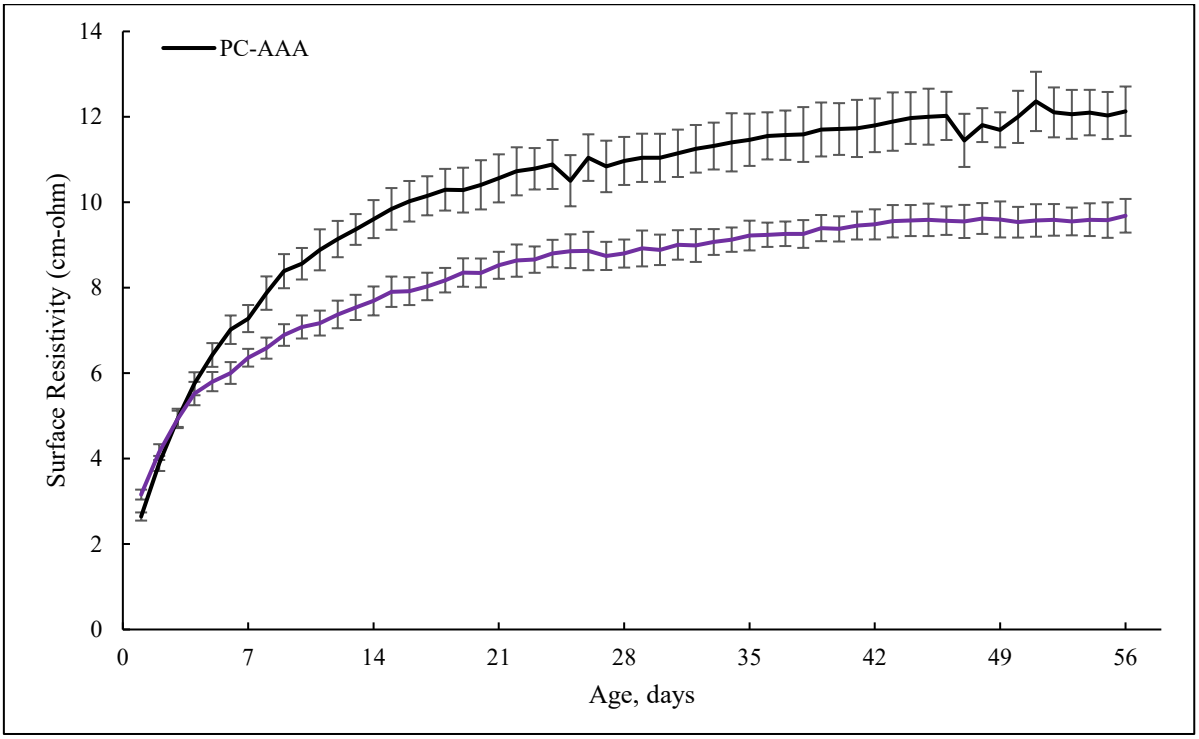

Figure 29. Graph. Surface Resistivity Successful Identification of the Depleted Moisture Transport Properties Due to the Addition of an Inert Quartz Filler

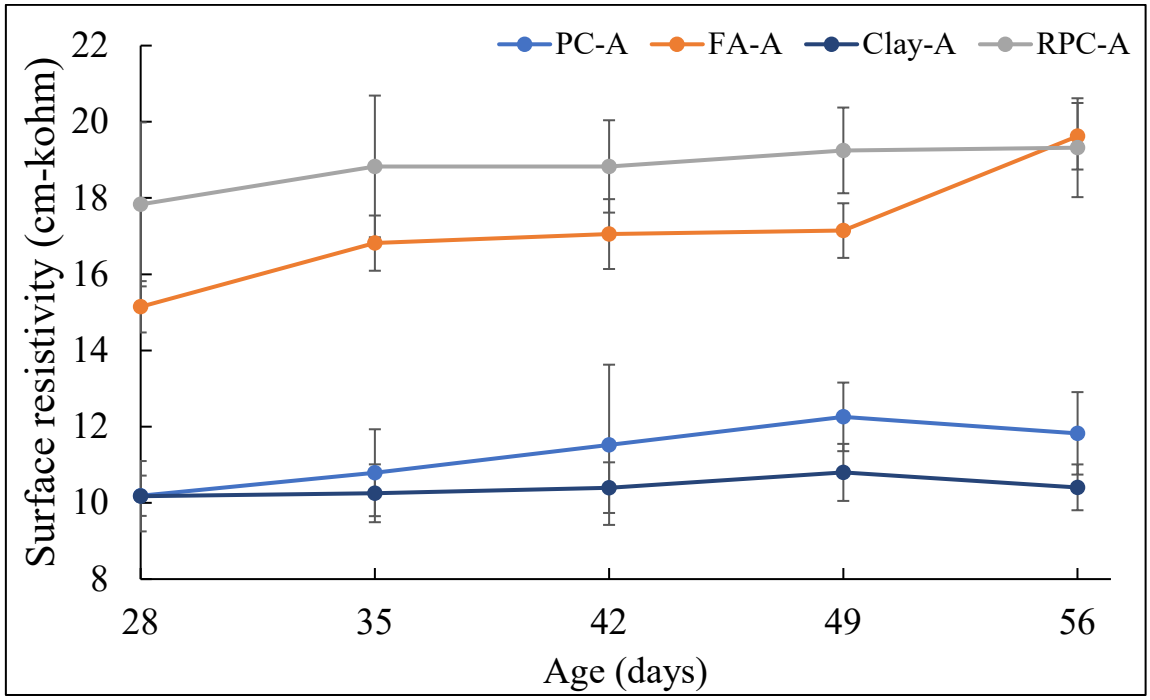

Figure 30. Graph. A Comparison Between Surface Resistivity Measurements

Conclusions

In the testing performed, surface resistivity measurements were shown to be sensitive to the decreased porosity and pore connectivity that resulted from the use of a Class C fly ash and metakaolin. Based on the results, it can be concluded that for concrete samples tested at the same age, and made with the with the same cement, fine aggregate, coarse aggregate, and paste fractions, comparing surface resistivity measurements can be used as an indication of the concretes moisture transport properties. Under the same conditions, surface resistivity measurements can be used as an indication of the pozzolanicity of an SCM. The results also demonstrated that comparing surface resistivity measurements for concrete mixtures with different paste fractions can lead to misleading results.

UPV AND REBOUND HAMMER TESTING

UPV Precision

The Olson UPV device contains software analysis options which automatically determine the transit time, thereby improving measurement efficiency and reducing operator bias. However, in some instances, especially in cases where there was a large amount of ambient noise, the software had difficulty differentiating the received signal, leading to inaccurate transit time values. An example of an inaccurate transit time is shown in Figure 31, where the vertical red line shows the software selected transit time.

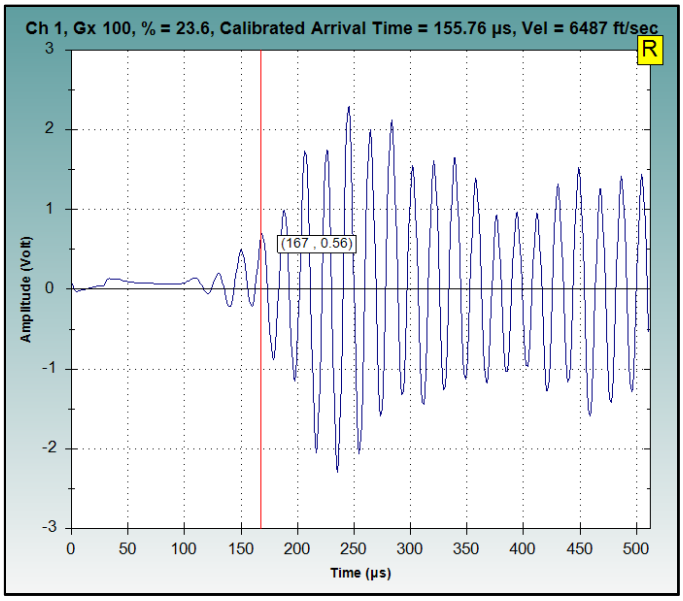

Figure 31. Graph. Olson UPV Incorrect Software Selection of Transit Time

In these cases, the most consistent results were achieved when a constant scale was used to view the waveform, and the transit time was manually selected rather than using the software analysis options. The precision of UPV measurements using this procedure was determined for three different stress wave path lengths. For each path length, five measurements were taken at a single

location. The population standard deviation of measurements at each location are presented in Table 15. For all three samples, the standard deviation was less than 1 µs (the time discretization of the software).

Table 15: UPV Precision for Manually Determined Transit Times

Transit Time (µs)	Population Standard Deviation (µs)
33	0.83
93	0.90
180	0.97

In other instances, the noise was large enough in amplitude that it even became difficult to manually differentiate the received signal, as shown in Figure 32.

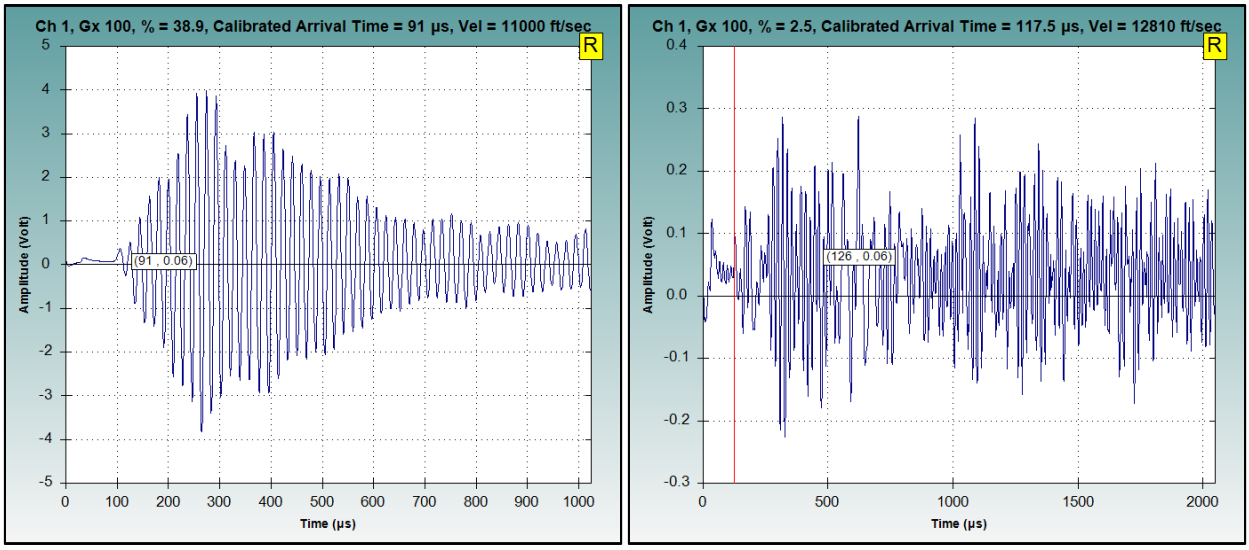

b) Low Amplitude Noise **(a) High Amplitude Noise**

Figure 32. Graph. A Comparison of UPV Waveforms

The Influence of Rebar

Ten direct transmission measurements were taken on the class AA1 sample at various locations. Locations were selected such that no reinforcing bars were in the vicinity of the assumed path length. The mean velocity was 13,840 ft/s with a coefficient of variation (CoV) of 1.82%. Direct transmission measurements were also taken approximately parallel to the axis of the rebar to determine the influence of reinforcement on the pulse velocity. The transducers were positioned as close to the rebar as possible, with the maximum offset (measured from the rebar to the edge of the transducer) being 0.88". A diagram of the measurement set up is shown in Figure 33 where the rebar are shown in black and the concrete is shown in dark grey.

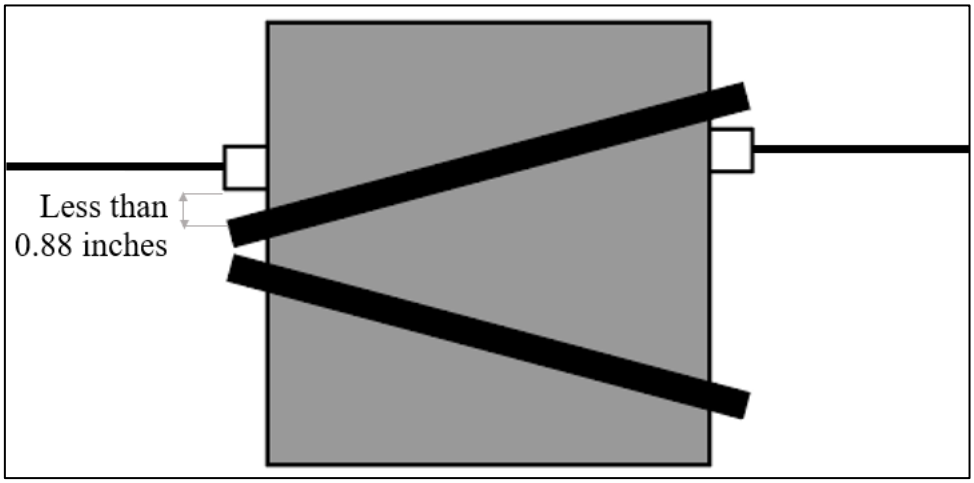

Figure 33. Diagram. Measurement Diagram

The velocity measurements taken along #3, #5 and #8 rebar were 13,960 ft/s, 13,720 ft/s, and 13,840 ft/s, respectively. These results are displayed in Table 16.

Table 16: The Influence of Reinforcing Steel on Stress Wave Velocities

	UPV (ft/s)	CoV (%)	Difference from Mean (%)
No Reinforcement	13,840	1.82	-
#3 Rebar	13,960	-	0.86
#5 Rebar	13,720	-	-0.92
# 8 Rebar	13,840	-	-0.04

All three velocities were within one standard deviation of the mean, indicating that the influence of steel reinforcing bars with diameters of 1 inch or less is negligible. The influence of rebar perpendicular to the path length would have less of an effect on the velocity because the stress wave passes through rebar for a shorter distance.

It should be noted that the results in this study conflict with the formula presented in a past version of the British UPV standard (BS 1881-203: 1986) as well as a more recent study on the influence of reinforcing steel (Fodil, 2019). The fact that the reinforcement was not perfectly parallel could have reduced its effect. The quality of the concrete-rebar bond is also known to affect the influence of rebar on UPV measurements (Concha, 2020).

Direct Transmission Void Detection

Seven direct transmission UPV measurements were taken along Beam 1 at locations selected to avoid rebar and embedded defects. The measurements had a path length of 12.125”. The average pulse velocity was 11,100 ft/s with a coefficient of variation of 1.75%. The pulse velocity through a 6” x 6.5” embedded Styrofoam ovoid was 10,470 ft/s (3.23 standard deviations below the mean). These results are shown in Figure 34, where the error bar represents one standard deviation.

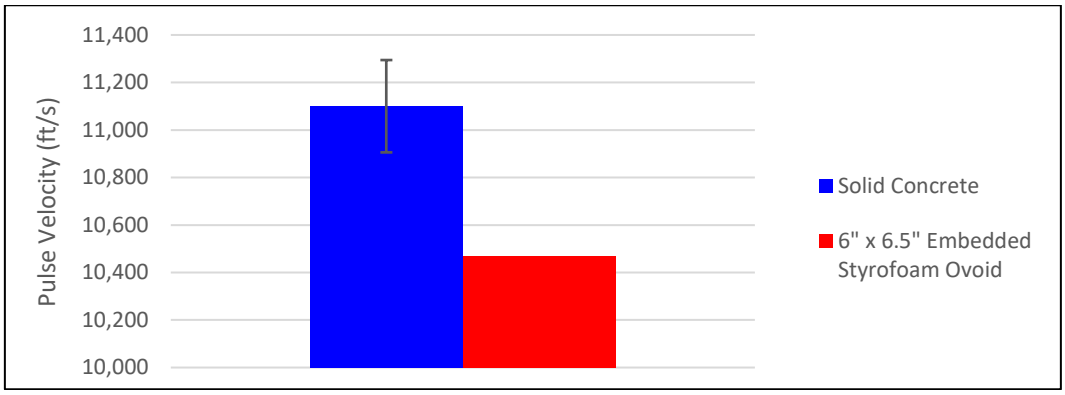

Figure 34. Graph. Beam 1 UPV Results

Six direct transmission UPV measurements were taken along Beam 2 at locations selected to avoid rebar and embedded defects. The measurements had a path length of 12.0625”. The average pulse velocity was 11,830 ft/s with a CoV of 1.47%. Five measurements were taken on either side of an embedded 4” diameter, 8” long cylindrical void with the path of the stress wave perpendicular to the axis of the void. The average pulse velocity was 11,020 ft/s (4.65 standard deviations below the mean). These results are shown in Figure 35, where the error bar represents one standard deviation.

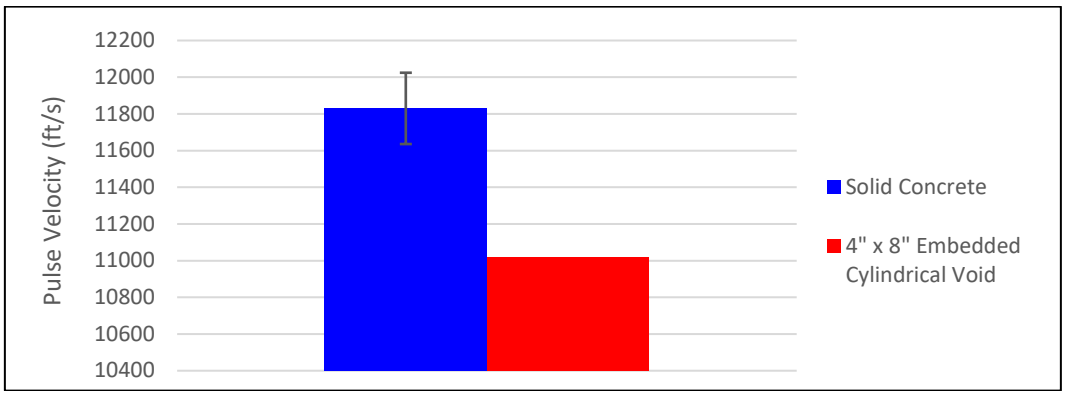

Figure 35. Graph. Beam 2 UPV Results

Indirect Transmission Measurements

Six indirect transmission measurements were taken on the Test Slab 2 sample. The mean pulse

velocity was 11,793 ft/s and the coefficient of variation was 3.82%. A lower velocity of 10,262 ft/s (3.40 standard deviations below the mean) was measured through an embedded cylindrical void with a radius of 3 inches and a height of 1 inch. A velocity of 10,411 ft/s (3.06 standard deviations below the mean) was measured through a 1.5 inch deep concrete patch of inferior quality. The velocity of the stress wave in the patch of inferior quality can be calculated by assuming that the velocity of the wave through the regular concrete is the mean velocity of 11,793 ft/s, and applying equation 17:

$$V_{patch} = \frac{d_{patch}}{\frac{d_{total}}{V_{total}} - t_{concrete}} \quad (17)$$

where V_{patch} = velocity through concrete patch, V_{total} = measured velocity, d_{patch}= twice the depth of concrete patch, d_{total}= twice the total depth, and $t_{concrete}$= transit time of wave in normal concrete. The velocity of the wave through the patch of inferior quality was calculated to be 8,619 ft/s (7.04 standard deviations below the mean).

These results are displayed in Figure 36, where the error bar represents one standard deviation. The coefficient of variation for these measurements is significantly higher than what was found during direct measurement testing. This is most likely due to changes in the slab depth which could not be accounted for.

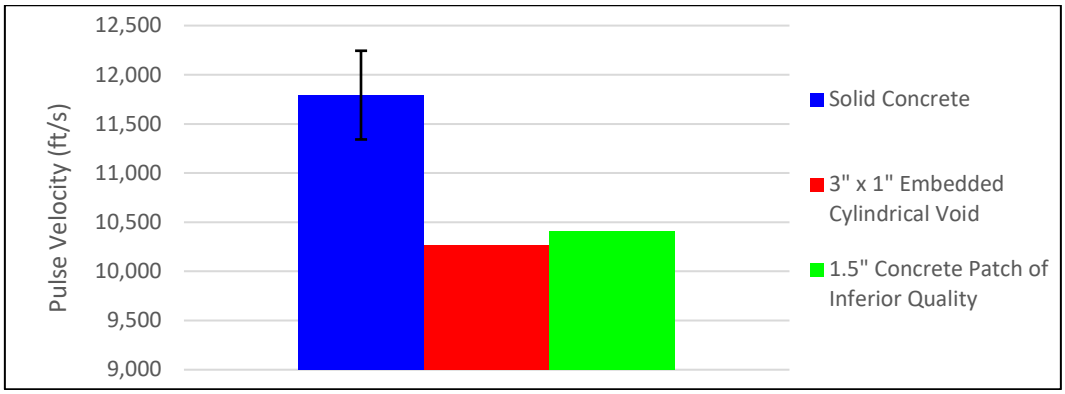

Figure 36. Graph. Test Slab 2 UPV Indirect Transmission Results

Rebound Hammer Testing

The Proceq Silver Schmidt Hammer was used to make nine measurements on the sample with the inferior concrete patch. The hammer was oriented as vertically as possible using the naked eye, and the angle correction setting was used. The mean rebound number was 44.4, with a coefficient of variation of 3.14%. A higher coefficient of variation (3.45%) was found prior to implementing the angle correction, demonstrating the benefit of the correction. Three measurements were taken on the concrete patch of inferior quality, and the mean rebound number was 32.7 (8.38 standard deviations below the mean).

Crack Depth Measurement

An artificial crack ranging in depth from 2.83 inches to 3 inches was cut into the Pavement Control Sample using a concrete saw. The crack depth was estimated using the technique outlined in *Testing of Concrete in Structures* (Bungey, 2006) and described in the literature review section. The first measurement was taken with the transducers positioned 4 inches from the crack (measured from the center of the crack to the center of the transducer). The second measurement was taken with the transducers positioned 10 inches from the crack. The crack depth was then calculated using a form

of Bungey's equation, generalized for arbitrary transducer distances:

$$h = \frac{1}{2} \times \sqrt{\frac{x_2{}^2 t_1{}^2 - x_1{}^2 t_2{}^2}{t_2{}^2 - t_1{}^2}} \quad (18)$$

where h = crack depth, x_1 = first distance from transducer to crack, x_2 = second distance from transducer to crack, t_1 = first transit time, and t_2 = second transit time. The crack depth was calculated to be 2.8 inches. As mentioned in the literature review section, there are a variety of factors in the field which can influence the accuracy of crack depth measurement which were not simulated in the current study, such as the tapering of the crack, and the presence of debris and moisture.

UPV – Compressive Strength Correlations

UPV measurements and compressive strength tests were performed on a set of (19) 4 inch by 8 inch cylinders representing typical concrete pavement mixtures with a variety of mix designs and material properties. As discussed in the literature review section, UPV measurements are commonly used to estimate the in-place strength for concrete mixtures for which correlations have previously been made. UPV measurements can also be used as a relative assessment of concrete quality within a structure.

An initial single variable regression, shown in Figure 37. had an R^2 of 0.7147. While there is a clear correlation between the two values, it is weakened by differences in other concrete properties. The goal of the current work is to study how mix design parameters and fresh concrete properties effect the UPV-compressive strength relationship.

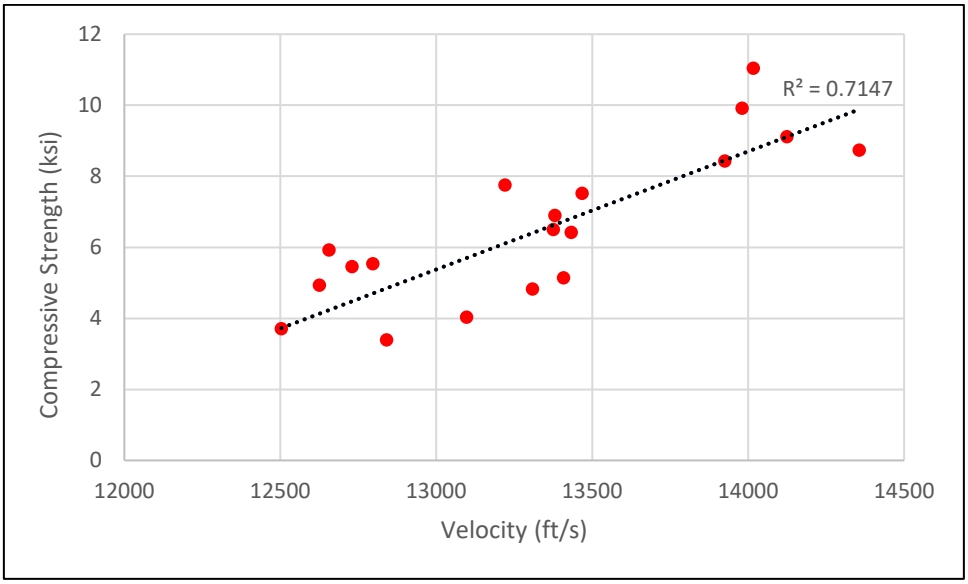

Figure 37. Graph. Correlation Between UPV and Compressive Strength

Least absolute shrinkage and selection operator (LASSO) regressions were performed with mix design parameters, fresh concrete properties, and UPV measurements as independent variables. The long-term concrete compressive strength (F_c) was the dependent variable used to identify which parameters have the greatest potential to predict compressive strength. LASSO is a regression technique which regularizes, or shrinks, coefficients with less statistical significance (Tibshirani, 1996). The degree of shrinkage is controlled by the variable λ, and the regression can shrink the coefficients of less important parameters to zero. In the current study, the λ value which produced the smallest root mean square error (RMSE) was used. Water-to-cement ratio (w/c), air content (AC), air in paste (AIP, air content normalized by paste fraction), and fresh concrete density (δ) were all initially included as independent variables. All variables were initially standardized using equation 19

$$x' = \frac{x-\mu_x}{\sigma_x} \quad (19)$$

where x' = standardized value, x = original value, μ_x = mean, and σ_x = population standard deviation. The standardization of variables removes the influence of units and allows for the coefficient magnitudes to be representative of the extent to which the parameter explains the variation in compressive strength (parameter importance).

An initial LASSO regression had a RMSE of 0.4902. The regression coefficients are shown in Table 17.

Table 17. First LASSO regression

	w/c	AC	AIP	δ	UPV
Coefficient	-0.3697	0	-0.0456	0.3179	0.3513

The coefficient for air content was shrunk to zero, most likely due to its redundancy with air in paste and its dependence on the paste fraction. Air in paste was retained, although the coefficient implies that it is much less important than the other three parameters.

A second LASSO regression, shown in Table 18, was performed with the air content removed. The regression had a lower RMSE of 0.4387. Similarly, the air in paste was retained but had a coefficient with much lower magnitude than the other three parameters.

Table 18. Second LASSO regression

	w/c	AIP	δ	UPV
Coefficient	-0.3638	-0.0279	0.3230	0.3398

An initial multiple linear regression is given in Equation 20. Air in paste values were given as percentages, density values had units of pounds per cubic foot, UPV measurements had units of feet per second, and compressive strength measurements had units of kips per square inch. The model had a RMSE of 0.8601 and an R^2 of 0.8795 $ksi^{0.5}$. It should be noted that unstandardized variables were used; therefore, the parameter coefficients and RMSE cannot be compared with the LASSO regressions.

$$F_c = -11.6062(w/c) + 0.0059(AIP) + 0.0014(\delta) + -0.0176(UPV) - 29.0992 \quad (20)$$

The covariance between independent variables was evaluated to determine whether the inclusion of interaction terms had the potential to improve the model. The covariance is shown visually in Figure 38.

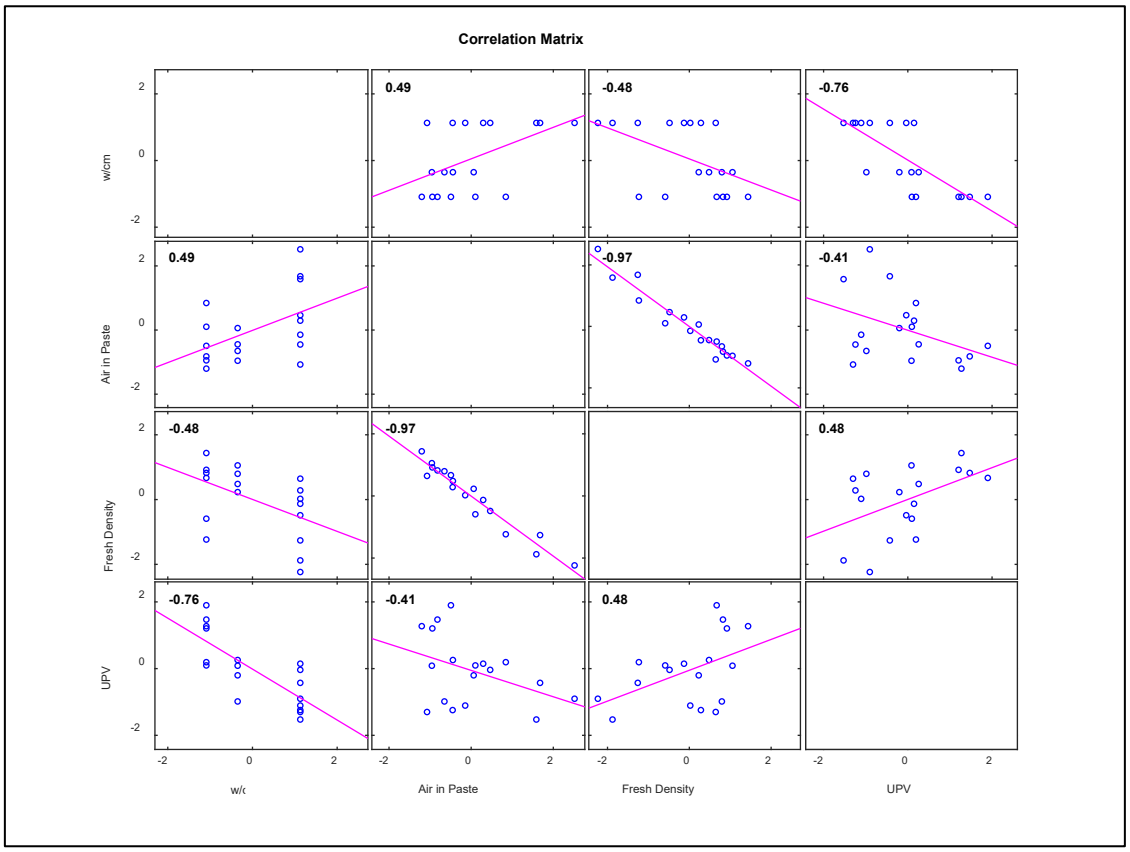

Figure 38. Graph. Covariance Between Independent Variables

As expected, strong correlations were detected between the UPV measurements and w/c ratios, and air in paste and fresh concrete density. An interaction term for the w/c-UPV relationship was included, however the air in paste-density interaction term was omitted because it was discovered through experimentation that it negatively influenced the model accuracy. A multiple linear fit with interaction terms is given in Equation 21. The model had a RMSE of 0.7882 ksi$^{0.5}$, and an R^2 of 0.9066.

$$F_c = 166.8140(w/c) + 0.0451(AIP) + 0.0102(\delta) + 0.0074(UPV) - 0.0136\,(w/c \times UPV) - 125.8637 \quad (21)$$

Finally, a multiple linear regression was conducted with three datapoints removed such that only mixtures with 1 inch nominal maximum size aggregate (NMAS) were used. The model is given in Equation 22.

$$F_c = 44.9865(w/c) + 0.2197(AIP) + 0.0262(\delta) + 0.0018(UPV) - 0.052(w/c \times UPV) - 109.8156 \quad (22)$$

The model had an RMSE of 0.5307 ksi$^{0.5}$ and an R^2 of 0.9672, indicating superior performance. This result shows that the effect of changes in coarse aggregate size cannot be accounted for solely by changes in density and UPV measurements. This is most likely due to the effect of the larger interfacial transition zone (bond between coarse aggregate and cement paste) on the concrete compressive strength. As a discretized variable, the NMAS, performs poorly when used in a regression.

Conclusions

Overall, the Olson UPV device was able to achieve the sensitivity required to be used as a relative measure of concrete quality and detect voids / defects. From the UPV results, the following conclusions were drawn:

1. The precision of the Olson UPV device was determined to be 1 μs.
2. Under the conditions of the current study, the effect of #3, #5, and #8 rebars on the measured velocity was negligible.
3. The UPV device was able to confidently detect a 4-inch diameter cylindrical void in direct transmission with a 12.0625-inch path length, with a measured velocity 4.65 inches below the mean. A 3-inch diameter cylindrical void embedded in a 4.25-inch deep slab was

successfully detected with indirect transmission measurements, with a measured velocity 3.4 standard deviations below the mean.

4. The rebound hammer had greater precision than the UPV device used in indirect transmission, with coefficient of variations of 3.14% and 3.82%, respectively. The UPV device had greater precision in direct transmission with a mean coefficient of variation of 1.75% for a 12.0625-inch path length. Both the UPV device and the Proceq Silver Schmidtt rebound hammer were capable of detecting a 1.5-inch patch of inferior quality concrete. The rebound hammer had higher sensitivity with a rebound number 8.38 standard deviations below the mean, compared to the UPV device which measured a velocity 7.04 standard deviations below the mean.
5. The UPV device measured the depth of an 2.83” to 3” deep crack to be 2.8”.
6. Using LASSO regressions, the w/c ratio, fresh concrete density, and UPV measurements were identified as the most important parameters for predicting the long-term concrete compressive strength, with approximately equal importance. The percentage of air in the cement paste was also deemed a significant parameter, although it had less of an influence on the variance in compressive strength. A model was developed to predict the compressive strength from the four parameters, and it was found that the inclusion of an w/c ratio-UPV measurement interaction term improved the accuracy of the model. The final model had a RMSE of 0.5306 $ksi^{0.5}$ and an R^2 of 0.9672.

IMPACT ECHO TESTING

Measurements were taken on Test Slab 1 and Test Slab 2 using the Olson Concrete Thickness Gauge 2 device (CTG–2) and the James Instruments VuCon Device. Before measurements were taken, the stress wave's velocity was determined by taking a reading 10 inches away from the edge of the slab for both devices. Thickness measurements were used for the calibration of the VuCon device instead of the built-in surface wave velocity calibration to avoid inaccuracies due to the presence of rebar. For both devices, three calibrations were performed and the average of the three velocities was used.

For readings with calibrated velocities, measurement accuracies should be within 2% according to the CTG-2 reference manual. No expected accuracy is specified in the VuCon operating instructions. For Test Slab 1, which is approximately 5.75 inches in depth, the mean error from seven CTG-2 measurements was 1.38% (0.078 inches), and the maximum error was 3.5% (0.19 inches). The mean error from seven VuCon measurements was 1.23% (0.070 inches) and the maximum error was 3.07% (0.17 inches). For Test Slab 2, which is approximately 4.25 inches in depth, the mean error from eight CTG-2 measurements was 2.8% (0.12 inches), and the maximum error was 4.2% (0.19 inches). When 25 measurements were taken in a single location, the coefficient of variation was 0.22% (0.0103 inches).

A 0.75 inch artificial delamination embedded in Test Slab 1 at a depth of 5.00 inches was successfully detected using the VuCon. The depth to the delamination was measured as 5.11 inches. A cylindrical void with a radius of 3.00 inches and a depth of 2.50 inches, embedded at a depth of 1.25 inches, was detected with the VuCon device as a 2.40 inch increase in measured pavement

depth. The increase in the path length associated with the stress wave traveling around the void was calculated to be 2 inches using the Pythagorean theorem.

Conclusions

In the presence of two layers of #4 rebar, the James Instruments VuCon device was able to measure a 5.75 inch slab with slightly superior accuracy (1.38% mean error) to the Olson CTG-2 device (1.38% mean error). The CTG2 -2 device was able to measure the depth of a 4.25 inch slab with two layers of #4 rebar with a mean error of 2.85%. The increase in percent error was most likely due to the increased variation in stress wave velocity due to increased reinforcement ratio (0.21 for Test Slab 2 and 0.17 for Test Slab 1).

With the measured accuracies, both devices are capable of enforcing the 0.2 inch thickness tolerance. The coefficient of variation for 25 measurements taken in a single location was 0.22% (0.0103 inches), which can be considered the device's precision in the absence of rebar and concrete inhomogeneities. This precision is more than sufficient for the enforcement of the 0.2 inch thickness tolerance, however it may be difficult to distinguish concrete inhomogeneities from variations in pavement depth.

The James Instruments VuCon device successfully detected a 0.75 inch thick delamination and a 3 inch X 2.5 inch embedded cylindrical void.

CHAPTER 5. RECOMMENDATIONS

Based on the AASHTO CoMP survey results, literature reviewed, and validation testing performed, recommendations are made for what NDT techniques and devices should be used for a given quality assurance application.

FOR THE MEASUREMENT OF REBAR

Commercially available GPR and cover meter devices can be used in place of drilling for the acceptance or rejection of rebar placement.

From the validation testing, it was determined that for cover depths less than 3.19 inches, the Proceq cover meter (Profometer 650) has the greatest accuracy. For rebar cover depths greater than 4.25 inches, the Proceq GPR (GP 8000) has the greatest accuracy. For cover depths between 3.19 and 4.25 inches it is expected that either the James Instruments cover meter (Rebarscope) or the Proceq GPR would have the greatest accuracy depending on the conditions. The cover meter accuracy would decrease for concrete members with high concentrations of steel, and the GPR accuracy would decrease in the presence of moisture or interfering EM wave reflections from either concrete-steel or concrete-air interfaces. GPR devices have the added benefit of being able to simultaneously check for delaminations and measure pavement depth.

A model was developed to predict the precision of GPR cover measurements for a given cover depth and concrete dielectric constant. During the development of the model, it was determined that GPR operator experience plays an important role in the precision of GPR measurements, and the methodology could be repeated to develop a model with experienced GPR operators.

FOR THE MEASUREMENT OF CONCRETE THICKNESS

For concrete members in which the bottom face is a concrete-steel interface and rebar are available for the determination of EM wave velocity (such as bridge decks with SIP forms), a GPR device is likely going to be the most effective for the measurement of pavement depth. GPR thickness measurements can be used as a partial or complete replacement for drilling depending on the depth and concrete dielectric constant. For concrete-air or concrete-gravel interfaces stress-wave based technologies are recommended. When the member is thin enough, a UPV SAFT device will have the most accurate non-destructive determination of concrete thickness and can be used as a replacement for coring without velocity calibration. For deeper members such as pavements, impact echo devices are recommended and can be used as a complete or partial replacement for coring depending on the depth.

FOR THE RELATIVE MEASUREMENT OF CONCRETE QUALITY AND THE DETECTION OF DEFECTS

Stress wave-based NDT techniques are known to be more sensitive to changes in concrete quality and are more effective for the measurement of concrete-air interfaces. In the validation testing program, a UPV pitch-catch device was shown to be effective for the detection of changes in concrete compressive strength and the detection of embedded voids. The use of a UPV pitch-catch device is recommended when both sides of a member are accessible. For thin members (up to 2.58 feet for the MIRA device and 6.6 feet for the Proceq PD8000 device) where only one side of the member is accessible (such as shallow pavements), the use of a UPV SAFT device is recommended. For deep pavements and foundations, an Impact Echo device is recommended because of the

superior penetration depth. For all three technologies, the measured wave velocities can be used for the acceptance of concrete quality and to identify coring locations when potential problems are detected.

While they are less sensitive to concrete-air interfaces, GPR devices have the benefit of being able to detect voids and delaminations while the rebar is being measured. The dielectric constant can also be used as an indication of the susceptibility of rebar to corrosion.

FOR THE DETERMINATION OF CONCRETE MOISTURE TRANSPORT PROPERTIES

From the review of literature and validation testing performed by the RP 20-19 team, it was found that surface resistivity measurements can be used as an indication of concrete moisture transport properties (i.e., diffusion, permeability, and sorption). In-situ surface resistivity measurements can be used as a relative measure of concrete quality. The concrete formation factor can be calculated from surface resistivity measurements and estimated pore solution conductivities (Bentz, 2007) and can be used to predict the initiation of corrosion.

REFERENCES

AASHTO R 37, (2004). “Standard Practice for Application of Ground Penetrating Radar (GPR) to Highways.” American Association of State Highway and Transportation Officials, Washington, DC

AASHTO T 259. (2002). “Standard Method for Resistance of Concrete to Chloride Ion Penetration,” American Association of State Highway and Transportation Officials, Washington, DC

AASHTO T 277, (2007). “Standard Test Method for Electrical Indication of Concrete’s Ability to Resist Chloride.” American Association of State Highway and Transportation Officials, Washington, DC.

AASHTO T 358-17 (2017). “Standard Method for Resistance of Concrete to Chloride Ion Penetration,” American Association of State Highway and Transportation Officials, Washington, DC.

ACI Committee 228. (2013). “228.2R-13: Report on Nondestructive Test Methods for Evaluation of Concrete in Structures”

ACI Committee 228. (2019). “228.1R-19: Report on Methods for Estimating In-Place Concrete Strength.” https://doi.org/10.14359/51715516

Alldred, J. C. (1993) "An improved method for measuring reinforcing bars of unknown diameter in concrete using a cover meter." *CONFERENCE PROCEEDINGS OF THE BRITISH INSTITUTE OF NON-DESTRUCTIVE TESTING INTERNATIONAL CONFERENCE, NDT IN CIVIL ENGINEERING 14-16 APRIL 1993, LIVERPOOL UNIVERSITY. VOLUME 2*.

ASTM C 1074 -17 (2017). “Standard Practice for Estimating Concrete Strength by the Maturity Method,” ASTM International, West Conshohocken, PA.

ASTM C192-14 (2014). “Standard Test Method for Making and Curing Concrete Test Specimens in the Laboratory,” ASTM International, West Conshohocken, PA.

ASTM C192/C192M-19 Standard Practice for Making and Curing Concrete Test Specimens in the Laboratory, West Conshohocken, PA, 2019.

ASTM C1202-12, (2012). “Standard Test Method for Electrical Indication of Concrete’s Ability to Resist Chloride Ion Penetration.” ASTM International, West Conshohocken, PA.

ASTM C1383-15. (2012). “Standard Test Method for Electrical Indication of Concrete’s Ability to Resist Chloride Ion Penetration,” ASTM International, West Conshohocken, PA.

ASTM C1543-10a, “Standard Test Method for Determining the Penetration of Chloride Ion into Concrete by Ponding” ASTM International, West Conshohocken, PA, 2010

ASTM D4748-10, (2020) “Standard Test Method for Determining the Thickness of Bound Pavement Layers Using Short-Pulse Radar,” ASTM International, West Conshohocken, PA, 6 pp.

ASTM D6087-08, (2015) “Standard Test Method for Evaluating Asphalt-Covered Concrete Bridge Decks Using Ground Penetrating Radar,” ASTM International, West Conshohocken, PA, 6 pp.

Barnes, R., and Zheng, T. (2008) "Research on factors affecting concrete cover measurement." *The e-Journal of Nondestructive Testing. Austrália*.

Bentz, D.P. (2007). "A Virtual Rapid Chloride Permeability Test," *Cement and Concrete Composites*, 29(10), pp. 723–731.

British Standard. (1881) "Recommendations for Testing Concrete."

Bungey, John H., and Michael G. Grantham. *Testing of concrete in structures*. CRC Press, 2006.

Carino, N. J. (2015). "Impact Echo: The Fundamentals." *Proceedings of the International Symposium Non-Destructive Testing in Civil Engineering (NDT-CE), Berlin, Germany*.

Chopperla, K. S. T., and Ideker, J. H.. (2022). "Using Electrical Resistivity to Determine the Efficiency of Supplementary Cementitious Materials to Prevent Alkali-Silica Reaction in Concrete." *Cement and Concrete Composites* 125, p. 104282.

Collins, C., and Hill, C. (2019). *The Investigation of Chloride Ion Penetration Utilizing Two Methods*.

Concha, N., and Oreta, A.W. (2020) "An improved prediction model for bond strength of deformed bars in rc using upv test and artificial neural network." *GEOMATE Journal* 18.65: 179-184.

Emmenegger, L. P. (2020). *Extending the Lifespan of Reinforced Concrete Bridge Decks: Historical Analysis, Modeling, and Improved Contracting*. Dissertation. Georgia Institute of Technology

Fodil, N., Chemrouk, M., and Ammar, A. (2019). "The Influence of Steel Reinforcement on Ultrasonic Pulse Velocity Measurements in Concrete of Different Strength Ranges." *IOP Conference Series: Materials Science and Engineering*, 603(2). IOP Publishing.

García, F.G., Pérez-Gracia, V., and Abad I.R., (2008) "GPR evaluation of the damage found in the reinforced concrete base of a block of flats: A case study." *NDT & e International* 41.5: 341-353.

Ghosh, P., and Tran, Q.. "Correlation between bulk and surface resistivity of concrete." *International Journal of Concrete Structures and Materials* 9.1 (2015): 119-132.

Khanal, S. (2020) *Review of Modern Nondestructive Testing Techniques for Civil Infrastructure*. West Virginia University, 2020.

Koyan, P., Tronicke J., Allroggen N., Kathage A., and Willmes, M., (2018) "Estimating moisture changes in concrete using GPR velocity analysis: potential and limitations," *2018 17th International Conference on Ground Penetrating Radar (GPR)*, pp. 1-6, doi: 10.1109/ICGPR.2018.8441572.

Kurtis K.E., Scott, D., (2013) "Forensic Slab and Beam" CEE 4803: Special Topics, Georgia Institute of Technology, Atlanta, Georgia

Lesnicki, K. J., Kim, J. Y., Kurtis, K. E., and Jacobs, L. J. (2013). "Assessment of Alkali–Silica Reaction Damage through Quantification of Concrete Nonlinearity." *Materials and Structures*, 46, pp. 497–509.

Ley, T. M., and Bradden, T. (2014) "A test method to measure the freeze thaw durability of fresh concrete using overpressure." T&DI Congress 2014: Planes, Trains, and Automobiles. 2

Liu Y., Francisco P., and Suares A. (2010) "Characterization of new and old concrete structures using surface resistivity measurements."

Liu, Yun-Lin, et al. (2019). “Grouting Defect Detection of Lapped Bar Connections Based on Impact-Echo Method.” *Shock and Vibration* 2019.

Maierhofer, C. (2003) "Nondestructive evaluation of concrete infrastructure with ground penetrating radar." *Journal of materials in civil engineering* 15.3, 287-297.

Malhotra, V. M., and Carino, N. J. (2003). *Handbook on Nondestructive Testing of Concrete*. CRC Press.

McDonald, D. B. (1994). “The Rapid Chloride Permeability Test and its Correlation to the 90-Day Chloride Ponding Test.” *PCI Journal* 39(1), pp. 38–47.

Moradllo, M. K., et al. (2018). “Relating Formation Factor of Concrete to Water Absorption.” *ACI Materials Journal* 115(6), pp. 887–898.

Morris, W., Moreno, E. I., and Sagüés, A. A. (1996). “Practical Evaluation of Resistivity of Concrete in Test Cylinders Using a Wenner Array Probe.” *Cement and Concrete Research*, 26(12), 1779–1787.

Ndagi, A., et al. (2019). “Non-Destructive Assessment of Concrete Deterioration by Ultrasonic Pulse Velocity: A Review.” *IOP Conference Series: Earth and Environmental Science,* 357(1). IOP Publishing.

Neto, P.X., and Eugênio de Medeiros, W., (2006) "A practical approach to correct attenuation effects in GPR data." *Journal of Applied Geophysics* 59.2: 140-151.

Popovics, J. S., and Rose, J. L. (1994). “A Survey of Developments in Ultrasonic NDE of Concrete.” *IEEE Transactions of Ultrasonics, Ferroelectrics and Frequency Control*, 41, pp. 140–143.

Popovics, J. S., et al. (2017). *Ultrasonic Imaging for Concrete Infrastructure Condition Assessment and Quality Assurance*. No. FHWA-ICT-17-007. Illinois Center for Transportation.

Profometer Operating Instructions, Proceq, (2017).

Rebarscope Instruction Manual, James Instruments, (2018).

Rios, Renee T., et al. “Screening Candidate Supplementary Cementitious Materials under Standard and Accelerated Curing through Time-Series Surface Resistivity Measurements and Change-Point Detection.” *Cement and Concrete Research*, vol. 148, 2021, p. 106538. https://doi.org/10.1016/j.cemconres.2021.106538.

Saleem, M. (2017). “Study to Detect Bond Degradation in Reinforced Concrete Beams Using Ultrasonic Pulse Velocity Test Method.” *Structural Engineering and Mechanics: An International Journal* 64(4), pp. 427–436.

Senin, S. F., and Hamid, R., (2016) "Ground penetrating radar wave attenuation models for estimation of moisture and chloride content in concrete slab." *Construction and Building Materials* 106: 659-669

Shalan, L., Kahn, K., and Nadelman, E. (2016). “Assessment of High Early Strength Limestone Blended Cement for Next Generation Transportation Structures: Final Report,” Georgia Institute of Technology, Atlanta, Georgia

Snyder, K. A., Feng, X., Keen, B.D., and Mason, T. O. (2003). "Estimating the Electrical Conductivity of Cement Paste Pore Solutions from OH-, K+ and Na+ Concentrations," *Cement and Concrete Research*, 33(6), pp. 793–798.

Soutsos, M.N, (2001) "Dielectric Properties of Concrete and Their Influence on Radar Testing." *NDT & E International*, vol. 34, no. 6, pp. 419–425., https://doi.org/10.1016/s0963-8695(01)00009-3

Stain, RT, and Dixon, S., (1919) "Inspection of cables in post-tensioned bridges." *Construction repair* 8.1.

Tibshirani, R. (1996) "Regression shrinkage and selection via the lasso." *Journal of the Royal Statistical Society: Series B (Methodological)* 58.1: 267-288.

Weiss, W. J., Barrett, T. J., Qiao, C., and Todak, H. (2016). "Toward a Specification for Transport Properties of Concrete Based on the Formation Factor of a Sealed Specimen." *Advances in Civil Engineering Materials* 5(1), 179 194.

Weiss, W. J., et al. (2018)"Toward Performance Specifications for Concrete: Linking Resistivity, RCPT and Diffusion Predictions Using the Formation Factor for use in Specifications." In D.A. Hordijk and M. Luković (Eds.), *High Tech Concrete: Where Technology and Engineering Meet* (pp. 2057–2065). Springer, Cham.

Whiting, D., "Rapid Determination of the Chloride Permeability of Concrete," Report No. FHWA/RD-81/119, Federal Highway Administration, Washington, DC, 1981, 174 pp.

APPENDIX A. SURVEY RESULTS DIAGRAM

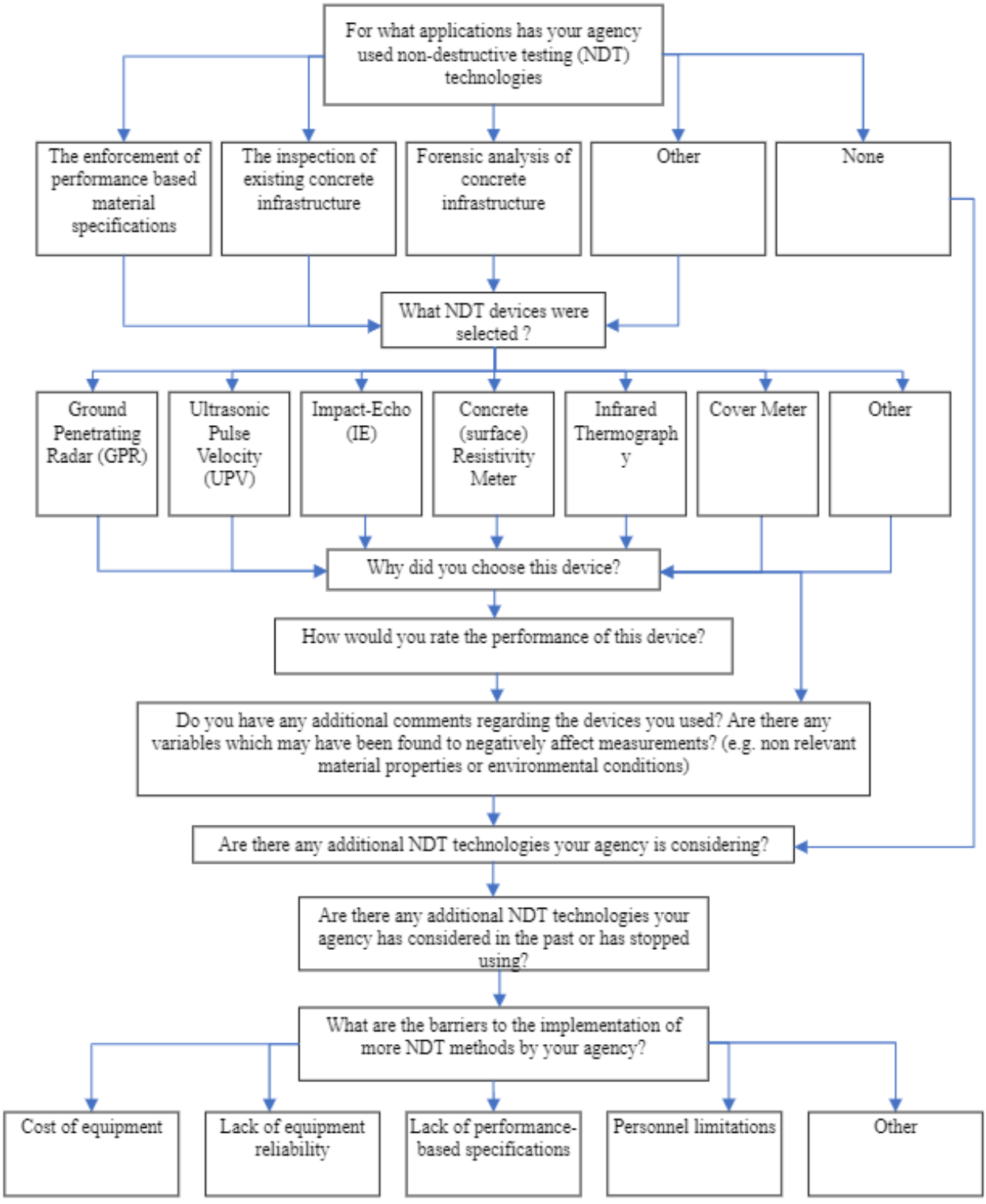

APPENDIX B. SAMPLE DETAILS AND IMAGES

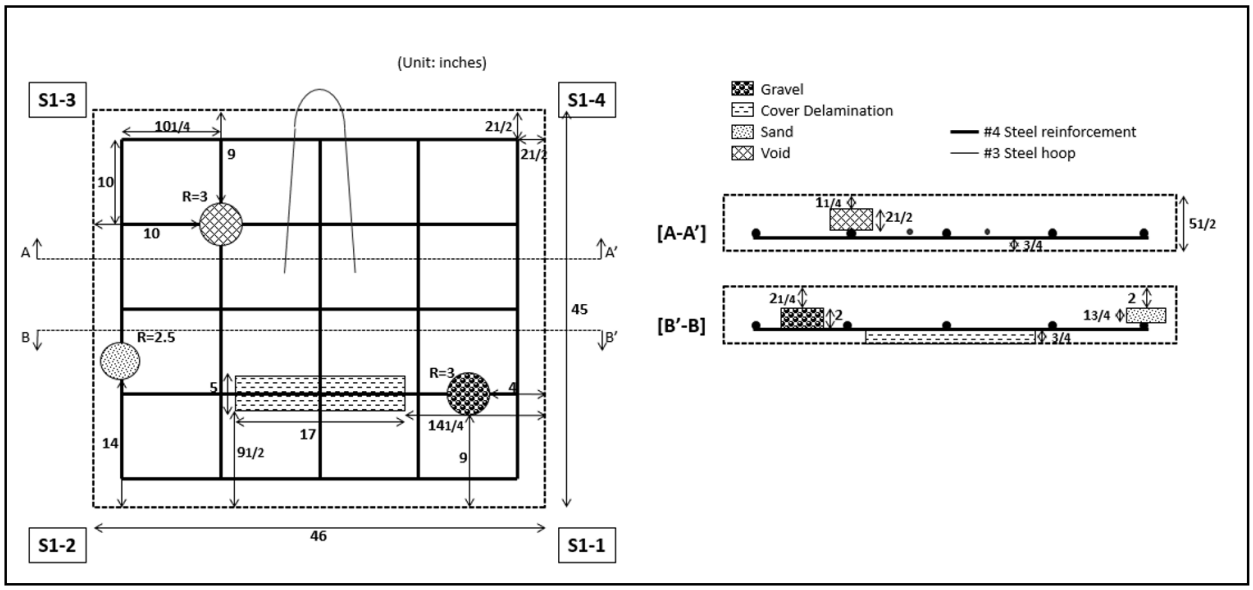

Figure 39. Diagram. Test Slab 1 Details

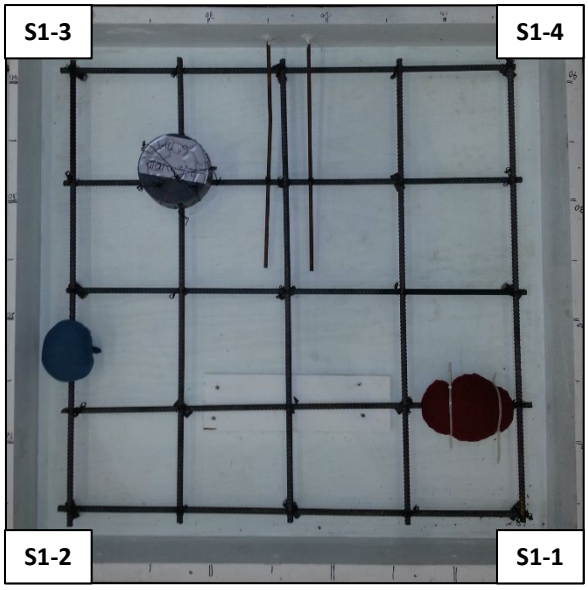

Figure 40. Photo.Test Slab 1 Before Casting

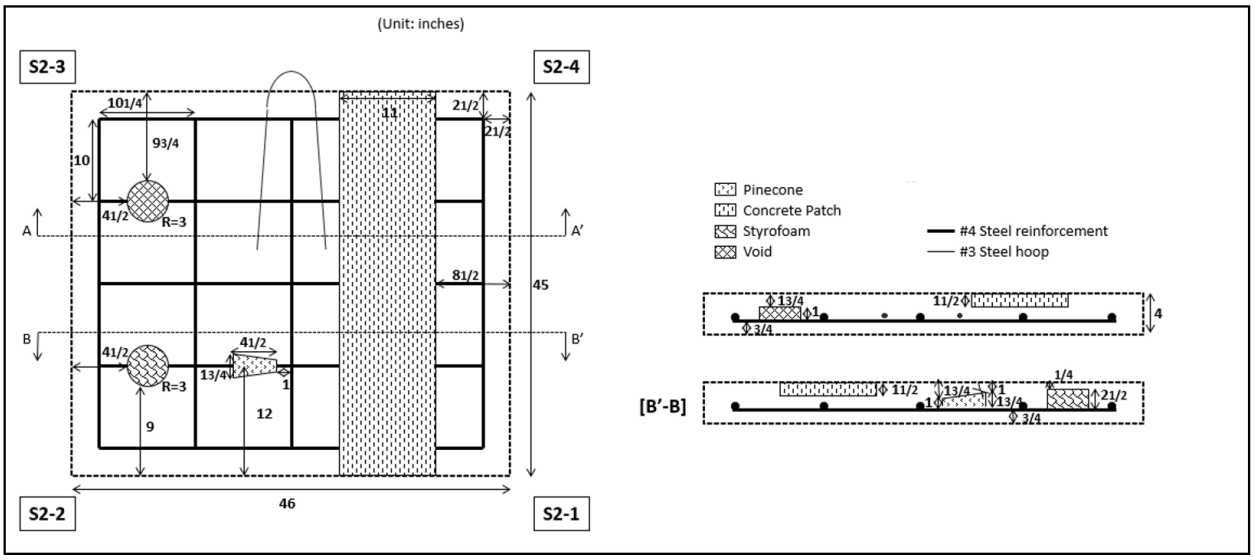

Figure 41. Diagram. Test Slab 2 Details

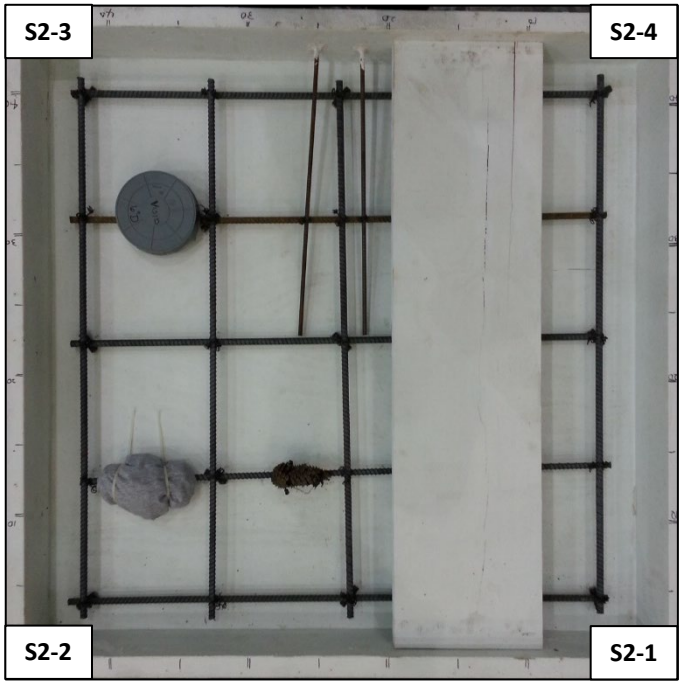

Figure 42. Photo. Test Slab 2 Image Before Casting

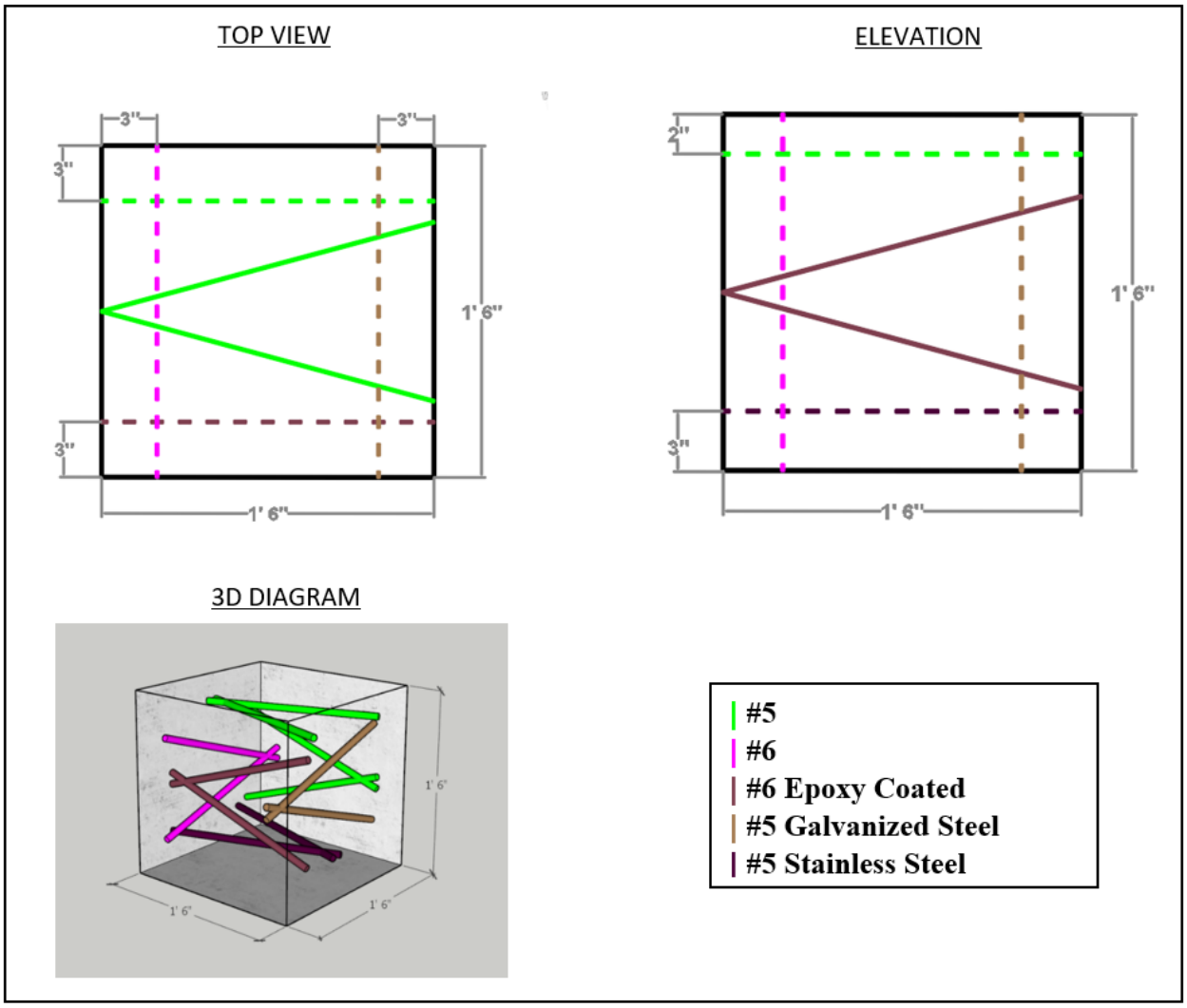

Figure 43. Diagram. Alternative Rebar Sample

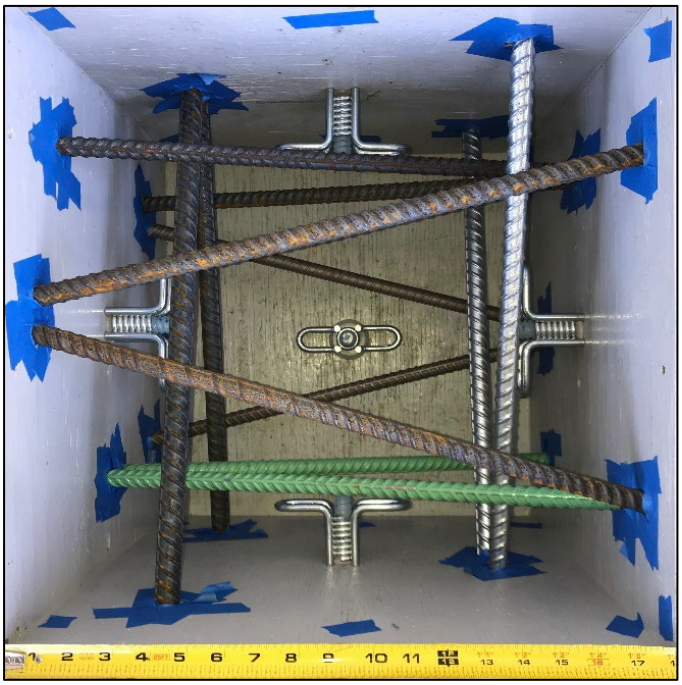

Figure 44. Photo. Alternative Reinforcement Sample Image Before Casting

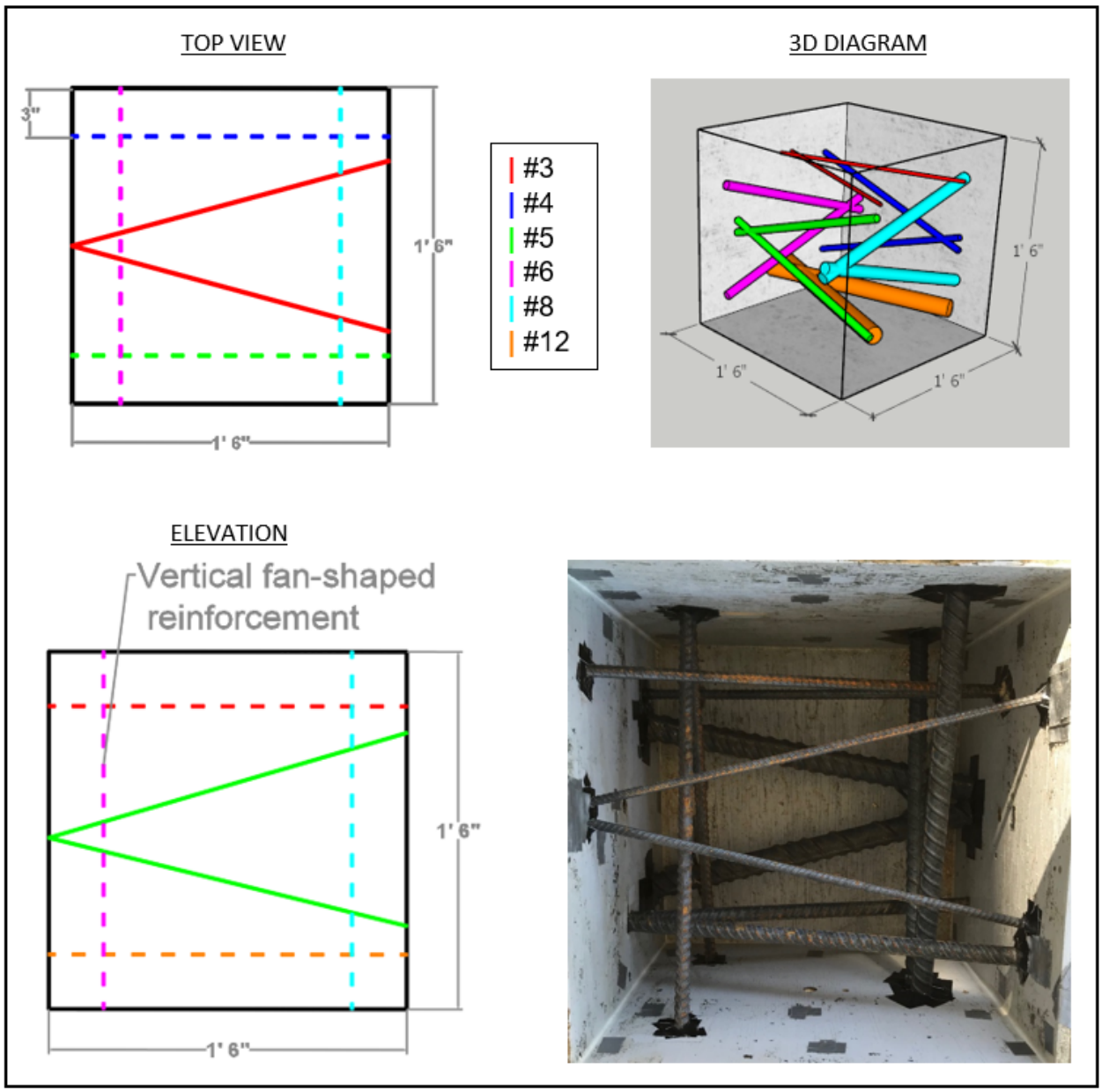

Figure 45. Diagram. Rebar Size Sample Details and Image Before Casting

Figure 46. Photo. Dowel Bar Sample Image Before Casting

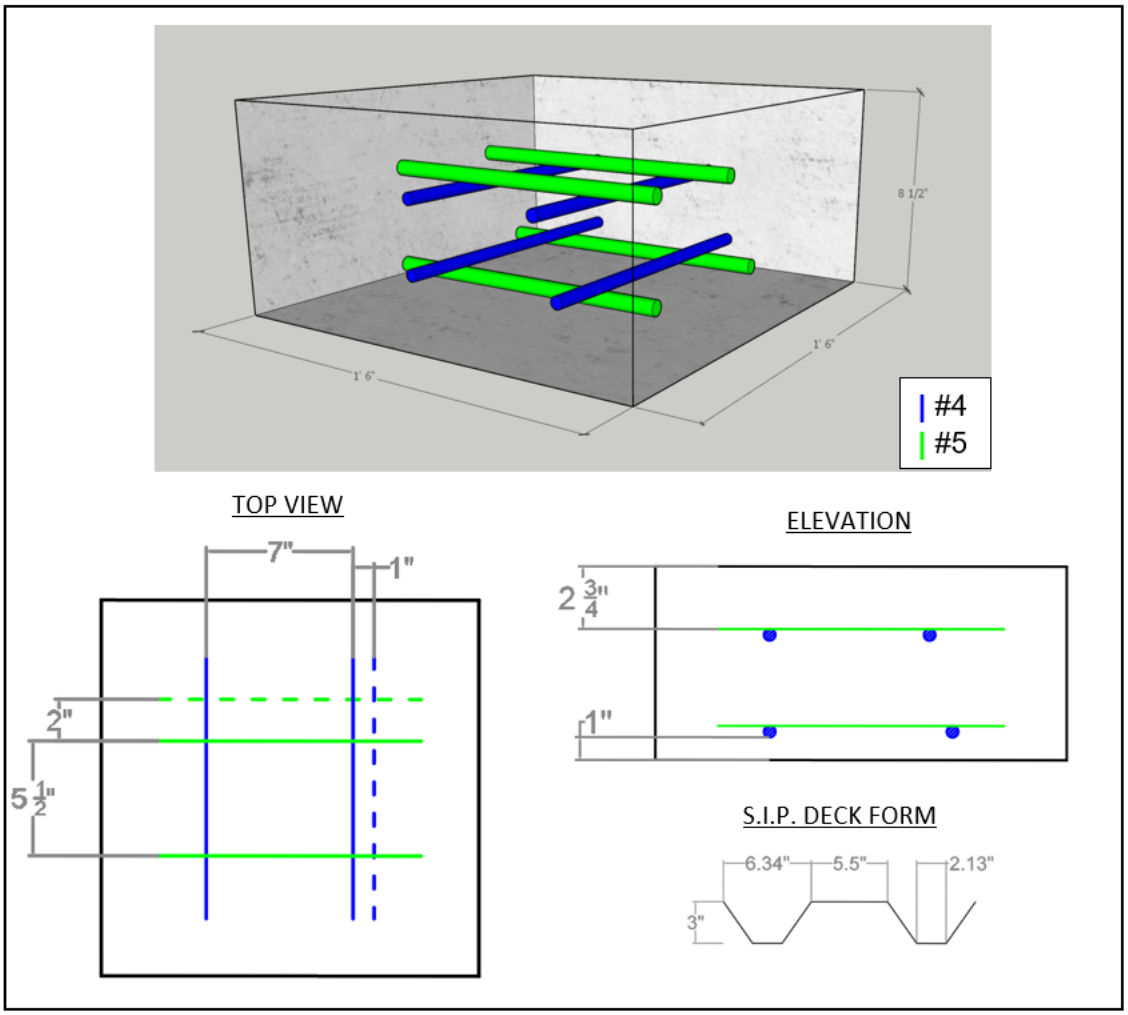

Figure 47. Diagram Bridge Deck Sample Details

Figure 48. Photo. Bridge Deck Sample Image Before Casting and SIP Form

APPENDIX C. SAMPLE MIX DESIGNS WITH AGGREGATES IN SATURATED SURFACE DRY (SSD) CONDITION

Table 19. UPV-Compressive Strength Sample Mix Designs

Sample	Water (lb/cyd)	Cement (lb/cyd)	Coarse Aggregate (lb/cyd)	Sand (lb/cyd)	AEA (mL)	WRA (mL)
C01	283	708	1682	1205	8	0
C02	283	708	1682	1205	8	20
C03	310	775	1682	902	8	50
C04	297	539	1682	1401	0	9
C05	283	515	1682	1368	8	10
C06	297	539	1682	1225	15	10
C07	310	564	1682	1081	15	10
C08	297	742	1899	1012	4	0
C09	283	708	1899	987	6	25
C10	297	742	1899	836	10	22
C11	310	775	1899	684	13	0
C12	310	564	1899	1128	0	20
C13	283	515	1899	1150	5	10
C14	297	539	1899	1006	12	15
C15	297	539	1899	1006	12	0
C16	283	630	1899	1053	3.6	5
C17	283	504	1899	1033	2.9	5
C18	283	630	1899	1053	6	5
C19	283	630	1790	1163	4.5	10

Table 20. New Sample Mix Proportions and Fresh Concrete Properties

Sample	CA Size	Water	Cement	Fly Ash	Coarse Aggregate	Sand	Pressure Air	Unit Weight
	AASHTO #	lbs/yd^3	lbs/yd^3	lbs/yd^3	lbs/yd^3	lbs/yd^3	%	lbs/yd^3
Alternative Rebar Sample	#57	275	688	0	1920	920	3.18	3680
Rebar Size	#67	305	871	0	1800	808	5.85	3560
Bridge Deck Sample	#57	275	584	103	1920	902	3.55	3630
Dowel Bar Sample	#457	250	386	68.2	2030	1080	8.08	3650

Table 21. Surface Resistivity Sample Mix Designs

Sample	Water	Cement	Fine Aggregate	Coarse Aggregate	SCM
	lbs/yd^3	lbs/yd^3	lbs/yd^3	lbs/yd^3	lbs/yd^3
PC-AAA	340	850	1000	1783	0
Qz-AAA	340	680	1000	1783	170
MK-AAA	340	782	1000	1783	68
FA-AAA	340	680	1000	1783	170
PC-A	284	611	1189	1880	0
Clay-A	284	550	1189	1880	61
FA-A	284	489	1189	1880	122
RPC-A	270	581	1586	1674	0

APPENDIX D. GPR ANALYSIS QUANTILE-QUANTILE PLOTS

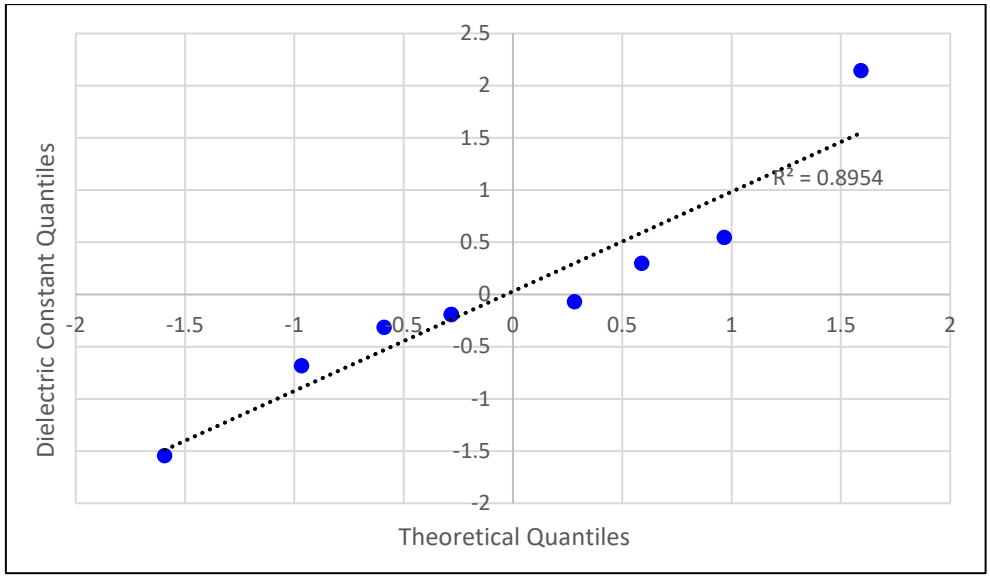

Figure 49. Graph. Test Slab 1 Dielectric Constant Q-Q Plot

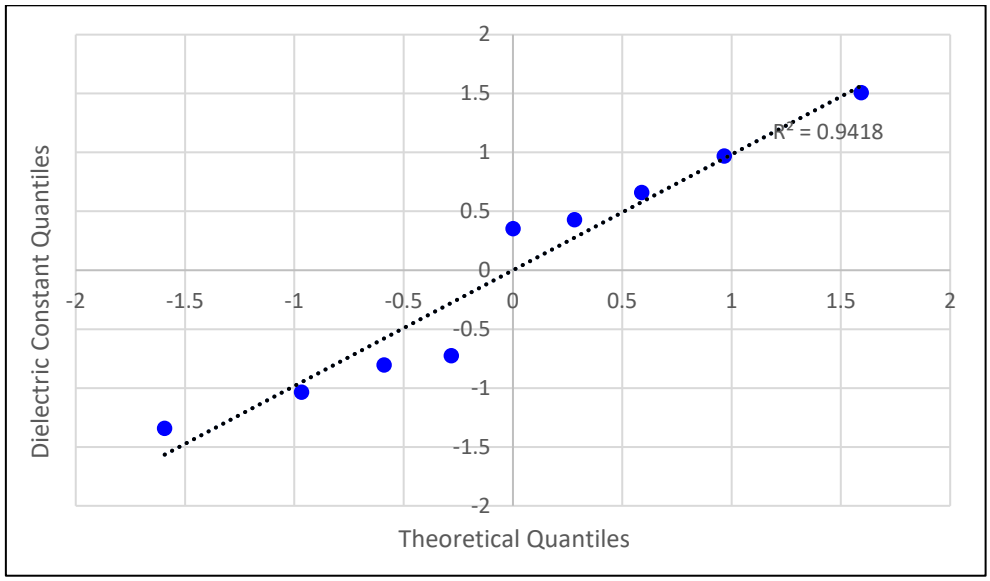

Figure 50. Graph. Slab 2 Dielectric Constant Q-Q Plot

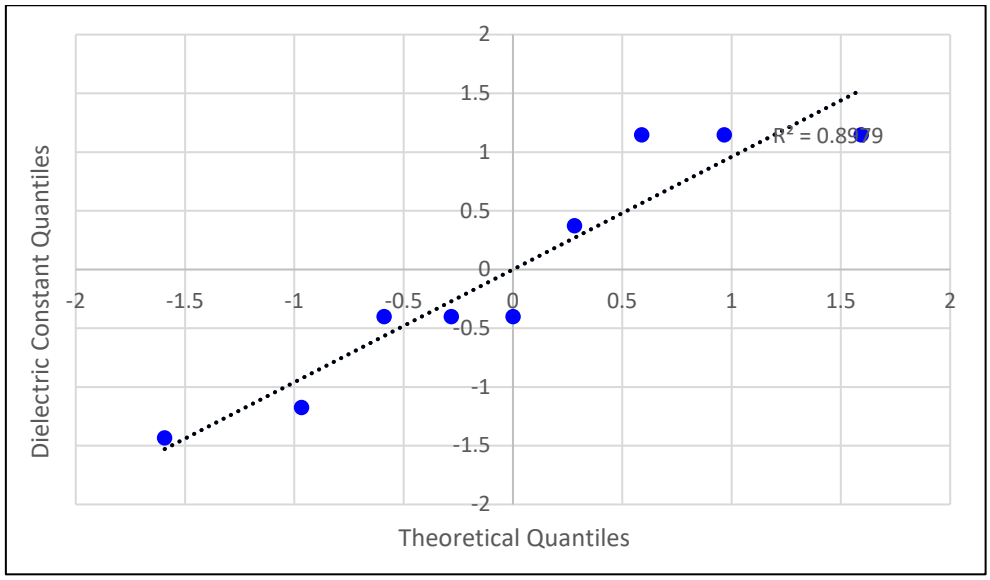

Figure 51. Graph. Dowel Bar Sample Dielectric Constant Q-Q Plot

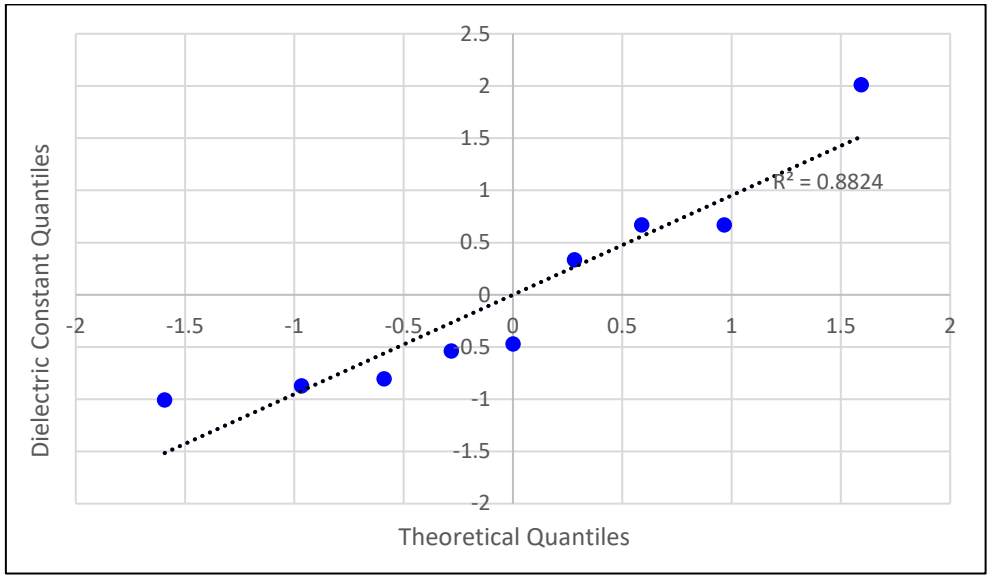

Figure 52. Graph. Bridge Deck Sample Dielectric Constant Q-Q Plot

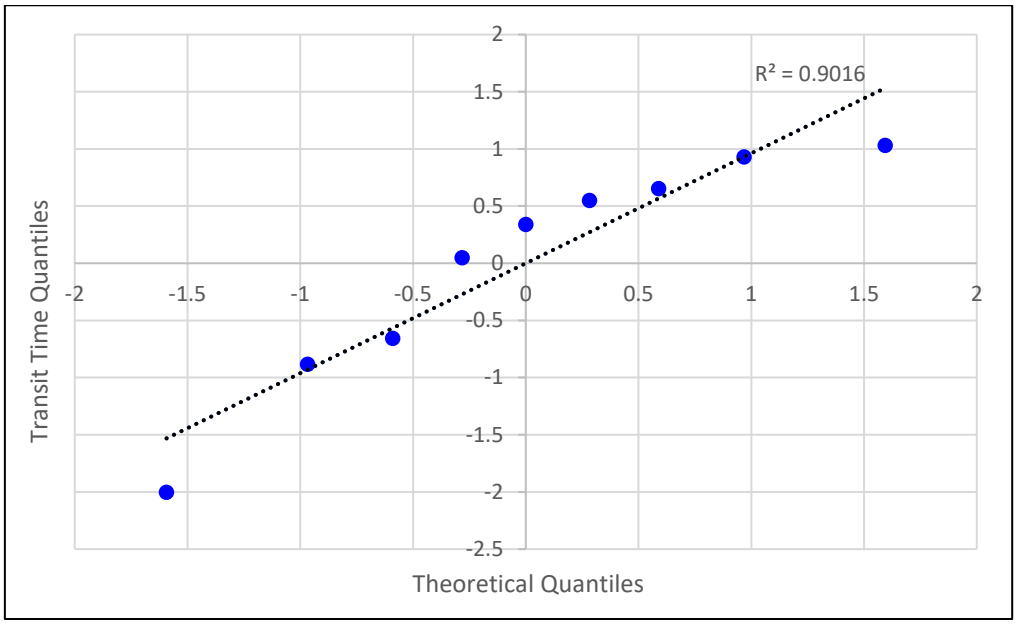

Figure 53. Graph. Test Slab 1 Transit Time Q-Q Plot

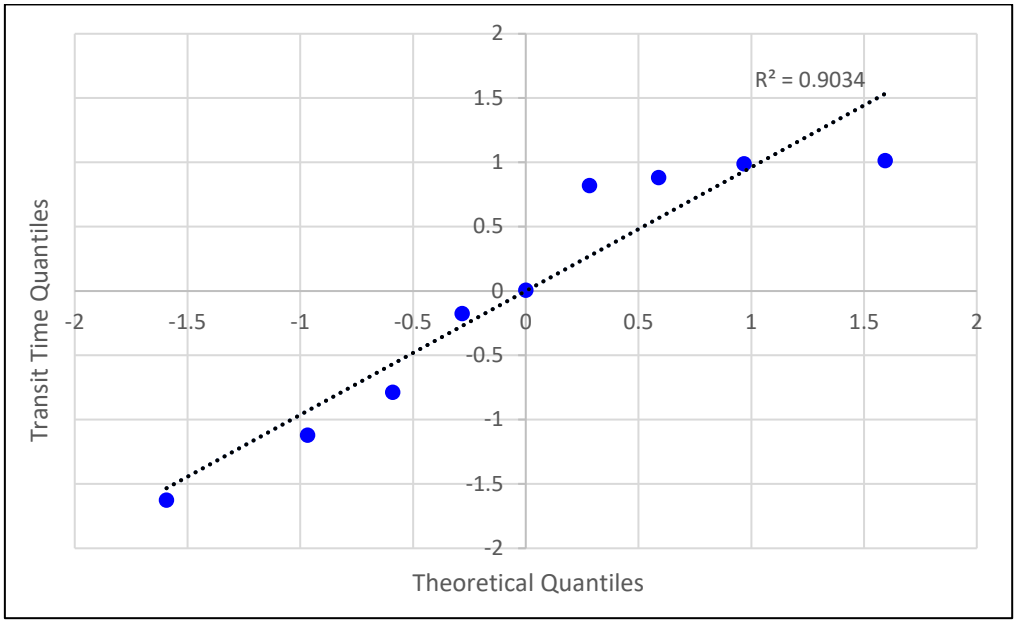

Figure 54. Graph. Test Slab 2 Transit Time Q-Q Plot

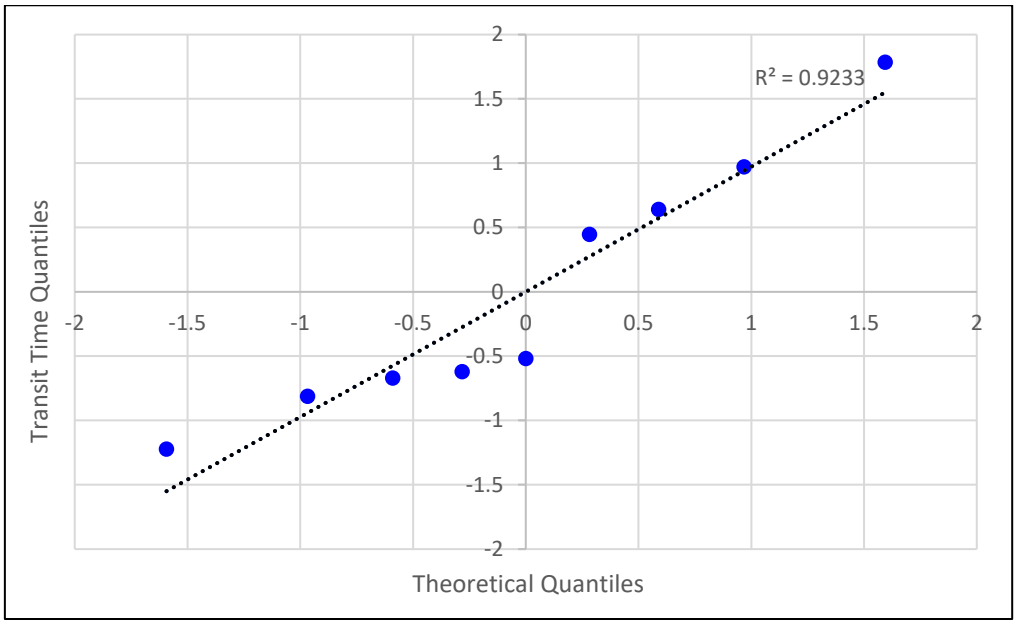

Figure 55. Graph. Bridge Deck Sample Transit Time Q-Q Plot

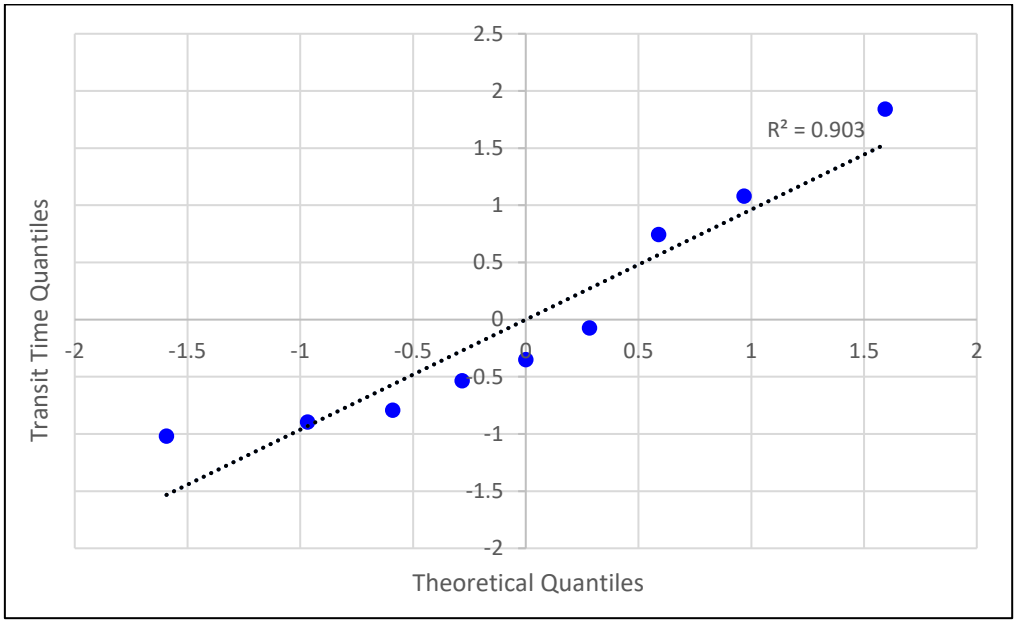

Figure 56. Graph. Dowel Bar Sample Transit Time Q-Q Plot

APPENDIX E. UPV–COMPRESSIVE STRENGTH DATA

Table 22. UPV–Compressive Strength Data

	w/c	Fresh Air Content	Air in Paste	CA NMAS	Fresh Density	UPV	Compressive Strength
Unit		%	%	In.	lbs/yd^3	ft/s	ksi
C01	0.4	3.75	12.5	1	3890	13930	8.43
C02	0.4	3.42	11.4	1	3910	14360	8.74
C03	0.4	7.29	22.1	1	3700	13430	6.42
C04	0.55	3.97	14.2	1	3840	12730	5.50
C05	0.55	7.77	28.8	1	3700	13100	4.00
C06	0.55	9.94	35.5	1	3590	12840	3.39
C07	0.55	8.14	28.1	1	3630	12500	3.70
C08	0.4	2.81	8.78	1	3930	14120	9.11
C09	0.4	1.71	5.71	1	4000	14020	11.04
C10	0.4	2.49	7.78	1	3940	13980	9.91
C11	0.4	5.34	16.2	1	3770	13380	6.89
C12	0.55	1.96	6.74	1	3910	12630	4.93
C13	0.55	4.78	17.7	1	3820	13410	5.14
C14	0.55	3.29	11.73	1	3870	12660	5.92
C15	0.55	5.34	19.06	1	3790	13310	4.82
C16	0.55	4.60	15.83	0.75	3860	13220	7.75
C17	0.45	3.42	11.78	1	3890	13470	7.52
C18	0.45	2.94	10.13	1.25	3930	12800	5.54
C19	0.45	2.23	7.68	1.25	3950	13390	6.50